UNIVERSITÀ
DEGLI STUDI
FIRENZE

UGO SCHIFF
DIPARTIMENTO
DI CHIMICA

DOTTORATO DI RICERCA IN SCIENZE CHIMICHE

CICLO XXXII

COORDINATORE Prof. PIERO BAGLIONI

Metal based drugs with potential anticancer and antibacterial properties: synthesis, interaction with biological targets and mechanistic studies

Settore Scientifico Disciplinare CHIM/03

Dottorando

Dott. Cirri Damiano

Tutore

Prof. Luigi Messori

_____ _____

Coordinatore

Prof. Piero Baglioni

_____

Anni 2016/2019

This work is dedicated to Piero Angela, the Man who inspired my deep love for Science

Table of contents

1. Introduction

Metal compounds in medicine: a short overview

Since the antiquity transition metals have been used as therapeutic agents on a simple empirical basis, in some cases with appreciable results. Among these, silver, gold and mercury salts have been extensively employed to treat various bacterial diseases such Tuberculosis, Syphilis and Gonorrhea [1-3]. Anyway, more recently, due to the discovery of Penicillin G (Fig.1) [4] and to grounded concerns on their conspicuous systemic toxicity, metal-based agents were gradually abandoned.

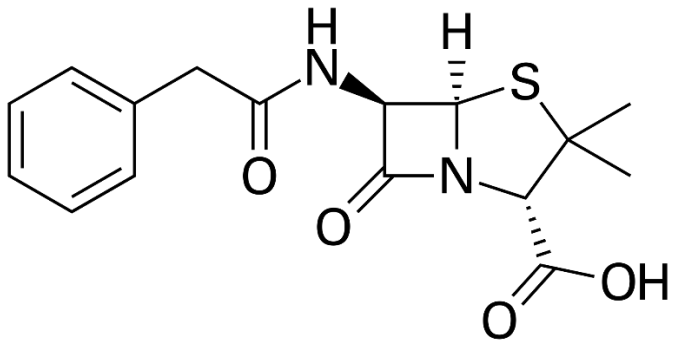

Fig.1: The molecular structure of Penicillin G.

Nowadays only a few metal-based compounds resist in clinical use, but, despite their low appeal in current research, transition metals are still of great importance in Medicinal Chemistry. Indeed, since the serendipitous discovery of the anticancer properties of Cisplatin in the late 1960s [5] (a simple Platinum(II) compound synthesized for the first time by Peyrone in 1844 [6]) and its approval in 1978 by the FDA for the treatment of testicular and ovarian cancer [7-9], metal-based drugs have gained a great interest in academic research. This unexpected discovery encouraged scientific community to investigate the properties of other Platinum related compounds and in a few decades other two diamminoplatinum-based molecules, i.e. Carboplatin and Oxaliplatin, were approved worldwide for the treatment of neoplastic diseases (Fig.2) [10, 11].

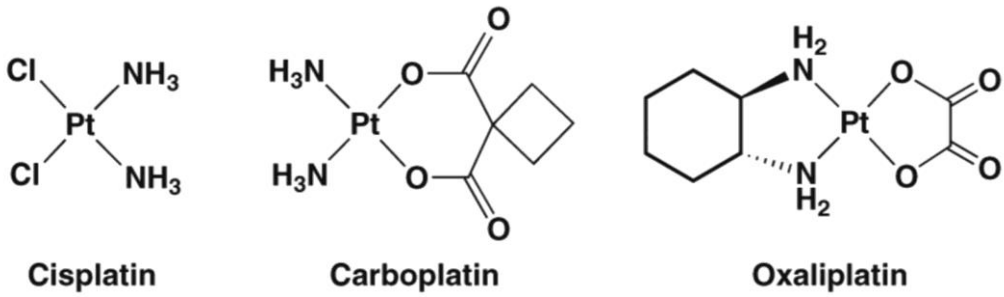

Fig.2: The three platinum related compounds approved worldwide for the treatment of cancer.

The introduction in clinical use of Platinum compounds has represented a revolution in the field of oncology and medicinal chemistry: as showed in Fig.3 [12], since the approval of clinical protocols based on Cisplatin, the death rate in the USA due to lung cancer stops for the first time his growth.

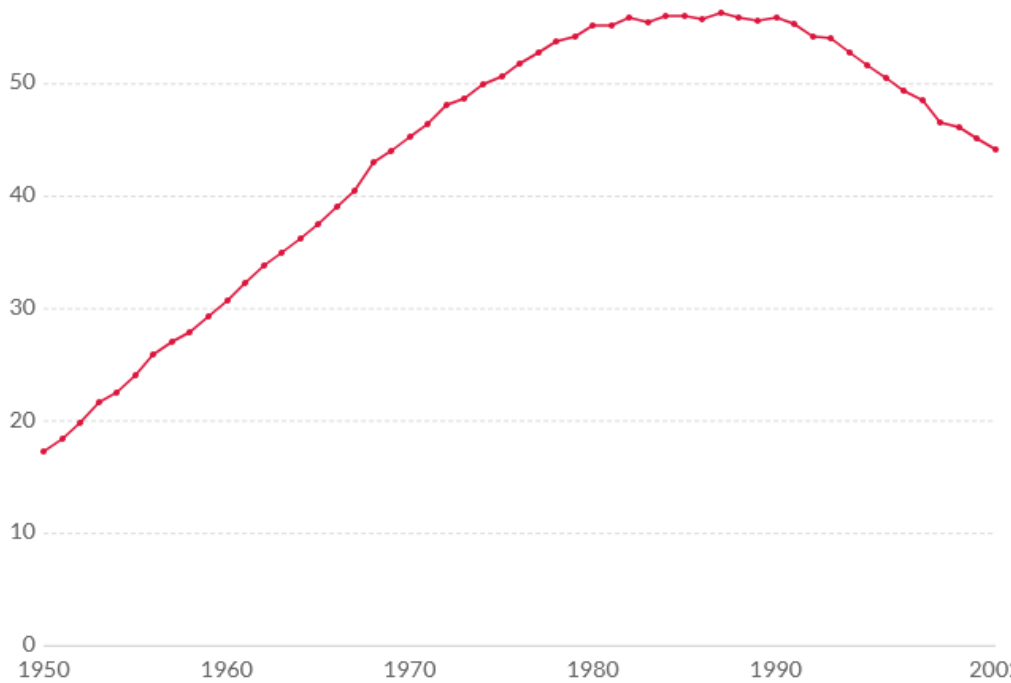

Fig.3: Lung cancer death rates per 100000 peoples (males) in the United States since 1950 to 2002 [12].

At present days Cisplatin, Carboplatin and Oxaliplatin still represent the most important established molecules for the treatment of malignances. Anyway, despite these impressive results obtained in the cure rate of oncologic patients, chemists are still looking for other valuable structures. This intense research is fully justified by the relevant flaws showed from the Cisplatin related compounds. Indeed, despite their high activity against tumoral cells, these molecules usually show invalidating side effects on treating patients (nephrotoxicity, ototoxicity, neurotoxicity, severe nausea and vomiting, hemolitic anemia and electrolytic disturbance) [13]. Another central topic concerning the administration of established Platinum compounds, is the development of drug resistance by cancer cells due to a low drug uptake [14]. The efforts of scientists for solving these problems have conducted to the development of new structures (some of them, such as Nedaplatin, Heptaplatin, Lobaplatin approved in specific areas [15-17]), but none of the new Platinum(II) compounds has reached the goal of solving the above mentioned problems. Ironically, after four decades since his approval, Cisplatin in still the most important anticancer agent.

Due to these considerations, the scientists have moved their attention on octahedral Platinum(IV) compounds. Indeed, due their high kinetic inertia, Platinum(IV) complexes are usually less reactive towards non wanted targets such serum proteins due to a higher stability. This property should contribute, at least in principle, to reduce the severe side effects associated to Platinum(II) compounds. More precisely, Platinum(IV) compounds act as prodrugs. Indeed, they are usually inert until their activation, that usually occurs through a redox process possible only in the reducing environment of cellular cytosol, followed from the release of two axial ligands (Fig.4) [18].

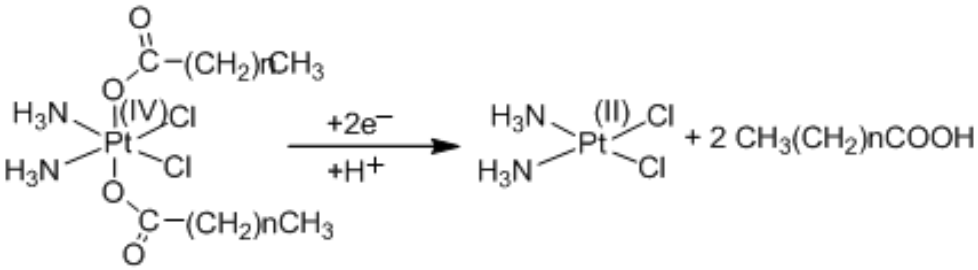

Fig:4: Reduction mechanism of Platinum(IV) prodrugs.

For expanding the possibilities of discovering new valuable structures, the interest of chemists had moved from Platinum to other transition metals. Indeed, in four decades of research concerning d block, many examples of complexes with interesting anticancer and antimicrobial activity have been reported in literature (based, for

example, on Iron, Copper, Silver, Iridium, Rhodium, Palladium and more others) [19-22]. In Fig.5 are reported some examples of Silver N-heterocyclic carbenes showing interesting anticancer properties: the activity of these compounds turned out to be in the nanomolar range (30-75 nM) against HCT116, MCF-7 and HL-60 cell lines [23].

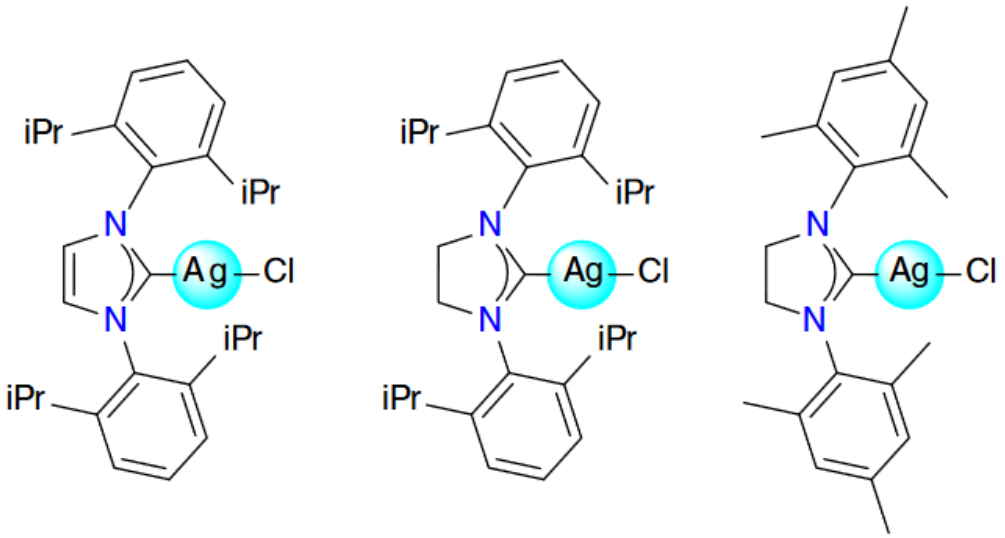

Fig.5: Examples of Silver N heterocyclic carbenes active in the nanomolar range against different cancer models (HCT116, MCF-7 and HL-60) [23].

Anyway, the most promising alternatives are actually limited to a few other transition elements such Ruthenium and Gold. More precisely, many Ruthenium derivatives have demonstrated interesting anticancer properties [24]. In particular, some imidazole and indazole derivatives such NAMI-A and KP1019 (Fig.6) reached the clinical trials and showed the capability of inhibiting the cellular growth associated with a lower cytotoxicity and lower side effects in comparison with Cisplatin and its derivatives [25].

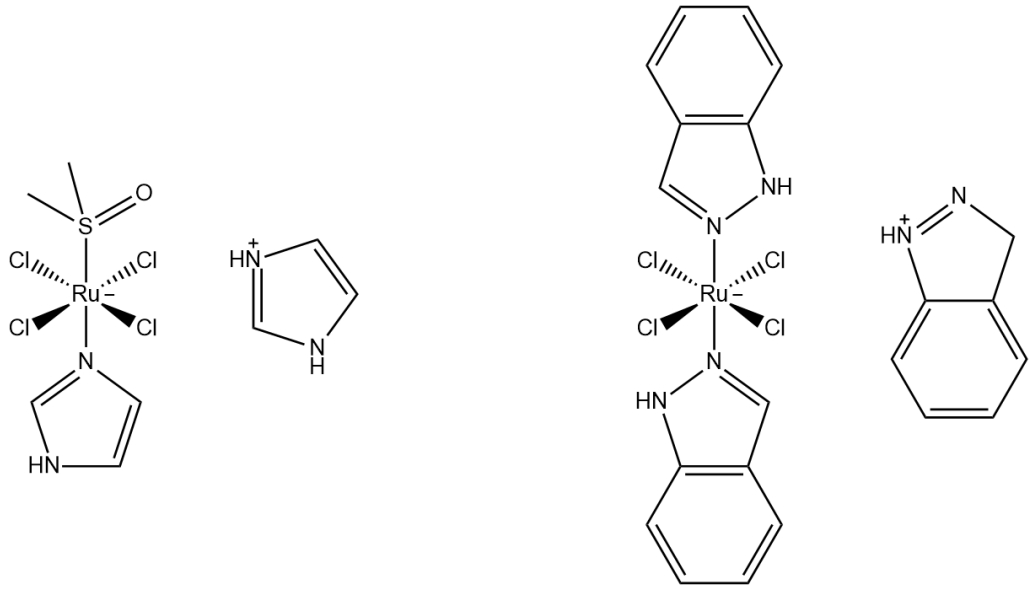

Fig.6: NAMI-A and KP1019 structures.

Other compounds of interest are, undoubtedly, the molecules bearing a Gold(III) center. As in the case of Platinum(II) complexes, Gold(III) molecules show square-planar coordination geometry. For this reason, based on their structural and electronic affinity to Cisplatin and cisplatin-related antitumor drugs, Gold(III) species represent a promising class of potential anticancer agents. However, the development of Gold(III) complexes as therapeutic drugs has been hampered by their low stability under physiological conditions and remains a critical parameter in the drug development of these species. More precisely, in comparison with Platinum(II) compounds, Gold(III) analogues turned out to be light sensitive and to undergo easy reduction to metallic gold under physiological conditions [26]. Anyway, kinetically stable Gold(III) complexes with various ligands have been prepared and biologically investigated. Most of them are complexes with Au–N bonds (eventually containing additional Au–O and Au–Cl bonds) but also some species with Au–S or Au–C bonds and their bioactivities have been described (Fig.7) [27].

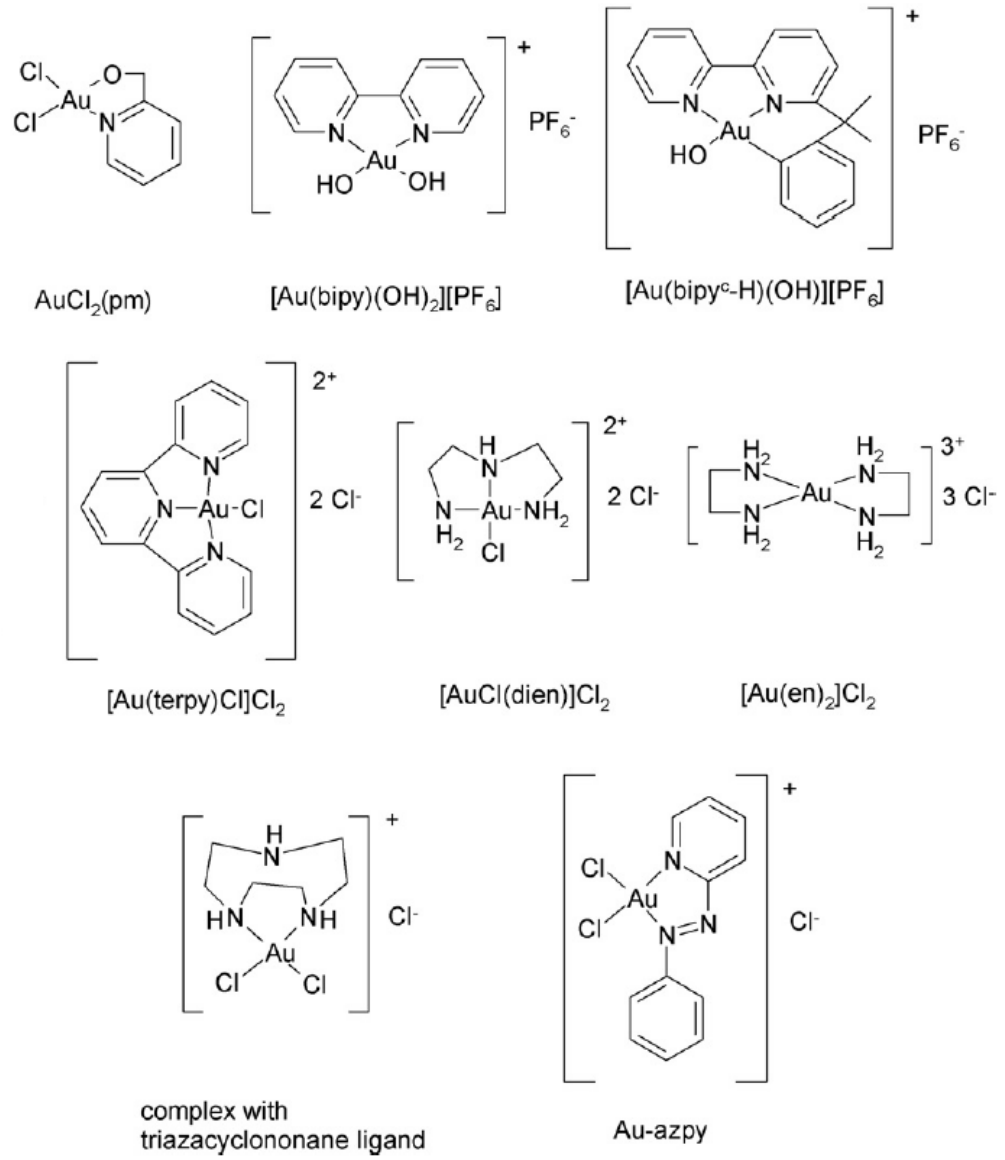

Fig.7: Examples of Gold(III) complexes [27].

On the other hand, the linear Gold(I) complexes show a greater stability associated with many interesting pharmacological properties: many of them act as immunosuppressive, anti-inflammatory, antiretroviral and anticancer compounds. At present days Sodium Aurothiomalate and Auranofin (Fig.8), two examples of this class of molecules, are established drugs in clinical use for the treatment of severe forms of autoimmune rheumatoid arthritis [28].

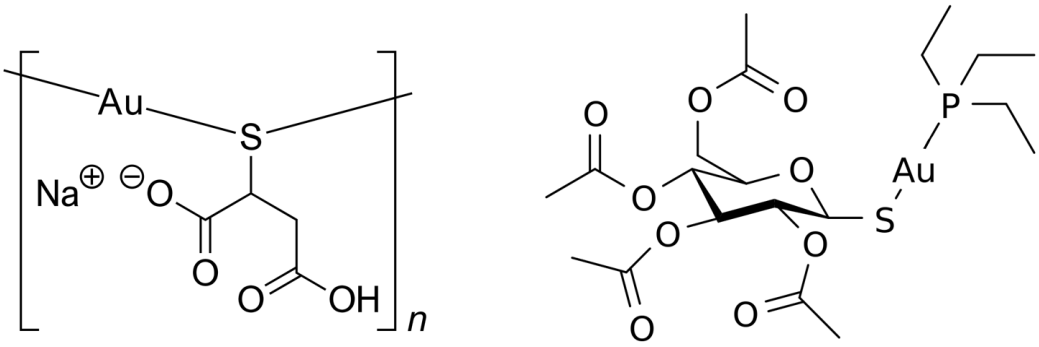

Fig.8: Structures of Sodium Aurothiomalate and Auranofin, respectively.

Moreover, in the frame of a repurposing approach of already established drugs, the latter of these two compounds has recently gained a growing attention of bioinorganic community due to its antibacterial, antiparastitic and anticancer activity [29].

The purpose of the thesis

For all these reasons, the research concerning metal-based compounds as possible antimicrobial or anticancer candidates, is a field of interest still keeping valuable alternatives to organic chemistry. The aim of this work is to present the most relevant results obtained in the years of my PhD, more precisely, all the data presented in this thesis are extracted from the following papers (from chapter 2 to chapter 7, respectively):

- D. Cirri, S. Pillozzi, C. Gabbiani, J. Tricomi, G. Bartoli, M. Stefanini, E. Michelucci, A. Arcangeli, L. Messori, T. Marzo, *Dalton Trans.*, **2017**, 46, 3311–3317.
- T. Marzo, A. Pratesi, D. Cirri, S. Pillozzi, G. Petroni, A. Guerri, A. Arcangeli, L. Messori, C. Gabbiani, Inorganica Chimica Acta, 2018, 470, 318–324.
- T. Marzo, D. Cirri, S. Pollini, M. Prato, S. Fallani, M. I. Cassetta, A. Novelli, G. M. Rossolini, L. Messori, *ChemMedChem*, **2018**, 13, 2448–2454.
- T. Marzo, D. Cirri, C. Gabbiani, T. Gamberi, F. Magherini, A. Pratesi, A. Guerri, T. Biver, F. Binacchi, M. Stefanini, A. Arcangeli, L. Messori, *ACS Med. Chem. Lett.*, **2017**, 8, 997−1001.
- T. Marzo, L. Massai, A. Pratesi, M. Stefanini, D. Cirri, F. Magherini, M. Becatti, I. Landini, S. Nobili, E. Mini, O. Crociani, A. Arcangeli, S. Pillozzi, T. Gamberi, L. Messori, *ACS Med. Chem. Lett.*, **2019**, 10, 656−660.

- M. G. Fabbrini, D. Cirri, A. Pratesi, L. Ciofi, T. Marzo, A. Guerri, S. Nistri, A. Dell'Accio, T. Gamberi, M. Severi, A. Bencini, L. Messori, *ChemMedChem*, **2019**, 14, 182–188.

The above mentioned chapters were written as an independent sections, containing each of them its own introduction to the specific problem and its conclusions. Anyway, all the chapters of the document are linked from drug discovery as a common thread. More precisely, chapters from 2 to 6 are dedicated to a "small modification approach" merged with repurposing strategies. Indeed, all the presented molecules were obtained from minor modifications of two parent compounds, i.e Oxaliplatin (Fig.2) and Auranofin (Fig.8). The choice of modifying two clinically established compounds comes from the advantages of dealing with molecules owning an already know pharmacological profile, and from the possibility of elucidating some structure-activity relationships. On the other hand, chapter 7 is dedicated to the study of a fluorescent complex belonging to the class of Silver N-heterocyclic carbenes, being these compounds very interesting due their high activity against many tumoral cell lines. Moreover, the presence of a fluorescent probe bounded on the structure, allowed to perform some confocal studies for determining the biodistribution of the complex inside the cells.

References

[1]: T. Marzo, D. Cirri, S. Pollini, M. Prato, S Fallani, M. I. Cassetta, A. Novelli, G. M. Rossolini, L. Messori, ChemMedChem, 2018, 13, 2448-2454.

[2]: Pimple, K.D. Pedroni, J.A. Berdon, V. (2002, July 09). Syphilis in history Archived 2008-04-30 at the Wayback Machine. Poynter Center for the Study of Ethics and American Institutions at Indiana University-Bloomington. Retrieved on April 20, 2008.

[3]: Vaupel, E. (2005), Arthur Eichengrün—Tribute to a Forgotten Chemist, Entrepreneur, and German Jew Angew. Chem. Int. Ed., 44, 3344–3355.

[4]: Fischer, Janos; Ganellin, C. Robin (2006). Analogue-based Drug Discovery. John Wiley & Sons. p. 490. ISBN 9783527607495. Archived from the original on 20 December 2016.

[5]: B. Rosenberg, L. Van Camp, J. E. Trosko, V. H. Mansour, Nature, 1969, 222, 385–386.

[6]: M. Peyrone, Ann. Chem. Pharm., 1844, 51, 1-29.

[7]: S. Trzaska, Chemical & Engineering News, 2005, 83 (25).

[8]: Carpenter, D. P. (2010). Reputation and power: organizational image and pharmaceutical regulation at the FDA. Princeton, NJ: Princeton University Press. ISBN 978-0-691-14180-0.

[9]: "Approval Summary for cisplatin for Metastatic ovarian tumors". FDA Oncology Tools. Food and Drug Administration, Center for Drug Evaluation and Research. 19 December 1978. Archived from the original on 8 February 2008. Retrieved 15 July 2009.

[10]: "Carboplatin". The American Society of Health-System Pharmacists. Archived from the original on 21 December 2016. Retrieved 8 December 2016.

[11]: A. Ibrahim, S. Hirshfeld, M. H. Cohen, D. J. Griebel, G. A. Williams, R. Pazdur, The Oncologist, 2004, 9, 8-12.

[12]: International Agency for Research on Cancer, http://www-dep.iarc.fr/WHOdb/WHOdb.htm

[13]: R. Oun, Y. E. Moussa, N. J. Wheate, Dalton Trans., 2018, 47, 6645-6653.

[14]: D. Shen, L. M. Pouliot, M. D. Hall, M. M. Gottesman, Pharmacol. Rev., 2012, 64, 706–721.

[15]: M. Shimada, H. Itamochi, J. Kigawa, Cancer Manag. Res., 2013, 5, 67–76.

[16]: C.-H. Choi, Y.-J. Cha, C.-S. An, K.-J. Kim, K.-C. Kim, S.-P. Moon, Z. H. Lee, Y.-D. Min, Cancer Cell Int., 2004, 4, 6.

[17]: M. J. McKeage, Expert Opin. Investig Drugs., 2001, 10, 119-128.

[18]: M. D. Hall, H. R. Mellor, R. Callaghan, T. W. Hambley, J. Med. Chem., 2007, 50, 3403-3411.

[19]: W. A. Wani, U. Baig, S. Shreaz, R. A. Shiekh, P. F. Iqbal, E. Jameel, A. Ahmad, S. H. Mohd-Setapar, L. T. Hun, New J. Chem., 2016, 40, 1063-1090.

[20]: S. J. Tan, Y. K. Yan, P. Peng Foo Lee, K. H. Lim, Future Med. Chem., 2010, 2, 1591–1608.

[21]: J. M. Hearn, I. Romero-Canelón, B. Qamar, Z. Liu, I. Hands-Portman, P. J. Sadler, ACS Chem. Biol. 2013, 8, 1335−1343.

[22]: Buckley R.G. (1994) Rhodium, iridium and palladium compounds as experimental anticancer drugs. In: Fricker S.P. (eds) Metal Compounds in Cancer Therapy. Springer, Dordrecht.

[23]: S. Kankala, N. Thota, F. Björkling, M. K. Taylor, R. Vadde, R. Balusu, Drug Dev. Res., 2019, 80, 188-199.

[24]: A. Levina, A. Mitra, P. A. Lay, Metallomics, 2009, 1, 458-470.

[25]: E. Alessio, L. Messori, Molecules, 2019, 24, 1995-2014.

[26]: C. Gabbiani, A. Casini, L. Messori, Gold Bulletin, 2007, 40, 73-81.

[27]: I. Ott, Coordination Chemistry Reviews, 2009, 253, 1670-1681.

[28]: W. F. Kean, I. R. L. Kean, Clinical pharmacology of gold, 2008, 16, 112–125.

[29]: C. Roder, M. J. Thomson, Drugs R D, 2015,15, 13-20.

2. Platinum(II) compounds as promising chemotherapeutic agents: the case of PtI_2(DACH)

Introduction

Today, colorectal cancer (CRC) is the fourth most common cause of death due to cancer worldwide. Prognosis is highly correlated with TNM staging (widely used cancer staging system. T refers to the size and extent of the primary tumor; N refers to the number of nearby lymph nodes that have cancer; M refers to whether the cancer has metastasized. Numbers after each letter are used to give more details on the stage of a tumor), with a 5-year survival of 90% for patients in earlier stages but less than 25% for those with metastatic disease [1]. The cornerstone of therapy is represented by "en bloc" surgical resection of tumour and regional nodes, although perioperative chemotherapy may provide important advantages in subjects with advanced disease and metastases [2]. Adjuvant chemotherapy for CRC mainly relies on fluoropyrimidine compounds combined with platinum-based drugs, mainly cisplatin and its analogue oxaliplatin. Oxaliplatin (Eloxatin™) is a third-generation platinum compound approved by United States Food and Drug Administration (FDA) in 2002 for the treatment of advanced colorectal cancer. To date thousands of patients worldwide have been treated with oxaliplatin, especially in combination with other drugs [3]. Indeed, either the FOLFOX (5-FU, leucovorin, and oxaliplatin) or CapeOx (capecitabine and oxaliplatin) regimens are used most often [4, 5]. Despite its success, important side effects such as acute and chronic neurotoxicity are, still today, limiting factors to its clinical use [6]. With the aim to overcome the main drawbacks of oxaliplatin treatment i.e. side effects as well as frequent intrinsic or acquired pharmacological resistance, in the last few decades, many analogues of this clinically established drug have been synthesised and tested [7–11]. In this framework, we have prepared the oxaliplatin analogue {(1R,2R)-cyclohexane-1,2-diamine}diiodidoplatinum(II), (PtI_2(DACH) hereafter) (Fig.1) where the bidentate oxalate ligand of oxaliplatin is replaced by two iodide ligands.

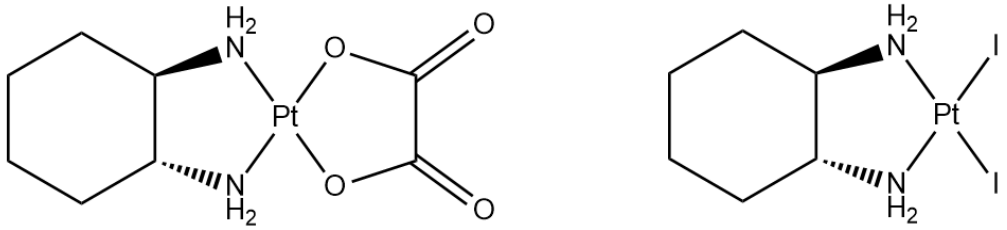

Fig. 1: Schematic drawing of oxaliplatin and its iodide analogue.

Notably, this oxaliplatin derivative was reported and structurally characterised in 2011 by R. Pažout and coworkers [12], but no biological studies were then attempted. Reasons that make PtI_2(DACH) of particular interest for inorganic medicinal chemists are essentially twofold.

(i) We believe that the replacement of the bidentate oxalate ligand with two iodides may affect mainly the activation process of the Pt centre, both kinetically and thermodynamically, influencing accordingly its overall biological profile.

(ii) In addition, insertion of two iodide ligands in the place of oxalate is expected to increase considerably the lipophilic character of the resulting drug hopefully enhancing cellular uptake and bioavailability.

It is worth reminding that this kind of strategy was recently exploited, in our research group, and applied to cisplatin. Indeed, the iodide analogue of cisplatin was prepared, characterised and shown to possess interesting chemical and biological properties that are definitely distinct from those of cisplatin [13]. The obtainment of the desired Pt compound, i.e. PtI_2(DACH), was confirmed and supported by NMR and CHN analysis. Afterward, the complex was studied in depth in terms of its solution behaviour and its interactions with model proteins (i.e. lysozyme, RNase) and with a short single strand oligonucleotide bearing the GG motif. Also, cytotoxic and proapoptotic effects were investigated in a few representative CRC cell lines and mechanistic hypotheses for the different pharmacological effects were proposed. Finally, uptake experiments were carried out to assess whether the replacement of the oxalate ligand with two iodide ligands affords indeed an enhanced uptake hopefully improving the drug's bioavailability.

Experimental

Chemicals and reagents

Chemicals were purchased from Sigma-Aldrich and used without further purification. Dodecameric oligonucleotide ODN2, with sequence CTACGGTTTCAC and proteins were also purchased from Sigma-Aldrich.

Chemistry

Synthesis and characterisation of PtI_2(DACH): For the synthesis of PtI_2(DACH), 99.3 mg of K_2PtCl_4 (2.4×10^{-4} mol), have been solubilised in 1.5 mL of MilliQ water. A water solution (2 mL) of KI (158.7 mg, 9.6×10^{-4} mol) was added to K_2PtCl_4 and stirred (50 °C) in the dark for five minutes until quantitative conversion of K_2PtCl_4 to K_2PtI_4 was obtained. 1,2-Diaminocyclohexane (1R,2R)-(−): DACH (27.3 mg, 2.4×10^{-4} mol) was then solubilised in 2 mL of MilliQ water and the obtained solution was slowly added to the K_2PtI_4 water solution. After a further four hours of stirring, a precipitate appeared, and complete precipitation of yellow crystals of PtI_2(DACH) occurred overnight at room temperature. The solid was then collected through vacuum filtration and washed with hot water, ice-cooled ethanol and ether. 135.5 mg of PtI_2(DACH) were obtained (yield 81%). The complex was characterised by NMR and elemental analysis.

^{1}HNMR ($DMFd_7$, 400.13 MHz, 298 K): 5.56 (b, 1H); 4.96 (b, 1H); 2.50 (t, *J* = 8 Hz, 2H); 2.23 (d, *J* = 12 Hz, 2H); 1.56 (m, 4H); 1.15 (m, 2H).

Elemental analysis of C, N and H [calculated C: 12.8%, H: 2.32%, N: 4.98%, experimental: C: 12.5%, H: 2.32%, N: 4.86%];

Log P value determination

The octanol–water partition coefficient for PtI_2(DACH) was determined by modification of the reported shake-flask method. Water (50 mL, distilled after MilliQ purification) and n-octanol (50 mL) were shaken together for 72 h to allow saturation of both phases. A solution of the complex was prepared in the water phase (3×10^{-3} M) and an equal volume of octanol was added. Biphasic solutions were mixed for ten minutes and then centrifuged for five minutes at 6000 rpm to allow separation. Concentration in both phases was determined by UV-Vis. Reported log P is defined as $\log[complex]_{oct}/[complex]_{wat}$. Final values were reported as mean of three determinations.

UV-Vis experiments

Solution behaviour of PtI_2(DACH) was assessed through spectrophotometric experiments performed with a Varian Cary 50 Bio UV-Vis spectrophotometer (1 cm pathlength quartz cell) in buffered solutions without the use of DMSO and NaCl. A solution of the complex (10^{-4} M) was prepared in 50 mM phosphate buffer at pH = 7.4. The absorbance was monitored in the wavelength range between 200 and 800 nm for 72 h at 25 °C.

ESI-MS experiments

The ESI-MS spectrum of the ODN2–PtI_2(DACH) mixture was recorded by direct injection at 5 µl/min flow rate in an Orbitrap high-resolution mass spectrometer (Thermo, San Jose, CA, USA), equipped with a conventional ESI source. The working conditions were as follows: negative polarity, spray voltage −2.7 kV, capillary voltage −20 V, capillary temperature 280 °C, tube lens voltage −113 V. The sheath and the auxiliary gases were set at 23 and 4 (arbitrary units), respectively. For acquisition, Xcalibur 2.0 software (Thermo) was used and deconvoluted masses were obtained by using the ProMass 2.8 rev. 2 tool for Xcalibur (Novatia).

ESI-MS spectra of the PtI_2(DACH)–protein mixtures were recorded by direct injection at 3 µL/min flow rate in the same instrument. The working conditions were as follows: positive polarity, spray voltage 3.1 kV, capillary voltage 45 V, capillary temperature 220 °C, tube lens voltage 230 V. The sheath and the auxiliary gases were set at 17 and 1 (arbitrary units), respectively. For acquisition, Xcalibur 2.0 software (Thermo) was used and deconvoluted masses were obtained by using the integrated Xtract tool. For spectra acquisition a nominal resolution (at m/z 400) of 100 000 was used.

Chemicals and drugs

For cellular experiments, cisplatin, *cis*-$PtI_2(NH_3)_2$, oxaliplatin and PtI_2(DACH) were dissolved in MilliQ water at the concentration of 8.3, 1, 5 and 1 mM, respectively. All stock solutions were stored at −20 °C.

Cell culture

Human colorectal cancer cell lines (HCT-116, HCT-8 and HT29) and mouse fibroblast cell line L929 were cultured in RPMI-1640 medium (Euroclone; Milan, Italy), supplemented with 2% L-Glut, 10% fetal bovine serum (FBS) and 1%

penicillin/streptomycin (complete medium). HT29 cells were kindly provided by Dr R. Falcioni (Regina Elena Cancer Institute, Rome).

Cell viability assay

To evaluate the IC50 of each compound, cell viability was assessed through the Trypan Blue exclusion test (Sigma-Aldrich). Cells were seeded at $1x10^4$ per well in 96-well plates (Costar Corning) in complete medium and incubated for 24 h before the compound was added. Following the addition, cells were further incubated for 24 hours. Cells were then harvested and counted by the Trypan Blue exclusion test using a hemocytometer. All experiments were performed in triplicate. The IC50 values were calculated for each cell line and data fitted using a Hill1-type equation by using Origin Software (Microcal Origin 8.0 software; OriginLab Corporation, Northampton, MA).

Proliferation experiments

HCT116 cells were seeded at $1x10^4$ per well in 96-well plates (Costar Corning) in complete medium and incubated for 24 h before the compound was added. After 24, 48 and 72 h of incubation viable cells (determined by the Trypan Blue exclusion test) were counted in triplicate using a haemocytometer. Each experimental point represents the mean ± sem of three separate experiments.

Cell cycle analysis

Cell cycle distribution was assessed by flow cytometry after staining the cells with propidium iodide (PI). Cells were seeded and treated generally with different compounds at their IC50 (unless otherwise noted in the figure legend) for 24 h. At the end of incubation, cells were harvested, washed with PBS and resuspended in 300 µl propidium iodide staining solution and incubated in the dark for 20 minutes at room temperature. The DNA content of the cells was measured by using a BD FACSCanto (Becton Dickinson, Franklin Lakes, NJ, USA) and the percentage of cells in each cell cycle phase was determined using ModFit LT 3.0 analysis software (Verity Software House, Topsham, ME, USA).

Annexin/PI assay

Apoptosis was determined through the Annexin V/propidium iodide test (Annexin-VFLUOS staining kit; Roche Diagnostics, Mannheim, Germany). Cells, treated as above, were harvested after 24 h of treatment with different compounds (at their IC50 value, unless otherwise noted in the figure legend), washed with PBS, re-suspended in 100 µL of buffer and incubated with FITC-conjugated Annexin V and propidium iodide for 15

min. Flow cytometry was performed using the BD FACSCanto (Becton Dickinson, Franklin Lakes, NJ, USA). Data were analysed through the BD FACSDiva Software 6.1.3.

Statistical analysis

Data are generally given as mean values ± standard error of the mean (sem), unless otherwise specified in the figure legend. The normality of data distribution was checked with the Kolmogorov–Smirnov test. For multiple comparisons, we used one-way ANOVA, with the post-hoc Bonferroni test to derive P values.

Uptake measurement

The determination of platinum concentration in the cellular pellets was performed by using a Varian 720-ES Inductively Coupled Plasma Atomic Emission Spectrometer (ICP-AES) equipped with a CETAC U5000 AT+ ultrasonic nebulizer, in order to increase the method sensitivity as fully described in [13].

Results and discussion

Synthesis and characterization of PtI_2(DACH)

The synthesis of PtI_2(DACH) was performed as described in the Experimental section, with a good yield. Synthesis started from K_2PtCl_4 that was quantitatively converted into K_2PtI_4. In contrast to previously reported synthetic routes [12], 1,2-diaminocyclohexane(1R,2R)-(−) was used in the place of DACH tartrate and slowly added to K_2PtI_4, at room temperature. The purity of the resulting product was checked by ^{1}HNMR and elemental analysis and found to be >95%. A detailed description of all the procedures and of the chemical characterization is given in the experimental section. Remarkably, in the ^{1}HNMR spectrum, the two signals at 4.96 and 5.56 ppm, are assignable to the ammine protons. This attribution was validated by a direct comparison with the spectrum of $PtCl_2$(DACH) previously synthesized and recorded under the same conditions. It is interesting to note that in contrast to $PtCl_2$(DACH) for which the two signals attributable to the amine protons can be suppressed by adding D_2O to the DMF-d7 sample solution, for PtI_2(DACH) the exchange of a proton with deuterium (and thus amine signals suppression), doesn't occur even after 24 h after the addition of deuterated water, indicating that the replacement of chloride with iodide ligands strongly decreases the mobility of amine protons.

Log P determination

The octanol/water partition coefficient is an important parameter in drug design with a large impact on the overall ADME profile of the drug itself. Generally speaking, a more lipophilic character commonly facilitates cellular drug uptake and bioavailability. However, the situation is somewhat more complex when dealing with a prodrug requiring chemical activation prior to performing its pharmacological actions as is the case for anticancer Pt compounds. A log P value of 0.76 was determined for PtI_2(DACH) by modification of the classical flask method previously used (see the Experimental section for further details) [13, 14]. For comparison purposes log P values for a few parent Pt complexes are also reported in Table 1.

Complex	Log *P* value
Cisplatin	−2.40[a]
cis-$PtI_2(NH_3)_2$	−0.13
Oxaliplatin	−1.58[b]
PtI_2(DACH)	0.76

[a] Value previously determined in our laboratories, ref. 13. [b] The log *P* here determined for oxaliplatin is close to that reported in the literature (−1.76, ref. 15).

Table 1: Log P values for Pt-based drugs Complex Log P value.

As expected, the bis-iodide analogue i.e. PtI_2(DACH), manifests a far larger lipophilic character than oxaliplatin, being the most lipophilic compound in the series.

Solution chemistry

PtI_2(DACH) may be easily solubilised under physiological-like conditions (i.e. in phosphate buffer) upon short sonication, thus avoiding the use of DMSO and the associated chemical interferences. The solution behaviour of PtI_2(DACH) was then assessed through UV-Vis analysis. Similarly to *cis*-$PtI_2(NH_3)$, PtI_2(DACH) shows two main absorption bands located at 280 and 350 nm (Fig. 2) [13].

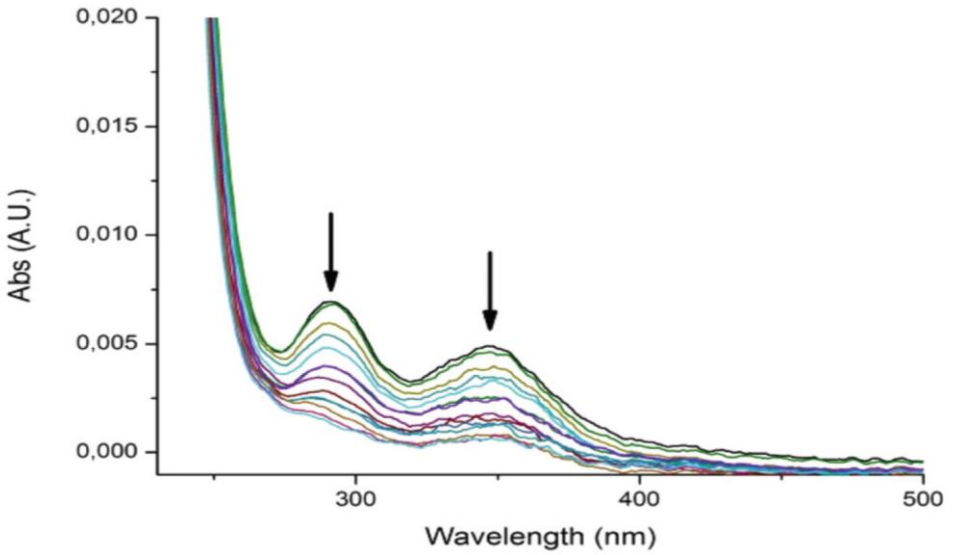

Fig. 2: Time course spectra of PtI_2(DACH), 10^{-4} M in 50 mM phosphate buffer recorded over 72 h, RT.

With time, the intensity of both bands slowly decreases; the residual band intensity after 72 hours is only ~20% of the original intensity according to a roughly monoexponential decay. The observed spectral changes are ascribed to the progressive release of the two iodido ligands [13, 14] with the hydrolysis of PtI_2(DACH) significantly slower than *cis*-$PtI_2(NH_3)_2$ but faster than oxaliplatin (see Table 2).

Complexes	k_{obs} (s^{-1}) $[1/t]$	$t_{1/2}$ (min) $[t \times \ln(2)]$
PtI_2(DACH)	9.75×10^{-6}	1184.58
cis-$PtI_2(NH_3)_2$ [a]	2.08×10^{-5}	555.58
Oxaliplatin [b]	6.32×10^{-6}	1827.92

[a] Value previously determined in our laboratories, ref. 13. [b] The k_{obs} here determined for oxaliplatin is close to that reported in the literature (7.76×10^{-6} s^{-1}, ref. 16).

Table 2: k_{obs} was calculated fitting the variation of absorbance as function of time with a single exponential function (UV-Vis time course spectra of complexes, 10^{-4} M in 50 mM phosphate buffer recorded over 72 h, RT).

Biomolecular interactions of PtI_2(DACH)

Next, to study its interactions with model biological targets, *cis*-PtI_2(DACH) was incubated with two model proteins i.e. hen egg white lysozyme and RNase (see the Experimental section for details) and the possible adduct formation was investigated. These two proteins were chosen since their structures have been often used to characterize the interactions occurring between proteins and metallodrugs; in addition, crystal structures of their adducts with both cisplatin and oxaliplatin are available [17–20]. Notably, these model proteins are well suitable also for ESI-MS studies, offering a very important substrate for comparative mechanistic studies of metal-based drugs. In both cases no metallodrug–protein adduct was detected, indicating that PtI_2(DACH), in contrast to oxaliplatin, is not able to bind these proteins [18–20]. An explanation for this unexpected behaviour is not straightforward. We previously reported that coordination of oxaliplatin to lysozyme and RNase implies a multi-step reaction at the level of aspartate residues. First, non-covalent coordination of oxaliplatin to the protein occurs; then detachment of one oxygen atom of oxalate from Pt coordination (a ring-opening step leading to monodentate oxalate) is observed with concomitant Pt coordination of the carboxylate group from an aspartate residue. Finally the oxalate ligand is fully released [19, 20]. We might hypothesize that, this multi-step mechanism is inhibited when the oxalate ligand is replaced by two iodides due to the lack of "recognition" of intact PtI_2(DACH) by these model proteins. Conversely, and in analogy with its parent drug oxaliplatin, PtI_2(DACH) interacts extensively with a standard oligonucleotide bearing the GG motif (ODN2) through a classical reaction pattern involving preferential release of iodide ligands (Fig. 3) [21].

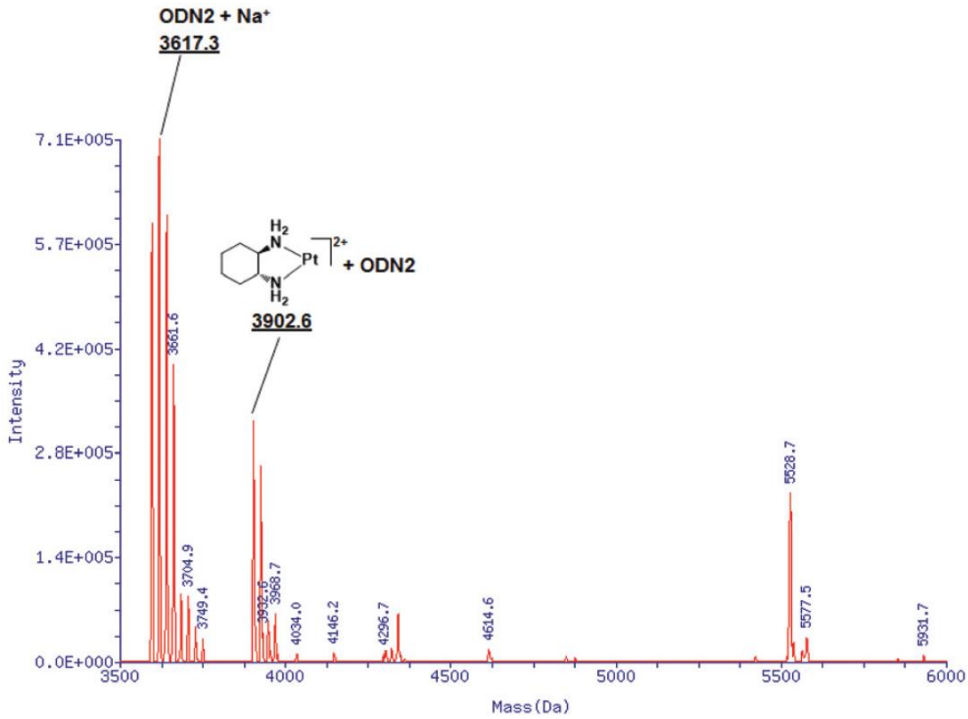

Fig. 3: Deconvoluted ESI-MS spectrum of PtI_2(DACH) 10^{-4}M incubated with ODN2 in LC-water 72 h, 37 °C, metal to oligonucleotide ratio 1 : 1.

These results are fully supported by theoretical calculations of ESI-MS peaks (Figure 4).

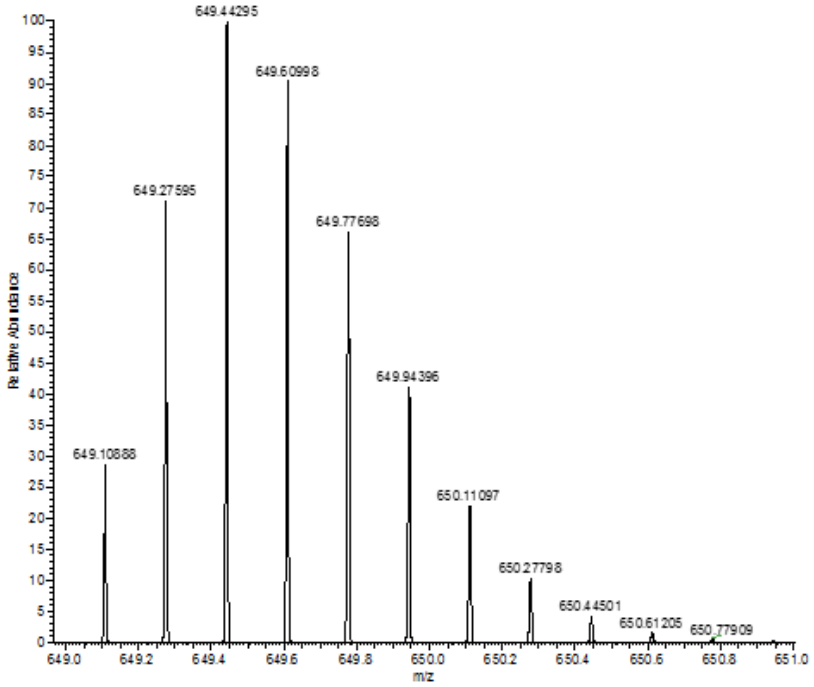

Fig.4: Simulated spectra of 6^- charge state of ODN2 + $[Pt(DACH)]^{2+}$.

Cellular effects

We then measured the cytotoxic effects of PtI_2(DACH) in a small panel of CRC cell lines (HT-29, HCT-116, HCT-8) in comparison with cisplatin, oxaliplatin and *cis*-$PtI_2(NH_3)_2$. A normal cell line (L929 fibroblast cells) was also included. The *cis*-$PtI_2(NH_3)_2$ compound was also evaluated since we previously showed that it is fairly active on a cisplatin resistant CRC cell line, and can hence be considered a potential drug candidate to overcome Pt resistance, at least partially [13]. Cells were exposed to increasing concentrations of the drugs, given in the 0–300 µM range, for 24 hours, and the respective IC_{50} concentrations were determined (Table 3).

Cell line	Cisplatin	*cis*-$PtI_2(NH_3)_2$	Oxaliplatin	PtI_2(DACH)
HT-29	15.2 ± 1.3	5.8 ± 0.3	19.7 ± 1.2	25.7 ± 1.6
HCT-116	22.9 ± 1.0	9.1 ± 0.2	49.2 ± 0.9	34.5 ± 1.2
HCT-8	9.3 ± 0.6	23.6 ± 1.0	33.1 ± 0.2	51.1 ± 2.0
L929	70.2 ± 1.5	72.1 ± 2.3	72.1 ± 1.1	82.4 ± 2.4

Table 3: IC50 (μM) of cisplatin, *cis*-$PtI_2(NH_3)_2$, oxaliplatin and PtI_2(DACH) in HT29, HCT116 and HCT8 CRC cell lines, as well as in a normal fibroblastic cell line (L929). Cell vitality was measured after 24 hours of treatment with the four different compounds, by the Trypan Blue exclusion test. IC50 values (means ± sem of four independent experiments) were calculated using the Origin Software (Microcal Origin 8.0 software; OriginLab Corporation, Northampton, MA) fitting experimental data with Hill1 type equation.

In line with our previous results [13], *cis*-$PtI_2(NH_3)_2$ turned out to be more active than cisplatin, and even more compared to oxaliplatin, especially in the case of partially cisplatin-resistant cell lines HT29 and HCT116. Though less cytotoxic than cisplatin and slightly less cytotoxic than oxaliplatin, PtI_2(DACH) was more effective than oxaliplatin in HCT116 cells that are poorly sensitive to either compounds. These data point out that PtI_2(DACH) maintains appreciable cytotoxic properties, not different from, and in some cases even better than oxaliplatin. This implies that the replacement of oxalate with two iodide does not impair the cellular effects of this drug that may be attributed mainly to the $[Pt(DACH)]^{2+}$ chemical moiety. Additionally, when evaluating the effects of all compounds on the fibroblast cell line L929, we can state that the cytotoxicity is on the whole similar and rather low, with the iodide analogue of oxaliplatin being slightly less cytotoxic. Based on these results we studied in detail the effects that Pt compounds produce on HCT-116 cells, determining both the distribution of the cells in the various phases of the cell cycle and the percentage of cells in the early apoptotic phase. These effects were measured in the absence or in the presence of the four compounds tested at their respective IC50 values. None of the tested Pt compounds caused relevant variation of cell cycle distribution of HCT 116 cells (Table 4 and Fig. 5).

	G0/G1 (%)	*S* (%)	G2/M (%)
Control	36.3 ± 0.6	41.5 ± 2.6	22.2 ± 2.8
Cisplatin	41.3 ± 1.3	36.3 ± 3.5	22.4 ± 1.3
cis-$PtI_2(NH_3)_2$	45.5 ± 2.8	35.5 ± 5.3	19.1 ± 2.5
Oxaliplatin	37.9 ± 3.6	37.0 ± 4.4	25.1 ± 1.9
PtI_2(DACH)	40.6 ± 2.3	36.4 ± 3.4	24.1 ± 3.7

Table 4: Cell cycle distribution of HCT 116 cells after 24 hours of treatment with the four different compounds at the IC50 values shown in Table 3. Data are means ± sem of three independent experiments, and are expressed as percentage of cells in each phase of the cell cycle, determined by flow cytometry after staining the cells with propidium iodide (PI).

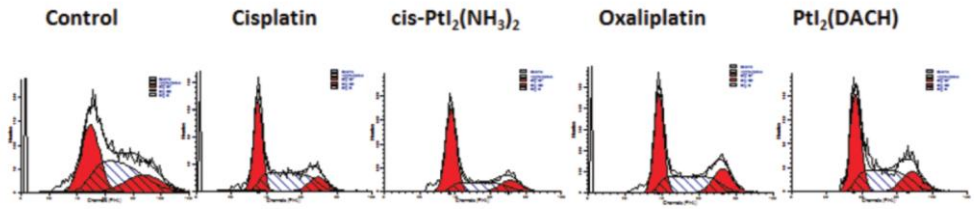

Fig.5: Representative histograms of data reported in Table 4.

On the contrary, both cisplatin and oxaliplatin increased the percentage of early apoptotic cells, as expected (Fig. 6A). Furthermore, the two iodide analogues showed an even more evident pro-apoptotic effect, higher than cisplatin and oxaliplatin. Interestingly, the analysis of dot plots (Fig. 6B) showed a shifting of the Annexin V/PI labelled population to higher fluorescence in HCT116 cells treated with PtI_2(DACH) compared to oxaliplatin. This suggests that the iodide compound exerts a stronger, possibly earlier, pro-apoptotic effect in HCT116 cells, which poorly respond to both cisplatin and oxaliplatin.

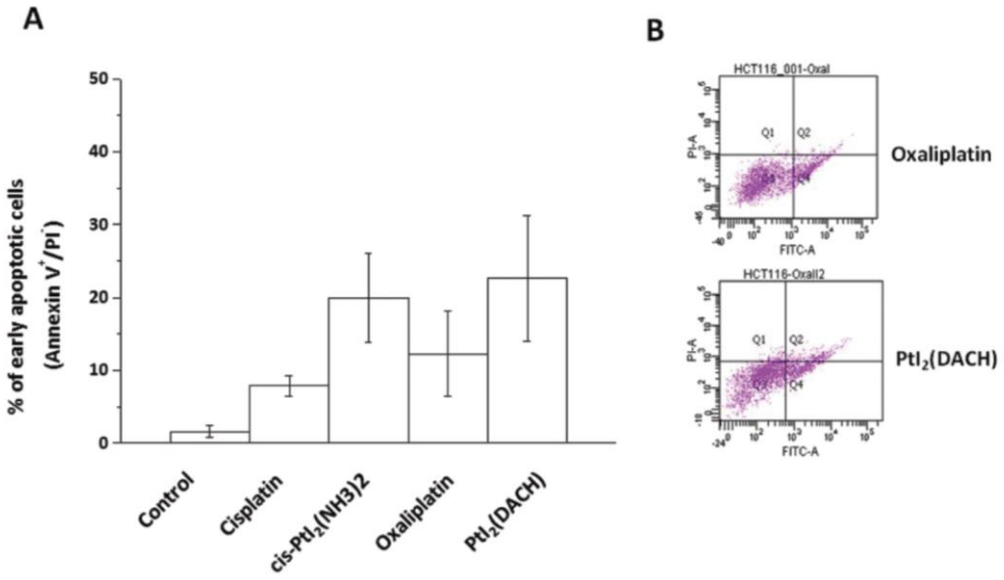

Fig.6: Percentage of early apoptotic HCT 116 cells (determined as Annexin V+/PI-cells) after 24 hours treatment with the four different compounds at the respective IC50 values. Histograms (panel A) are means ± sem of three independent experiments. B: Representative dot plots of the Annexin V/PI assay relative to treatments with oxaliplatin and PtI_2(DACH).

Pt uptake studies

Afterward, to confirm whether the enhanced lipophilic character of PtI_2(DACH) was related to an increase in drug internalisation, comparative uptake experiments were carried out on the HCT116 cell line. The results reveal that upon replacement of oxalate with iodide, a dramatic enhancement of cellular uptake (~7 fold increase) takes place (Table 5) most likely related to the strong increment in the lipophilic character.

Drug	Platinum level (μg)
Oxaliplatin	1.96×10^{-8}
PtI_2(DACH)	1.44×10^{-7}

Table 5: Platinum level (per cell) measured after exposure (24 hours) of cell lines to 25 μM of oxaliplatin and *cis*-PtI_2(DACH).

Conclusions

Despite the success of novel targeted anticancer therapies, cytotoxic platinum drugs still remain a cornerstone in the treatment of CRC being largely used in chemotherapeutic regimens combined with other cytotoxic molecules. Yet, clinically established Pt drugs, e.g. cisplatin and oxaliplatin, manifest important drawbacks often leading to treatment failure. Accordingly, new Pt based drugs are still urgently needed. These arguments led us to design and investigate some structural analogues of established anticancer Pt drugs that have been surprisingly overlooked; specifically, we have prepared a few analogues of established Pt drugs through incorporation of non-conventional halido ligands such as iodide and bromide. We report here on PtI_2(DACH), an analogue of oxaliplatin that is obtained through the replacement of the oxalate ligand with two iodide ligands. The kinetics of activation is significantly influenced by oxalate replacement; the biomolecular reactivity is also influenced. In contrast to oxaliplatin, PtI_2(DACH) is poorly reactive toward model proteins while retaining a significant affinity for a representative DNA molecule. The effects of PtI_2(DACH) on a small panel of CRC cells have been explored as well; PtI_2(DACH) similarly to *cis*-$PtI_2(NH_3)_2$ demonstrated an increased capability of inducing apoptosis in the HCT116 cell line, this cell line being the least sensitive to cisplatin. On the other hand, the cytotoxic properties of PtI_2(DACH) versus CRC cell lines were roughly comparable to those of oxaliplatin. This implies that the presence of the oxalate ligand is not crucial for the anticancer activity of oxaliplatin and that the latter may be replaced by other ligands such as iodide with nearly full retention of the cytotoxic properties. Furthermore, analysis of the proliferation (up to 72 h) of HCT116 cell line treated with oxaliplatin and PtI_2(DACH) reveal that, even for longer incubation time, differences in the cytotoxicity of these two drugs are comparable. This implies that there isn't any "kinetic" of the cytotoxic activity. Remarkably, PtI_2(DACH) manifests a larger lipophilicity than oxaliplatin and cisplatin. Increased lipophilicity leads to a strong enhancement of cellular uptake of this drug in HCT116 cells; however, this enhanced uptake does not result in a net enhancement of cytotoxicity possibly in relation to lower reactivity. The lower reactivity towards proteins might be associated with a better toxicological profile. Overall, we believe that this novel analogue of oxaliplatin manifests a number of peculiar chemical and biological features that render it particularly attractive and worthy of further preclinical testing in appropriate in vivo models of CRC.

References

[1] F. A. Haggar and R. P. Boushey, Clin. Colon Rectal Surg., 2009, 22, 191.

[2] C. C. Compton and F. L. Greene, CA-Cancer J. Clin., 2004, 54, 295.

[3] R. J. Mayer, J. Clin. Oncol., 2012, 30, 3325.

[4] H. S. Hochster, L. L. Hart, R. K. Ramanathan, B. H. Childs, J. D. Hainsworth, A. Cohn, L. Wong, L. Fehrenbacher, Y. Abubakr, M. Wasif Saif, L. Schwartzberg and E. Hedrick, J. Clin. Oncol., 2008, 26, 3523.

[5] P. J.O'Dwyer and S. W. Johnson, Semin. Oncol., 2003, 30, 78.

[6] G. D. Leonard, M. A. Wright, M. G. Quinn, S. Fioravanti, N. Harold, B. Schuler, R. R. Thomas and J. L. Grem, BMC Cancer, 2005, 5, 116.

[7] F. A. Thomet, P. Pinvol, J. Villena and P. G. Reveco, Inorg. Chim. Acta, 2012, 384, 255.

[8] V. Gandin, C. Marzano, G. Pelosi, M. Ravera, E. Gabano, D. Osella, ChemMedChem, 2014, 9, 1299.

[9] N. Margiotta, C. Marzano, V. Gandin, D. Osella, M. Ravera, E. Gabano, J. A. Platts, E. Petruzzella, J. D. Hoeschele and G. Natile, J. Med. Chem., 2012, 55, 7182.

[10] U. Jungwirth, D. N. Xanthos, J. Gojo, A. K. Bytzek, W. Körner, P. Heffeter, S. A. Abramkin, M. A. Jakupec, C. G. Hartinger, U. Windberger, Ma. Galanski, B. K. Keppler, W. Berger, Mol. Pharmacol., 2012, 81, 719.

[11] D. Pollak, R. Goddard and K. R. Pörschke, Inorg. Chem., 2016, 55, 9424.

[12] R. Pažout, J. Houskova, M. Dušek, J. Maixner and P. Kačer, Struct. Chem., 2011, 22, 1325.

[13] T. Marzo, S. Pillozzi, O. Hrabina, J. Kasparkova, V. Brabec, A. Arcangeli, G. Bartoli, M. Severi, A. Lunghi, F. Totti, C. Gabbiani, A. G. Quiroga and L. Messori, Dalton Trans., 2015, 44, 14896.

[14] T. Marzo, G. Bartoli, C. Gabbiani, G. Pescitelli, M. Severi, S. Pillozzi, E. Michelucci, B. Fiorini, A. Arcangeli, A. G. Quiroga and L. Messori, BioMetals, 2016, 29, 535.

[15] C. Rappel, M. Galanski, A. Yasemi, L. Habala, B. K. Keppler, Electrophoresis, 2005, 26, 878.

[16] W. G. Gao, S. P. Pu, W. P. Liu, Z. D. Liu and Y. K. Yang, Yaoxue Xuebao, 2003, 38, 223.

[17] A. Casini, G. Mastrobuoni, C. Temperini, C. Gabbiani, S. Francese, G. Moneti, C. T. Supuran, A. T. Scozzafava, L. Messori, Chem. Commun., 2007, 156.

[18] D. Marasco, L. Messori, T. Marzo and A. Merlino, Dalton Trans., 2015, 44, 10392.

[19] L. Messori, T. Marzo and A. Merlino, J. Inorg. Biochem., 2015, 153, 136.

[20] L. Messori, T. Marzo and A. Merlino, Chem. Commun., 2014, 50, 8360.

[21] S. Mowaka, M. Ziehe, D. Mohamed, U. Hochkirch, J. Thomale and M. W. Linscheid, J. Mass Spectrom., 2012, 47, 1282.

3. Platinum(II) compounds as promising chemotherapeutic agents: further studies on chloride and bromide derivatives

Introduction

PtI_2(DACH) shown to possess a number of peculiar chemical and biological features that make it particularly attractive. Despite its solution behaviour was characterized by a classical hydrolysis profile with halide release, yet, is scarcely reactive toward model proteins being instead highly reactive toward DNA ss oligonucleotides. Notably, we found PtI_2(DACH) capable to induce cytotoxic effects almost superimposable with those of oxaliplatin in representative CRC cell lines being this latter feature accompanied to a higher proapoptotic effect than cisplatin and oxaliplatin [1]. In light of these results, and in order to further expand the panel of oxaliplatin analogues, we decided to prepare and comparatively evaluate two other analogues of oxaliplatin bearing either chloride or bromido ligands in place of oxalate i.e. $PtCl_2$(DACH) and $PtBr_2$(DACH). Importantly, both these two oxaliplatin derivatives, have been previously synthesized and extensively investigated as prospective antineoplastic agents either in vitro and in vivo on leukemia, ovarian or sarcoma models; yet, no information are available in literature regarding their possible application in the treatment of colorectal cancer [2,3a]. It may be stressed that the presence of chlorido or bromide ligands may lead to a selective modulation of a few important properties of these compounds, such as the respective log P values and the kinetics of ligands release, leading to a different biological and pharmacological profile. Also, the comparative analysis allows to correlate relevant chemical features with biological and pharmacological effects, that, in turn, might allow specific design of more effective complexes for CRC treatment.

Experimental

Chemicals and reagents

Chemicals have been purchased from Sigma-Aldrich and were used without further purification. Dodecameric oligonucleotide ODN2 (sequence CTACGGTTTCAC), lysozyme (HEWL) and RNase have also been purchased from Sigma-Aldrich.

Chemistry

The two reported compounds were synthesized and purified according to literature procedures with slight modifications [3].

$PtCl_2$(DACH) has been obtained starting from 99,7 mg of K_2PtCl_4 ($2.40x10^{-4}$ mol) solubilised in 1.5 mL di of milli-Q water. 1,2-diaminocyclohexane (1R,2R)-(–), DACH (27.4 mg, $2.42x10^{-4}$ mol) was then solubilised in 2 mL of milli-Q water and the obtained solution slowly added to K_2PtCl_4 water solution. After further 4 h of stirring precipitate appeared, and complete precipitation of yellow crystals of $PtCl_2$(DACH) allowed over night at room temperature. The solid was then collected through vacuum filtration and

washed with hot water and ice-cooled ethanol and ether. 88.36 mg of $PtCl_2$(DACH) were obtained (yield 96%). Complex was characterized through ^{1}HNMR and elemental analysis.

^{1}HNMR (DMF-d_7, 400.13 MHz, 298 K): 2.45 (t, *J* = 8 Hz, 2H); 2.21 (d, *J* = 12 Hz, 2H); 1.52 (m, 4H); 1.16 (m, 2H).

Elemental analysis of C, N and H [calculated C: 18.96%, H: 3.71%, N: 7.37%, experimental: C: 18.84%, H: 3.66%, N: 7.30%].

For the synthesis of $PtBr_2$(DACH), 99.9 mg of K_2PtCl_4 ($2.41x10^{-4}$ mol), have been solubilised in 1.5 mL di of milli-Q water. A water solution (2 mL) of KBr (117.7 mg, $9.64x10^{-4}$ mol) was added to K_2PtCl_4 and stirred (50 °C) in the dark for 5 min until quantitative conversion of K_2PtCl_4 in K_2PtBr_4 was obtained. 1,2-diaminocyclohexane (1R,2R)-(–), DACH (27.2 mg, $2.41x10^{-4}$ mol) was then solubilised in 2 mL of milli-Q water and the obtained solution slowly added to K_2PtBr_4 water solution. After further 4 h of stirring precipitate appeared, and complete precipitation of yellow crystals of $PtBr_2$(DACH) allowed over night at room temperature. The solid was then collected through vacuum filtration and washed with hot water and ice-cooled ethanol and ether. 79.27 mg of $PtBr_2$(DACH) were obtained (yield 70%). Complex was characterized through ^{1}HNMR and elemental analysis.

^{1}HNMR (DMF-d_7, 400.13 MHz, 298 K): 2.50 (t, *J* = 8 Hz, 2H); 2.23 (d, *J* = 12 Hz, 2H); 1.56 (m, 4H); 1.15 (m, 2H).

Elemental analysis of C, N and H [calculated C: 15.36%, H: 3.01%, N: 5.97%, experimental: C: 16.50%, H: 3.14%, N: 6.30%].

Uv–Vis experiments

Solution behavior of $PtCl_2$(DACH) and $PtBr_2$(DACH) was assessed by spectrophotometric experiments performed with a Varian Cary 50 Bio UV–Vis spectrophotometer in the same condition used in our previous works [1].

LogP value determination

The octanol-water partition coefficients for $PtCl_2$(DACH) and $PtBr_2$(DACH) was determined by modification of reported shake-flask method as reported in our previous work [1].

ESI-MS experiments

For comparative purposes ESI-MS spectra of the ODN2-complexes and protein-complexes mixtures were recorded as already reported in literature [1].

Cell culture

Human colorectal cancer cell lines (HCT-116, HCT-8 and HT29) were cultured in RPMI-1640 medium (Euroclone; Milan, Italy), supplemented with 2% L-Glut and 10% fetal bovine serum (FBS) (complete medium). Human embryonic kidney HEK293 cell line was cultured in DMEM medium (Euroclone; Milan, Italy), supplemented with 2% L-Glut and 10% fetal bovine serum (FBS).

Cell viability assay

To evaluate the IC50 of each compound, cell viability was assessed through the Trypan Blue exclusion test (Sigma-Aldrich). Cells were seeded at $1x10^4$/well in 96-well plates (Costar Corning) in complete medium and incubated for 24 h before compound addiction. Following the addition, cells were further incubated for 24 h. Cells were then harvested and counted by the Trypan Blue exclusion test using a hemocytometer. All experiments were performed in triplicate. The IC50 values were calculated for each cell line and data fitted using a Hill1-type equation by using Origin Software (Microcal Origin 8.0 software; OriginLab Corporation, Northampton, MA).

Cell cycle analysis

Cell cycle distribution was assessed by flow cytometry after staining the cells with propidium iodide (PI). Cells were seeded and treated generally with different compound at their IC50 for 24 h, as already described [1].

Results and discussion

Synthesis and characterization of $PtCl_2$(DACH) and $PtBr_2$(DACH)

The same synthetic route already exploited for the synthesis of PtI_2(DACH), and based on modification of existing method [1,4] was used, as reported in more detail in the

material and methods section. Both complexes were obtained in good yield and their purity assessed through CHN analysis, was found to be higher than 95% (Scheme 1).

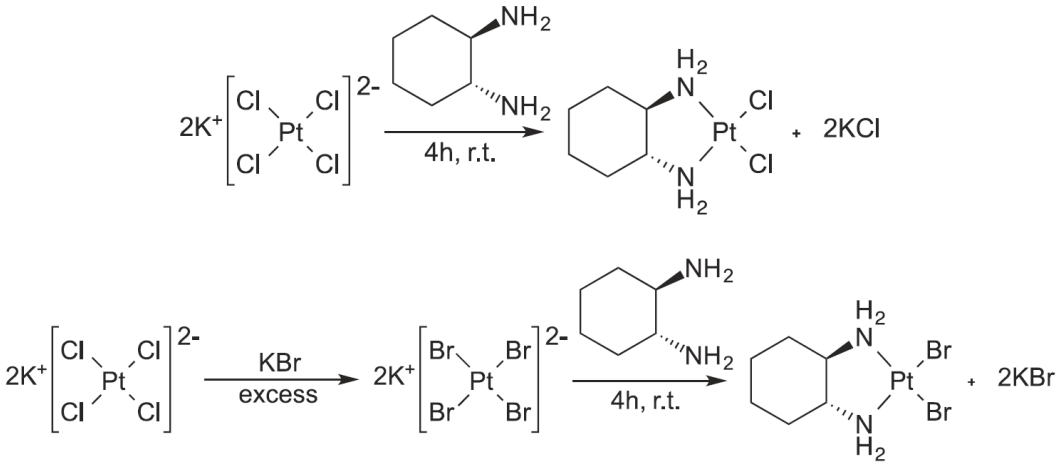

Scheme 1: Synthetic route for compounds 1 and 2, respectively.

LogP value determination

Octanol-water partition coefficient is an important parameter giving information related with the bioavailability and tendency of a compound to cross cell membranes. Through the modification of the classical flask-method and as already reported in our previous works [2,5a,6], we have determined for $PtCl_2$(DACH) and $PtBr_2$(DACH) a value respectively of -0,47 and -0,16. For comparison purposes log P values for a few parent Pt complexes are also reported in Table 1 and Table 2.

Compound	Log P[a]
$PtCl_2$(DACH)	−0,47
$PtBr_2$(DACH)	−0,16
Oxaliplatin	−1,58**
Cisplatin	−2,40*

Table 1: [a]Determination of LogP for compound $PtCl_2$(DACH) and $PtBr_2$(DACH) compared with cisplatin and oxaliplatin (for comparison purpose Log P for PtI_2(DACH) is 0,76**); *Ref. [5b], **Ref. [1].

IC_{50} value (μM, mean ± SEM)[b]			
HCT-116	HT-29	HCT-8	HEK293
9.86 ± 1.4	49.07 ± 1.1	30.83 ± 0.1	194.86 ± 6.8
30.96 ± 0.8	66.75 ± 2.0	48.64 ± 0.1	>200
49.9 ± 1.9	18.8 ± 2.5	33.1 ± 0.6	>200
24.4 ± 0.6	16.7 ± 2.3	9.2 ± 1.5	91.41 ± 4.15

Table 2: [b]IC50 (μM) of $PtCl_2$(DACH), $PtBr_2$(DACH), Oxaliplatin and Cisplatin (from top to bottom) in HCT-116, HT-29 and HCT-8 CRC cell lines, as well as in an embryonic kidney cell line cell line (HEK 293). Cell viability was determined after 24 h of treatment with the four different compounds (range 0 – 300 μM), by the Trypan Blue exclusion test. IC50 values (means ± sem of three independent experiments) were calculated using the Origin Software (Microcal Origin 8.0 software; OriginLab Corporation, Northampton, MA) fitting experimental data with Hill1 type equation. Remarkably, in line with results obtained for cisplatin analogues [5a], $PtBr_2$(DACH) manifests a larger lipophilic character than oxaliplatin and in less extent than $PtCl_2$(DACH), whereas shows a lower lipophilicity than PtI_2(DACH). It is well conceivable that this difference may have some appreciable effect in terms of pharmacological activity (Fig. 1).

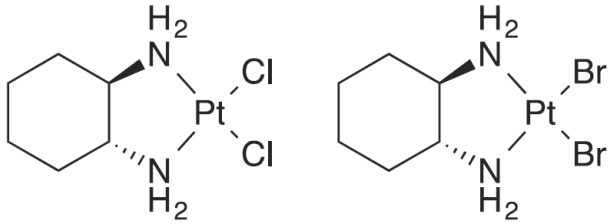

$PtCl_2$(DACH) (**1**) $PtBr_2$(DACH) (**2**)

Fig.1: The two synthesized molecules.

Solution behaviour

The solution behaviour of $PtCl_2$(DACH) and $PtBr_2$(DACH) was studied spectrophotometrically under physiological-like conditions. Freshly prepared aqueous solutions of $PtCl_2$(DACH) and $PtBr_2$(DACH), in 50 mM phosphate buffer, at pH = 7.4, manifest a band in the UV–visible region, located around 320 nm, that allows the continuous monitoring of the solution behaviour of this platinum complex (Fig. 2).

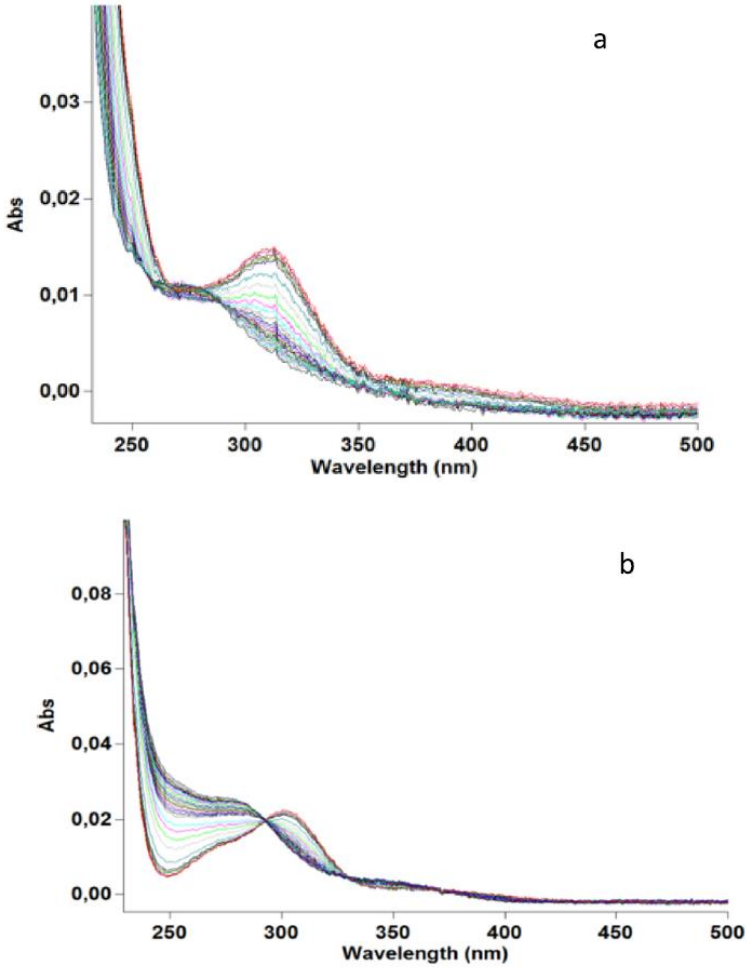

Fig.2: Time course spectra of (a) $PtCl_2$(DACH) and (b) $PtBr_2$(DACH) 10^{-4}M in 50 mM phosphate buffer recorded over 72 h, RT.

After dissolution of the selected compounds in the reference buffer, progressive spectral changes are observed, consisting in a decrease of the band centered at 330 nm and the appearance of a new band around 280 nm, tentatively assigned to a d–d and a LMCT transition, respectively [5a]. These changes, probably are ascribed to the progressive release of the two halide ligands [1,5]. The nature of the process and its kinetics are similar to what observed in the case of oxaliplatin despite release of halides in the case of $PtCl_2$(DACH) and $PtBr_2$(DACH) appears to be slightly faster than in case of oxaliplatin and PtI_2(DACH) (Fig. 3, Table 3).

Compound	K_{obs} (s^{-1})	$t_{1/2}$ (min)
$PtCl_2$(DACH)	$1{,}89 \times 10^{-5}$	611,3
$PtBr_2$(DACH)	$2{,}14 \times 10^{-5}$	538,4
PtI_2(DACH)*	$9{,}75 \times 10^{-6}$	1184,58
Oxaliplatin*	6,32 8 10^{-6}	1827,92

Table 3: Spectrophotometric determination of K_{obs} and t1/2 for the hydrolysis reaction of 1 and 2 10^{-4} M in phosphate buffer over 72 h. *The K_{obs} reported have been previously determined in our laboratory [1]. For oxaliplatin K_{obs} was found to be close to that reported in literature by other authors [7].

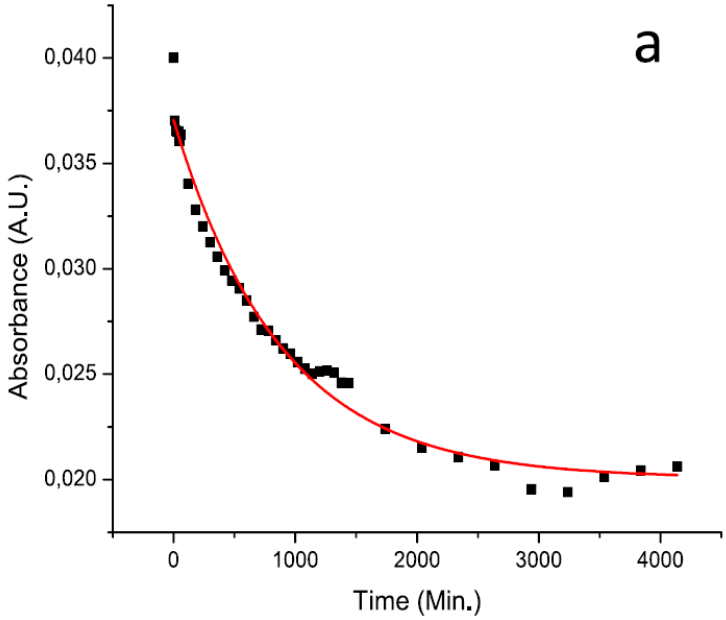

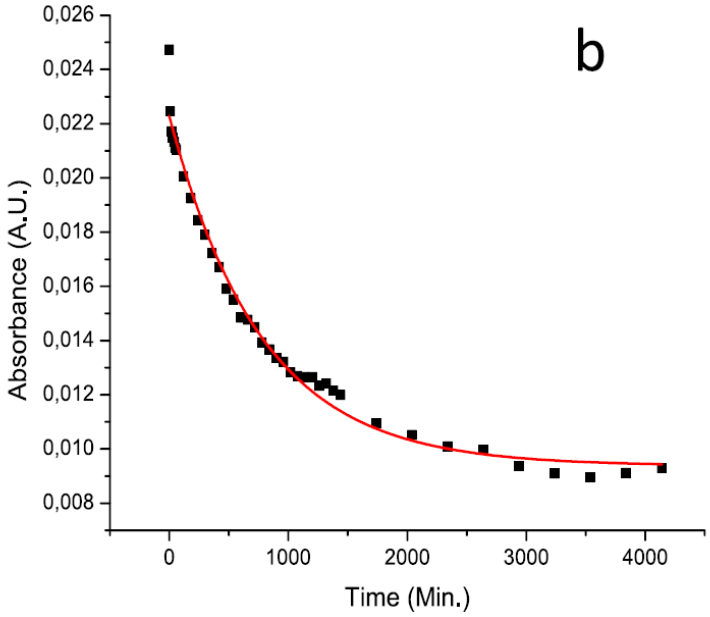

Fig.3: Experimental kinetic traces and calculated theoretical curve for the hydrolysis of the halido derivatives 1 (a) and 2 (b). k_{obs} was calculated fitting with a single exponential function (pH value = 7.4).

Interaction with model biomolecules, ESI-MS experiments

To investigate the possible interactions occurring between chloride and bromido oxaliplatin analogues and their potential biomolecular targets, the two complexes were incubated with RNase (Fig. 4) and possible adducts formation was investigated.

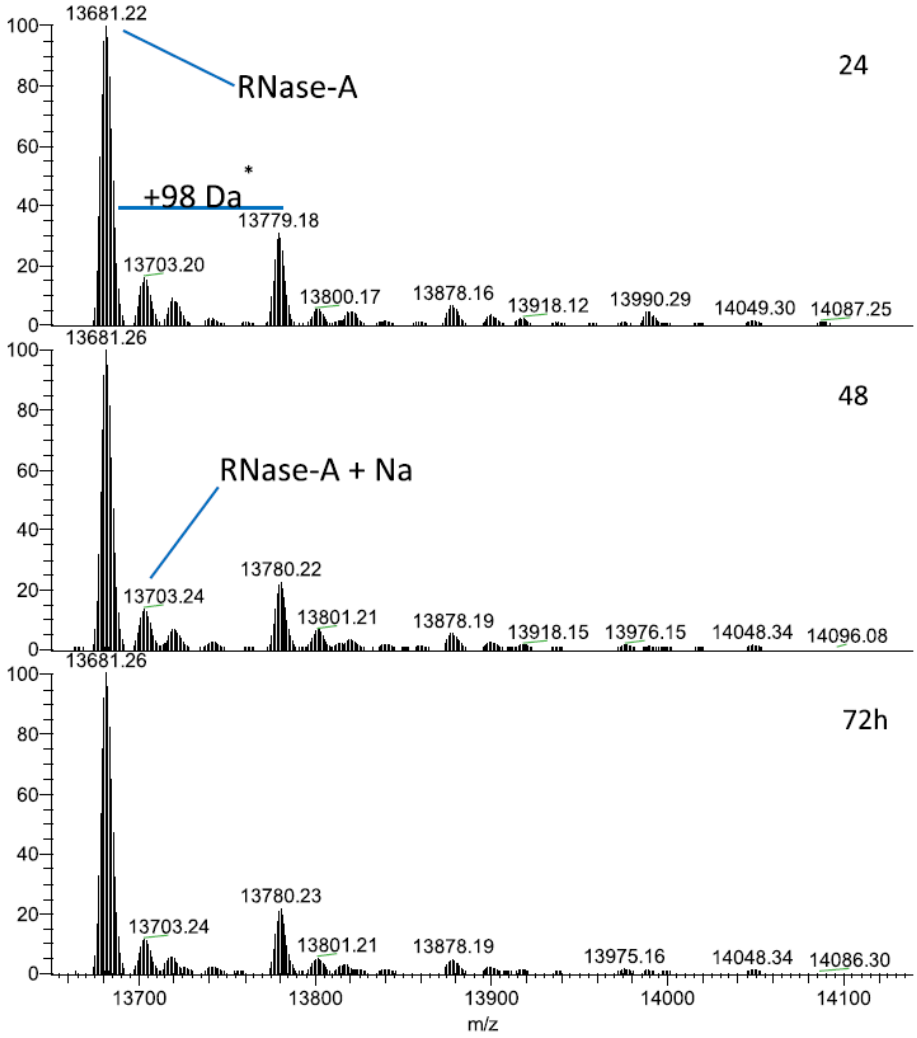

Fig.4: Deconvoluted ESI-MS spectra of RNase A in 20 mM ammonium acetate buffer, pH = 6.8 incubated with $PtBr_2$(DACH) after 24–72 h at 37 °C. The protein concentration was 10^{-4} M (with complex to protein molar ratio of 3:1). *The saline buffer can contain small amount of phosphoric acid or sulphuric acid that are responsible of the formation of undesired and isobaric adducts with Ribonuclease A (+98 m/z) [8].

RNase was chosen since his structure has been often used to characterize the interactions occurring between proteins and metallodrugs. These model proteins are well suitable for ESI-MS studies, offering a very important substrate for comparative mechanistic studies of metal-based drugs. We performed a few ESI-MS experiments

where the selected complexes were incubated in 20 mM ammonium acetate buffer, pH = 6.8 for increasing time intervals, from 24 to 72 h. ESI-MS spectra recorded for RNase in presence of $PtBr_2$(DACH) did not show any signal attributable to the metallated protein. The same results were obtained also for $PtCl_2$(DACH). This indicates that the two compounds are not able to bind this protein. Also, ESI-MS spectra recorded for Lysozyme in presence of $PtBr_2$(DACH) or $PtCl_2$(DACH) did not show any signal attributable to the metallated protein. In a previous study, similar results were obtained for PtI_2(DACH) [1]. Conversely, in other works, some of us have shown significant interactions between oxaliplatin and the two selected model proteins [9,10]. We hypothesized that an explanation for this different behaviour could be that coordination of oxaliplatin to lysozyme and RNase implies a multi-step reaction at the level of aspartate residues. This implies, at first a non-covalent coordination of oxaliplatin to the protein; then detachment of one oxygen atom of oxalate from Pt coordination with a ring-opening step leading to monodentate oxalate, with concomitant Pt coordination of the carboxylate group from an aspartate residue. Finally, the complete release of the oxalate ligand [4,6]. The replacement of the oxalate with the halide ligands could cause loss of the first non-covalent interaction, which could be an important step in the reactivity of oxaliplatin with these proteins.

Binding with model oligonucleotide: ESI-MS experiments

It is generally accepted that the distortion of DNA generated upon binding of cisplatin and oxaliplatin is largely responsible for their antitumor properties [11]. Subsequent drug activation via intracellular aquation reactions results in a variety of stable bifunctional DNA–platinum(II) adducts. 1,2-Intrastrand cross-links between two adjacent guanine bases d(GG) or between an adenine and a guanine residue d(AG) are primarily formed. The platinum centre of complexes, with a cis motif, preferentially coordinates to the N7 position of both adenine and guanine in the major groove of DNA [12]. For these reasons we tested the binding properties of the three oxaliplatin analogues with a simplified oligonucleotide model bearing the characteristic GG motif. The selected complexes interact extensively with the tested oligonucleotide bearing the GG motif (ODN2) through a classical reaction pattern involving preferential release of halide ligands (Fig. 5) [13]. $PtBr_2$(DACH), in this case, shows a greater reactivity compared to $PtCl_2$(DACH) and PtI_2(DACH), as highlights the ESI-MS spectrum in Fig. 5, in which the peak of native ODN2 completely disappeared after adduct formation.

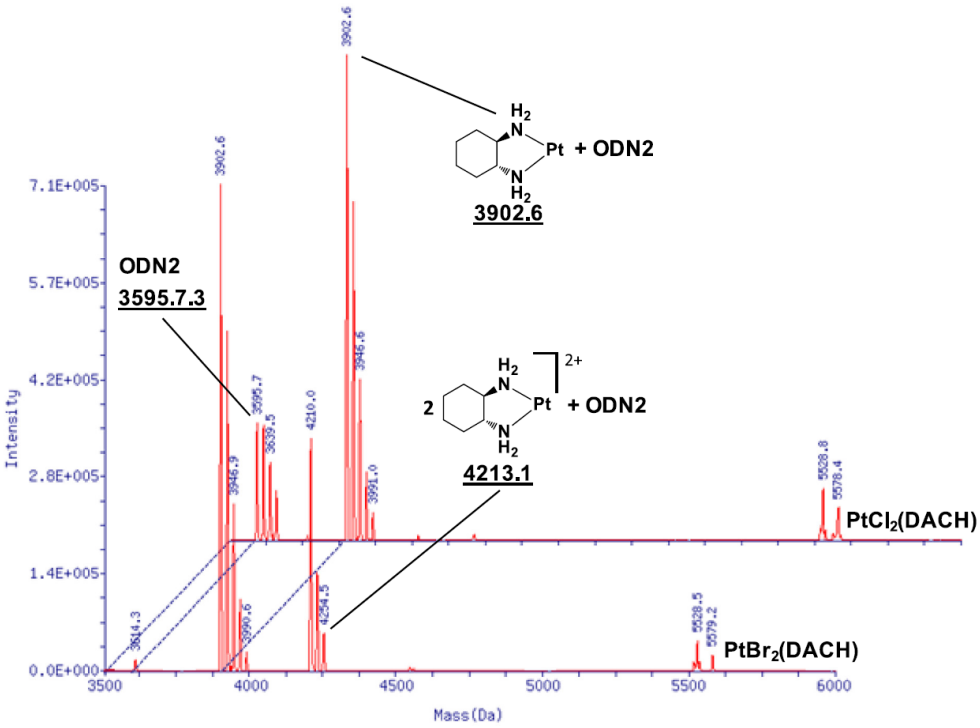

Fig.5: Deconvoluted ESI-MS spectra of ODN2 in Milli-Q water incubated with $PtCl_2$(DACH) and $PtBr_2$(DACH) after 72 h at 37 °C. The oligonucleotide concentration was 10^{-4} M (with complex to oligonucleotide molar ratio of 2:1).

Biological effects

The cytotoxic effects of $PtCl_2$(DACH) and $PtBr_2$(DACH) were then investigated in three CRC cell lines (HCT-116, HCT-8 and HT-29) in comparison with cisplatin and oxaliplatin. A normal cell line (HEK 293 cells) was also included. Cells were exposed to increasing concentrations of the drugs for 24 h, and the respective IC50 concentrations were determined by the Trypan blue exclusion test. As reported in Table 2, $PtBr_2$(DACH) and in particular $PtCl_2$(DACH), in comparison to oxaliplatin, show a greater cytotoxic effect only on the cell line least sensitive to cisplatin (i.e. HCT- 116) being less effective in the other cancer lines. The PtX_2(DACH) series conserves appreciable cytotoxic properties and is roughly similar to oxaliplatin. This implies that replacement of oxalate with two halido ligands does not impair the cellular effects of this drug. Additionally, when evaluating the effects of all compounds on embryonic kidney cell line HEK293, we can assert that the cytotoxicity is overall similar and rather low, being the $PtCl_2$(DACH) significantly less cytotoxic. Based on these results we studied the effects that

$PtCl_2$(DACH) and $PtBr_2$(DACH) (tested at their respective IC50s) produce on HCT-116 cells, determining the distribution of the cells in the various phases of the cell cycle. These effects were measured in the absence or in the presence of the four compounds tested at their respective IC50s. Preliminary results evidenced that as already reported for cisplatin, oxaliplatin and its iodido analogue [5b], $PtCl_2$(DACH) and $PtBr_2$(DACH) caused a variation of cell cycle distribution of HCT-116 cells (Table 4 and Fig. 6), with a block in G2/M phase. The same effect has been found also in HCT-8 cells (Fig.7).

	G0/G1 (%)	S (%)	G2/M(%)
Control	31.8 ± 0.6	31.2 ± 0.9	37.02 ± 1.4
$PtCl_2$(DACH)	20.2 ± 2.7	29.5 ± 6.1	50.2 ± 6.1
$PtBr_2$(DACH)	23.1 ± 3.4	20.4 ± 2.4	56.6 ± 4.1

Table 4: Cell cycle distribution of HCT-116 cells after 24 h of treatment with $PtCl_2$(DACH) and $PtBr_2$(DACH) at the IC50 values shown in Table 2. Data are means ± sem of four independent experiments, and are expressed as percentage of cells in each phase of the cell cycle, determined by flow cytometry after staining the cells with propidium iodide (PI).

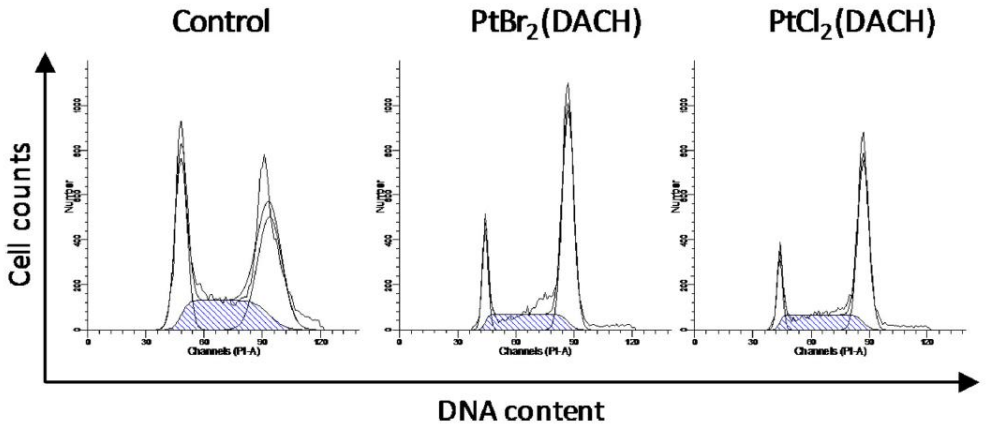

Fig.6: Cell cycle distribution of HCT-116 cells after 24 h of treatment with $PtBr_2$(DACH) and $PtCl_2$(DACH) at the IC50 values. Representative histograms of data reported in Table 4.

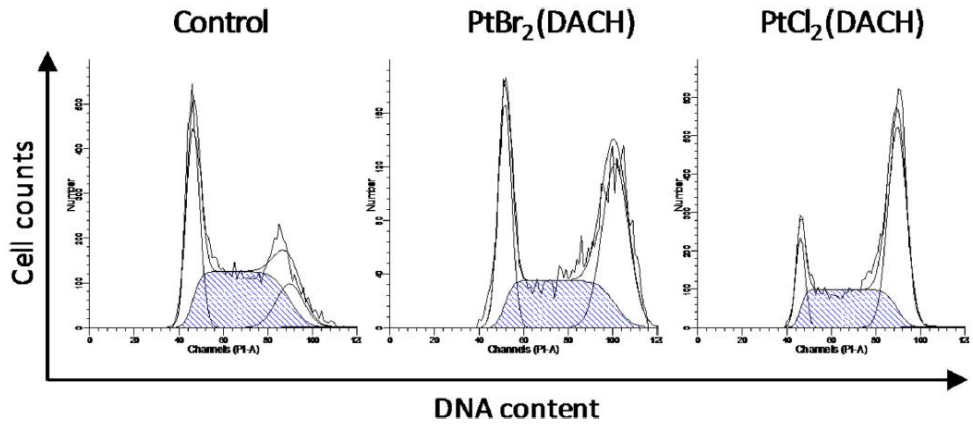

Fig.7: Cell cycle distribution of HCT-8 cells after 24 h of treatment with $PtBr_2$(DACH) and $PtCl_2$(DACH) at the IC50 values.

Conclusion

Colorectal cancer is a global health problem being the fourth most common cause of death due to cancer worldwide. Oxaliplatin plays a key role in current CRC treatment but shows serious drawbacks, such as a high systemic toxicity and the frequent insurgence of Pt resistance. This work continues a research line started a few years ago that is based on the idea that small modifications in the scaffold of established anticancer Pt drugs may lead to significant and hopefully positive changes in their pharmacological profile with appreciable effects in the overall spectrum of anticancer actions and in the ability to overcome Pt resistance in CRC. The exchange of halide ligands (e.g. replacement of chloride with iodide in cisplatin) represents indeed a small structural change with a relevant chemical and biological impact. Specifically, we have prepared here two analogues of oxaliplatin through incorporation of non-conventional halido ligands such as chloride and bromide. From the inspection of the solution behaviour, we have observed hydrolysis profiles similar to oxaliplatin, with a release of the halido ligand faster for chloride than bromide or iodide. At variance from oxaliplatin and in line with PtI_2(DACH), the selected compounds showed a scarce reactivity towards model proteins, while keeping affinity for a standard DNA oligo. These findings are of considerable interest; in fact, despite DNA is recognized as the main target for Pt-based anticancer agents, protein binding is nowadays considered a key aspect for the pharmacological profile. Interaction with aminoacidic residues of proteins may have a primary role in the pharmacokinetic and bioavailability of metal-based antineoplastic compounds. Also, the coordination of metal center to specific protein

sites, may result in an inhibition and damage of enzymes, leading in turn to augmented side effects [14]. Thus, the lack of reaction of the study compounds when reacted with model protein targets, and the concomitant conserved reactivity toward oligonucleotides may have important biological consequences. Furthermore, we have shown that CRC cells that were treated with $PtCl_2$(DACH) and $PtBr_2$(DACH) manifest at 24 h a clear spike in the G2/M fraction; the cytotoxic properties versus CRC cell lines of the two study compounds were roughly comparable to those of oxaliplatin. This implies that the presence of the oxalate ligand is not crucial for the anticancer activity of oxaliplatin and that the latter may be replaced by halido ligands with nearly full retention of the cytotoxic properties. Results collected indicated that treatments with $PtCl_2$(DACH) and $PtBr_2$(DACH) affect growth of human CRC cells and induce an evident cell cycle arrest ultimately triggering cellular apoptosis. Overall, a rather interesting picture emerges for these novel Pt drugs that merit, in our opinion, a deeper and more extensive preclinical evaluation.

References

[1] D. Cirri, S. Pillozzi, C. Gabbiani, J. Tricomi, G. Bartoli, M. Stefanini, E. Michelucci, A. Arcangeli, L. Messori, T. Marzo, Dalton Trans. 46 (2017) 3311–3317.

[2] (a) J. Maixner, R. Pazˇout, I. Nováková, J. Holakovská, P. Kacˇer, Powder Diffr. 27 (2012) 200; (b) Y. Kidani, K. Inagaki, S. Tsukagoshi, GANN 67 (1976) 921; (c) Y. Kidani, K. Inagaki, R. Saito, J. Clin. Hematol. Oncol. 7 (1977) 197; (d) Speer et al., J. Clin. Hematol. Oncol. 8 (1978) 44; (e) F.K.V. Leh, W. Wolf, J. Pharm. Sci. 65 (1976) 315.

[3] (a) Kidani, Yoshinori (2-1, Mataho-cho, Nishi-ku, Nagoya-shi, Aichi-ken, JP), Noji, Masahide (Nagoya, JP), 1981, Platinum Complex, United States, Patent n. 4256652.; (b) S.C. Dhara, Ind. J. Chem. 8 (1970) 193.

[4] R. Pazˇout, J. Houskova, M. Dušek, J. Maixner, P. Kacˇer, Struct. Chem. 22 (2011) 1325.

[5] (a) T. Marzo, G. Bartoli, C. Gabbiani, G. Pescitelli, M. Severi, S. Pillozzi, E. Michelucci, B. Fiorini, A. Arcangeli, A.G. Quiroga, L. Messori, Biometals 29 (2016) 535; (b) T. Marzo, S. Pillozzi, O. Hrabina, J. Kasparkova, V. Brabec, A. Arcangeli, G. Bartoli, M. Severi, A. Lunghi, F. Totti, C. Gabbiani, A.G. Quiroga, L. Messori, Dalton Trans. 44 (2015) 14896.

[6] M.V. Baker, P.J. Barnard, S.J. Berners-Price, S.K. Brayshaw, J.L. Hickey, B.W. Skelton, A.H. White, Dalton Trans. (2006) 3708.

[7] W.G. Gao, S.P. Pu, W.P. Liu, Z.D. Liu, Y.K. Yang, Yao Xue Xue Bao 38 (2003) 223.

[8] S.K. Chowdhury, V. Katta, R.C. Beavis, B.T. Chait, J. Am. Soc. Mass Spectrom. 1 (1990) 382.

[9] L. Messori, T. Marzo, A. Merlino, J. Inorg. Biochem. 153 (2015) 136.

[10] L. Messori, T. Marzo, A. Merlino, Chem. Commun. 50 (2014) 8360.

[11] J. Reedijk, J. Proc. Natl. Acad. Sci. USA 100 (2003) 3611.

[12] E.R. Jamieson, S.J. Lippard, Chem. Rev. 99 (1999) 2467.

[13] S. Mowaka, M. Ziehe, D. Mohamed, U. Hochkirch, J. Thomale, M.W. Linscheid, J. Mass Spectrom. 47 (2012) 1282.

[14] A. Casini, J. Reedijk, Chem. Sci. 3 (2012) 3135.

4. Gold(I) and Silver(I) compounds and their antibacterial properties

Introduction

Several metals and metal-based compounds have been used for centuries as anti-infective agents on a simple empirical basis, with some appreciable results. For instance, the complex dicyanoaurate(I) was proposed and used by Koch as an antitubercular agent during the pioneering times of modern pharmacology, and several bismuth, antimony and mercury compounds have been extensively used to combat various bacterial and parasitic diseases [1–4]. However, more recently, due to the advent of the golden era of antibiotics and owing to justified concerns about their systemic toxicity, metal-based agents have been gradually abandoned. Only a few exceptions remain in the clinic for specific therapeutic indications, such as bismuth salts for the eradication of Helicobacter pylori infection, and antimony compounds as antileishmanial agents [3, 5]. However, during the last two decades, the so-called "antibiotic resistance crisis"—arising from the emergence of bacterial strains with multidrug-resistant (MDR) and extensively drug-resistant (XDR) phenotypes, and from the simultaneous decline in the discovery rate of new and effective antibiotic molecules— has posed the dramatic problem of finding new substances capable of fighting life-threatening infections caused by these pathogens [6, 7]. Metal-based compounds are thus being reconsidered as a rich source of antimicrobial agents often having novel modes of action. In this context, Auranofin (AF), an antiarthritic agent still sporadically used to treat some severe forms of rheumatoid arthritis, has been revisited within the framework of drug repurposing strategies, with rather promising results. Indeed, remarkable antimicrobial and antiparasitic properties have been reported for this oral gold(I) drug, which has become the reference compound for the development of novel gold-based antibacterial agents or specific inhibitors of important enzymes [7, 8]. Some recent studies investigated in detail the mechanistic aspects of its antimicrobial action. It was shown that AF probably acts through a multifactorial and multitarget mechanism and that the low susceptibility of Gram-negative bacteria to this drug is probably the consequence of reduced intracellular gold accumulation [9–12]. However, the precise mechanisms of the antimicrobial action of AF, and the respective biomolecular targets, are not known. The promising antibacterial properties reported for AF prompted us to test not only AF but also a series of related metal complexes, prepared in our laboratory, against a panel of isolates, including major Gram-positive,

Gram-negative and fungal pathogens showing relevant resistance phenotypes. Due to the so-called “antibiotic resistance crisis” new antibacterial agents are urgently sought to treat multidrug-resistant pathogens. A group of gold- or silver-based complexes, of general formula [M(PEt_3)X] (with M=Au or Ag, and X=Cl, Br or I), alongside with three complexes bearing a positive or negative charge—[Au(PEt_3)$_2$]Cl, K[Au(CN)$_2$] and [Ag(PEt_3)$_2$]NO_3—were prepared and comparatively tested with AF on a representative panel of pathogens including Gram-positive, Gram-negative and Candida strains. Interestingly, all the gold and silver complexes tested were active on Gram-positive strains, with the gold complexes having greater efficacy. The effects of the gold compounds were potentiated to a larger extent than silver compounds when tested in combination with a permeabilizing agent. A number of relevant structure–activity relationships emerged from the comparative analysis of the observed antibacterial profiles, shedding new light on the underlying molecular mechanisms of the action of these compounds. Some classical gold complexes were also prepared and evaluated. We postulated that a comparative analysis of the antimicrobial behaviour of the various structurally related gold(I) and silver(I) complexes might provide valuable mechanistic insight on the activity of AF and its derivatives, and perhaps lead to drug improvement through chemical modification as well as to a better understanding of the observed pharmacological effects.

Results and Discussion

The panel of studied gold and silver compounds is shown in Figure 1. For gold-based complexes the panel includes, as well as AF, three gold complexes of general formula [Au(PEt_3)X] where X is a halide ligand; these latter compounds are known AF analogues in which the thiosugar ligand is replaced by chlorido, bromido or iodido ligand [13]. The cationic diphosphino gold(I) and the anionic dicyanoaurate(I) complexes, prepared according to reported procedures, were also included in the panel of test compounds (see the Experimental Section for details on their synthesis, CHN analysis, NMR and UV/Vis spectroscopic characterization) [14]. Careful analysis of the obtained results provides valuable insight on structure–activity relationships. Consistent with expectations, AF showed similar antimicrobial activity against all tested Gram-positive species, with the exception that it was poorly active against Candida albicans (Table 1). It is interesting to compare the behaviour of the [Au(PEt_3)X] compounds with AF. Remarkably, the [Au(PEt_3)X] complexes exhibit antimicrobial properties against Gram-positive bacteria, with a potency that is similar to or slightly lower than AF. Also, the

antibacterial profiles of the three [Au(PEt_3)X] complexes against these pathogens are similar to one another, being almost superimposable.

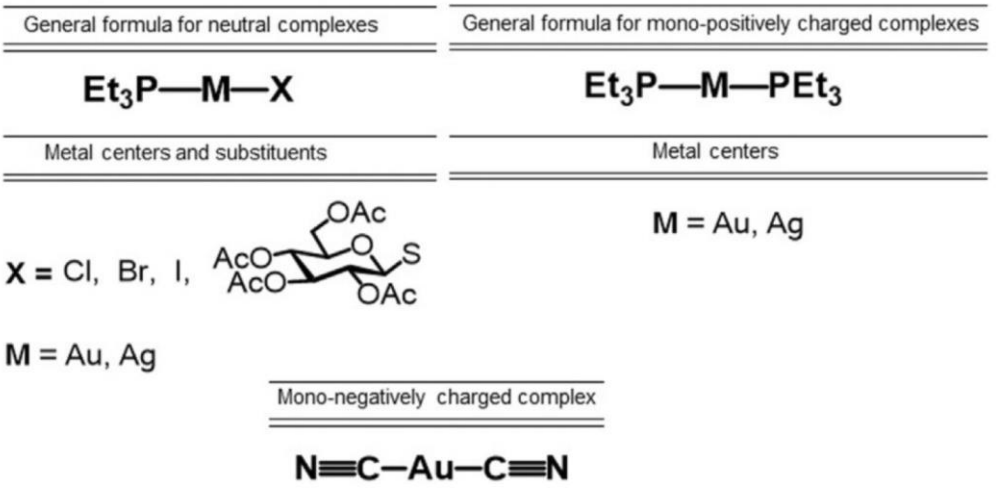

Fig.1: The panel of investigated gold and silver complexes. For clarity, the structure of the neutral silver complex, has been here reported in a simplified manner; those species are tetrameric with a structure of the type [Ag(PEt_3)X]$_4$.

These observations imply that the thiosugar ligand is not essential for the antimicrobial activity of AF. Similarly, the nature of the X ligand seems to play a minor role, if any, in determining the antimicrobial profiles of the three [Au(PEt_3)X] compounds, which are nearly identical. Altogether, these results point to the [Au(PEt_3)]$^+$ moiety as the "true pharmacophore". The strong similarity in the antimicrobial activity of the three [Au(PEt_3)X] complexes also suggests that their uptake is similar. Similarly to AF, the three [Au(PEt_3)X] compounds were less active against C. albicans.

Strain[a]	R profile[b]	AF		$[Au(PEt_3)Cl]$		$[Au(PEt_3)Br]$		$[Au(PEt_3)I]$		$[Au(PEt_3)_2]Cl$		$K[Au(CN)_2]$	
		[μg mL^{-1}]	[μM]	[μg mL^{-1}]	[μM]	[μg mL^{-1}]	[μM]	[μg mL^{-1}]	[μM]	[μg mL^{-1}]	[μM]	[μg mL^{-1}]	[μM]
1	Reference strain, wild type	0.062	0.09	≤0.062	≤0.18	≤0.062	≤0.16	≤0.062	≤0.14	≤0.062	≤0.13	8	27.77
2	OXA^r CL^r ERY^r LIN^r FQ^r AG^r	0.062	0.09	≤0.062	≤0.18	≤0.062	≤0.16	≤0.062	≤0.14	≤0.062	≤0.13	0.5	1.73
3	Reference strain, wild type	≤0.062	≤0.09	≤0.062	≤0.18	≤0.062	≤0.16	0.062	0.14	≤0.062	≤0.13	0.25	0.87
4	LIN^r	0.062	0.09	≤0.062	≤0.18	≤0.062	≤0.16	≤0.062	≤0.14	≤0.062	≤0.13	0.5	1.73
5	AG^r	0.25	0.37	≤0.062	≤0.18	≤0.062	≤0.16	0.062	0.14	≤0.062	≤0.13	0.5	1.73
6	–[c]	0.125	0.18	≤0.062	≤0.18	≤0.062	≤0.16	0.062	0.14	≤0.062	≤0.13	0.25	0.87
7	–	0.062	0.09	≤0.062	≤0.18	0.062	0.16	0.062	0.14	≤0.062	≤0.13	2	6.94
8	AMP^r VAN^r AG^r	0.125	0.02	≤0.062	≤0.18	0.062	0.16	0.062	0.14	≤0.062	≤0.13	2	6.94
9	AMP^r ESC^r	0.062	0.09	≤0.062	≤0.18	0.062	0.16	0.062	0.14	≤0.062	≤0.13	1	3.47
10	AMP^r	0.062	0.09	≤0.062	≤0.18	0.125	0.32	0.062	0.14	≤0.062	≤0.13	0.5	1.73
11	–	0.125	0.18	≤0.062	≤0.18	≤0.062	≤0.16	0.125	0.28	0.125	0.27	0.062	0.21
12	ESC^r CL^r AG^r	≤0.062	≤0.09	≤0.062	≤0.18	≤0.062	≤0.16	≤0.062	≤0.14	≤0.062	≤0.13	2	6.94
13	AMP^r CL^r AG^r	≤0.062	≤0.09	≤0.062	≤0.18	≤0.062	≤0.16	≤0.062	≤0.14	≤0.062	≤0.13	8	27.77
14	–	>8	>11.80	2	5.70	4	10.12	8	18.10	>8	>17.07	>8	>27.77

[a] Clinical strains: 1, *Staphylococcus aureus* ATCC 25923; 2, *Staphylococcus epidermidis* FI-1; 3, *Enterococcus faecalis* ATCC 29212; 4, *Enterococcus faecalis* FI-2; 5, *Enterococcus faecalis* FI-3; 6, *Enterococcus faecalis* FI-4; 7, *Enterococcus faecium* FI-5; 8, *Enterococcus faecium* FI-6; 9, *Streptococcus salivarius* FI-7; 10, *Streptococcus parasanguinis* FI-8; 11, *Streptococcus pyogenes* FI-9; 12, *Corynebacterium striatum* FI-10; 13, *Corynebacterium striatum* FI-11; 14, *Candida albicans* FI-12. [b] Resistance phenotype of the clinical strains; AMP^r, resistant to ampicillin; OXA^r, resistant to oxacillin; ESC^r, resistant to expanded-spectrum cephalosporins; CL^r, resistant to clindamycin; ERY^r, resistant to erythromycin; LIN^r, resistant to linezolid; VAN^r, resistant to vancomycin; FQ^r, resistant to fluoroquinolones (levofloxacin and/or ciprofloxacin); AG^r, resistant to aminoglycosides (gentamicin and/or amikacin and/or tobramycin). [c] Strain with no reported resistance phenotypes.

Table 1. MIC [μg/mL and μM] values obtained for gold compounds on Gram-positive strains and Candida albicans (strain 14).

To expand our analysis of structure–activity relationships, the two charged gold(I) compounds were then evaluated. Interestingly, the cationic diphosphine complex exhibited important antimicrobial properties similar to those of [Au(PEt_3)X] complexes. Again, this suggests that a single phosphine ligand is sufficient for the biological activity. In contrast, the dicyano gold(I) complex resulted much less active than [Au(PEt_3)$_2$]Cl. This observation might imply either that the negatively charged dicyano gold(I) complex is taken up less efficiently than neutral or positive gold complexes, or that the cyanide ligand is so strong that the biological action of the gold(I) center—probably linked to gold(I) coordination to a specific biomolecular target—is greatly inhibited. In considering this latter aspect, it is worth comparing the antimicrobial properties of two carbene complexes with the structures R-Au-R and R-Au-Cl (R= 1,3-Dimethylimidazol-2-ylidene) (Figure 2) that we tested previously on different bacterial strains (unpublished results: see the Table 2 for MIC values).

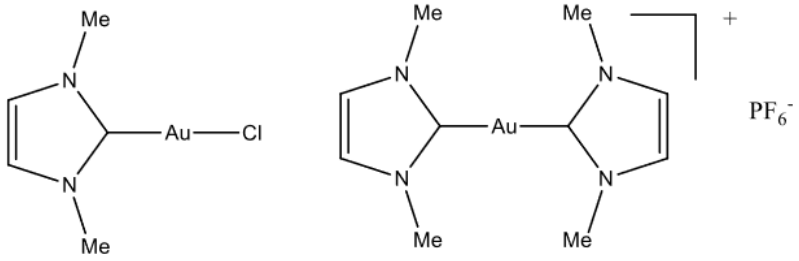

Fig.2: Structures of the two carbene gold compounds.

	S. aureus ATCC 25923
Au(NHC)Cl	0.5
Au(NHC)$_2$PF$_6$	8

Tab.2: MIC (μg/mL) values obtained for carbene gold compounds.

We observed that the dicarbene complex was far less active than the monocarbene on a Gram-positive strain (Staphylococcus aureus ATCC 2592). This lower activity is likely related to the greater stability of the R-Au-R Complexes [15, 16]. Conversely, the greater antimicrobial effects of the monocarbene gold complex, where Cl^- is a labile ligand, seems to support—at least indirectly—that its biological activity is linked to the ease of ligand displacement and to consequent gold coordination to relevant biological targets. As previously reported, AF is scarcely active on Gram-negative strains; this is tentatively attributed to reduced drug uptake [10]. To confirm these findings and assess whether such limited activity of gold compounds in Gram-negative bacteria is "conserved" upon replacement of a thiosugar with different ligands, we investigated the antibacterial effects of the experimental drugs on five Gram-negative strains of clinical origin. Also, to further understand the underlying mechanistic aspects of the activity, we repeated the same experiments on Gram-negative isolates in the presence of the permeabilizing agent polymyxin B nonapeptide (PMBN). The MIC values are summarized in Table 3.

Strain[a]	R profile[b]	AF		AF + PMBN		$Au(PEt_3)Cl$		$[Au(PEt_3)Cl]$ + PMBN		$[Au(PEt_3)Br]$		$[Au(PEt_3)Br]$ + PMBN	
		[μg mL^{-1}]	[μM]	[μg mL^{-1}]	[μM]	[μg mL^{-1}]	[μM]	[μg mL^{-1}]	[μM]	[μg mL^{-1}]	[μM]	[μg mL^{-1}]	[μM]
15	ESC^r NEM^r FQ^r AG^r	>32	>47.09	1	1.47	4	11.41	1	2.85	4	10.12	0.5	1.26
16	ESC^r NEM^r FQ^r AG^r COL^r	>32	>47.09	8	11.77	4	11.41	2	5.70	4	10.12	2	5.06
17	ESC^r NEM^r FQ^r AG^r	>32	>47.09	≤0.25	≤0.37	>8	>22.82	0.125	0.36	>8	>20.25	0.125	0.32
18	NEM^r FQ^r AG^r	32	>47.09	2	2.94	4	11.41	0.5	1.43	4	10.12	0.5	1.26
19	–[c]	16	>23.55	1	1.47	4	11.41	0.5	1.43	4	10.12	0.5	1.26

Strain[a]	R profile[b]	$[Au(PEt_3)I]$		$[Au(PEt_3)I]$ + PMBN		$[Au(PEt_3)_2]Cl$		$[Au(PEt_3)_2]Cl$ + PMBN		$K[Au(CN)_2]$		$K[Au(CN)_2]$ + PMBN	
		[μg mL^{-1}]	[μM]	[μg mL^{-1}]	[μM]	[μg mL^{-1}]	[μM]	[μg mL^{-1}]	[μM]	[μg mL^{-1}]	[μM]	[μg mL^{-1}]	[μM]
15	ESC^r NEM^r FQ^r AG^r	4	9.05	0.5	1.13	16	34.13	0.5	1.07	16	55.54	8	27.77
16	ESC^r NEM^r FQ^r AG^r COL^r	4	9.05	2	4.52	16	34.13	1	2.13	16	55.54	8	27.77
17	ESC^r NEM^r FQ^r AG^r	>8	>18.10	0.25	0.56	>32	>68.27	≤0.25	≤0.53	16	55.54	1	3.74
18	NEM^r FQ^r AG^r	4	9.05	0.5	1.13	8	17.07	0.5	1.07	16	55.54	8	27.77
19	–[c]	4	9.05	0.5	1.13	8	17.07	0.25	0.53	8	27.77	4	13.88

[a] Clinical strains: 15, *Escherichia coli* CV287; 16, *Klebsiella pneumoniae* KKBO4; 17, *Pseudomonas aeruginosa* Vr143/97; 18, *Acinetobacter baumannii* FI-13; 19, *Stenotrophomonas maltophilia* FI-14. [b] Resistance phenotype of the clinical strains; ESC^r, resistant to expanded-spectrum cephalosporins; NEM^r, resistant to carbapenems (imipenem and/or meropenem); FQ^r, resistant to fluoroquinolones (levofloxacin and/or ciprofloxacin); AG^r, resistant to aminoglycosides (gentamicin and/or amikacin and/or tobramycin); COL^r, resistant to colistin. [c] Strain with no reported resistance phenotypes.

Table 3. MIC [μg/mL and μM] values obtained for gold compounds in Gram-negative strains in the absence or presence of the permeabilizing agent polymyxin B nonapeptide (PMBN).

According to data reported in the literature, AF is poorly active against Gram-negative bacterial strains [10]. Although in general [Au(PEt_3)X] analogues, similarly to [Au(PEt_3)$_2$]Cl, show slightly greater activity than AF toward the six Gram-negative strains, their potency is still significantly lower than in Gram-positive isolates. The dicyano gold(I) complex was again the least active of the panel. However, if these gold compounds were administered in combination with the permeabilizing agent PMBN, a marked increase of the antibacterial effects was observed for AF and the [Au(PEt_3)X] series, as well as for [Au(PEt_3)$_2$]Cl, confirming that the difficulties in gold uptake reported for AF also arise with [Au(PEt_3)X] complexes. No significant increase of the antibacterial effects of K[Au(CN)$_2$] was observed in the presence of PMBN. This might offer indirect confirmation that the strong coordination of the cyanide ligand to the gold(I) center accounts for the weak antibacterial effects due to lack of ligand dissociation and of gold binding to bacterial targets. Interestingly, the MIC values determined for Pseudomonas aeruginosa Vr143/97 (strain 17) decreased markedly for all compounds if tested in the presence of PMBN, including the anionic dicyanide complex; this strong effect probably arises from the reported intrinsic higher susceptibility of this strain to PMBN [17]. Notably, a smaller decrease of MIC values in the presence of PMBN was observed for some compounds (e.g. AF and [Au(PEt_3)X]) for Klebsiella pneumoniae KKBO4 (strain 16); this strain shows a resistant phenotype to polymyxins (Table 3) owing to an alteration of the outer membrane lipopolysaccharide, that is also likely responsible for the lower susceptibility of this strain to the permeabilizing action of PMBN [18]. The above results and their implications prompted us to prepare a second set of compounds, strictly related to the gold panel, consisting of four distinct silver(I) complexes (Figure 1). The three silver compounds, of general formula [Ag(PEt_3)X], and the diphosphine cationic complex were prepared and characterized, as reported in the Experimental Section and in the Supporting Information. [Ag(PEt_3)X] complexes have been known for decades; studies carried out by Churchill et al. indicated that in the solid state these complexes possess a [Ag(PEt_3)X]$_4$ “cubane-like” skeleton of alternating silver and halogen [19]. By analogy with gold compounds, the solution behaviour of the silver complexes was assessed by NMR spectroscopy in dimethyl sulfoxide, phosphate-buffered saline (PBS) and in the presence of the media used for the biological experiments (details and spectra are reported in the Supporting Information). The studied complexes were highly stable both in organic solvents and in PBS. It should be noted that the ^{31}PNMR spectral linewidths of the silver complexes are larger than those of the corresponding gold complexes, this being an indication for the rapid equilibria that characterize silver compounds in solution and for a greater lability of ligands in the case of silver

complexes compared with gold ones. In addition, no evidence of $^{31}P–^{107/109}Ag$ coupling was found in our experimental conditions (i.e. at room temperature), which was further confirmation of the above interpretation [20]. Interestingly, if incubations were made in the Mueller–Hinton (MH) broth (the medium used for MIC determination), the ^{31}PNMR peaks converge toward a chemical shift of 37.20 ppm, indicating the formation of the same chemical species. This observation supports the view that silver compounds, in the presence of a high concentration of peptides and amino acids in the broth, rapidly react leading to the same species likely originating from the coordination of amino acid residues to the silver center. No evidence for precipitation was found in the experimental conditions used. From comparative analysis of the obtained results it is evident that silver compounds are less effective than gold compounds; this means that replacement of gold(I) with silver(I) results in a general decrease of the antibacterial potency (Table 4). This finding might be rather surprising in light of the well-known antimicrobial properties of silver compounds. However, the lower stability of the silver complexes in the biological medium revealed by the NMR experiments might account for this net decrease in biological effects. Also, it was observed that MIC values are similar for the $[Ag(PEt_3)X]$ series, with the exception of the cationic complex $[Ag(PEt_3)_2]NO_3$ for which the values are significantly larger.

Strain[a]	R profile[b]	[Ag(PEt$_3$)Cl]		[Ag(PEt$_3$)Br]		[Ag(PEt$_3$)I]		[Ag(PEt$_3$)$_2$]NO$_3$	
		[μg mL^{-1}]	[μM]	[μg mL^{-1}]	[μM]	[μg mL^{-1}]	[μM]	[μg mL^{-1}]	[μM]
1	Reference strain, wild type	0.25	0.96	0.25	0.82	0.5	1.42	8	16.72
2	OXA^r CL^r ERY^r LIN^r FQ^r AG^r	0.125	0.48	0.125	0.41	0.5	1.42	4	8.36
3	Reference strain, wild type	0.5	1.91	0.5	1.63	1	2.83	8	16.72
4	LIN^r	0.125	0.48	0.125	0.41	0.5	1.42	8	16.72
5	AG^r	0.125	0.48	0.25	0.82	0.25	0.71	8	16.72
6	–[c]	0.25	0.96	0.5	1.63	0.25	0.71	8	16.72
7	–	0.5	1.91	0.5	1.63	1	2.83	8	16.72
8	AMP^r VAN^r AG^r	0.5	1.91	0.5	1.63	1	2.83	8	16.72
9	AMP^r ESC^r	8	30.60	4	13.07	4	11.33	8	16.72
10	AMP^r	8	30.60	8	26.15	8	22.68	>8	>16.72
11	–	8	30.60	8	26.15	8	22.68	>8	>16.72
12	ESC^r CL^r AG^r	0.125	0.48	0.125	0.41	0.25	0.71	0.125	0.26
13	AMP^r CL^r AG^r	0.125	0.48	0.125	0.41	0.25	0.71	0.125	0.26
14	–	>8	>30.60	>8	>26.15	>8	>22.68	>8	>16.72

Table 4. MIC [μg/mL and μM] values obtained for silver compounds in Gram-positive strains and Candida albicans (strain 14). See Table 1 for strain features and notes.

This result can be explained by considering the nature of the ligands and the relative stability in the biological medium. Indeed, through comparative evaluation of the ^{31}PNMR spectra, it appears that after 72 h of incubation, complexes of the type [Ag(PEt_3)X] undergo quantitative conversion leading to the appearance of the same multiplet signal at 37.20 ppm, assignable to a species in which the halide ligands (or phosphine, to a minor extent), are replaced by sulfur or other coordinative atoms belonging to protein/peptides chains [20]. In Figure 3 are reported the spectra of Ag(PEt_3)Cl acquired at t_0 and after 72 h of incubation (Ag(PEt_3)Br and Ag(PEt_3)I show similar behaviour), in which is possible to observe the decreasing of the signal of Ag(PEt_3)Cl (10.51 ppm) with the rising of the specie at 37.20 ppm and a small formation of triethylphosphine oxide (peak at 61 ppm). On the contrary, for solutions of [Ag(PEt_3)$_2$]NO_3 incubated for 72 h, the peak assigned to the original species at 9.93 ppm is still strongly detected alongside the signal at 37.20 ppm (Figure 4). In this case, the peak assignable to triethylphosphine oxide (61 ppm) is clearly detectable even at t_0. Thus, even for the silver cationic complex, a ligand displacement process is likely to occur, that produces the same species as in the case of [Ag(PEt_3)X] compounds, with concomitant release of one triethylphosphine ligand that is oxidized to the corresponding oxide. However, in this latter case, the process is much slower. Next, the effects of silver compounds on the Gram-negative strains were studied (Table 5). The MIC values determined in Gram-negative strains, consistent with the findings on stability, reveal that all silver compounds exhibit similar antibacterial effects. Even in this case, the lowest activity was observed for the cationic complex. Interestingly, in contrast with the results obtained with the gold compounds (Table 3), for which a strong enhancement of the antibacterial effects was evident, the activity of the silver compounds in Gram-negative bacteria was weakly affected by pre-treatment with the permeabilizing agent. Again, this finding might reflect the chemical transformations of the silver complexes that occur in the biological medium.

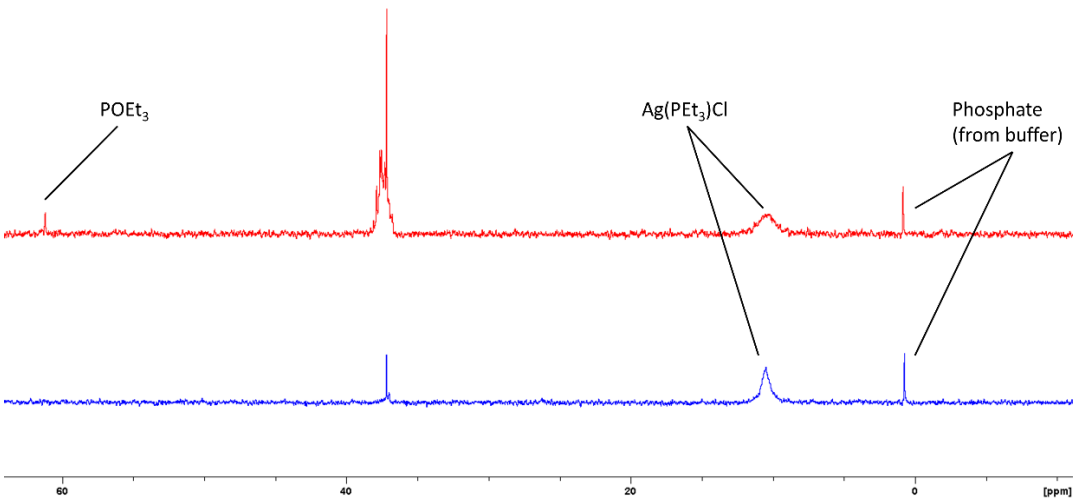

Fig.3: ^{31}PNMR analysis of $Ag(PEt_3)Cl$ (161.97 MHz, 298 K). Acquisition performed in a mixture of 250 µL MH Broth, 650 µL CH_3OH and 200 µL CD_3OD. The spectra were acquired at t_0 (blue) and after 72 h (red).

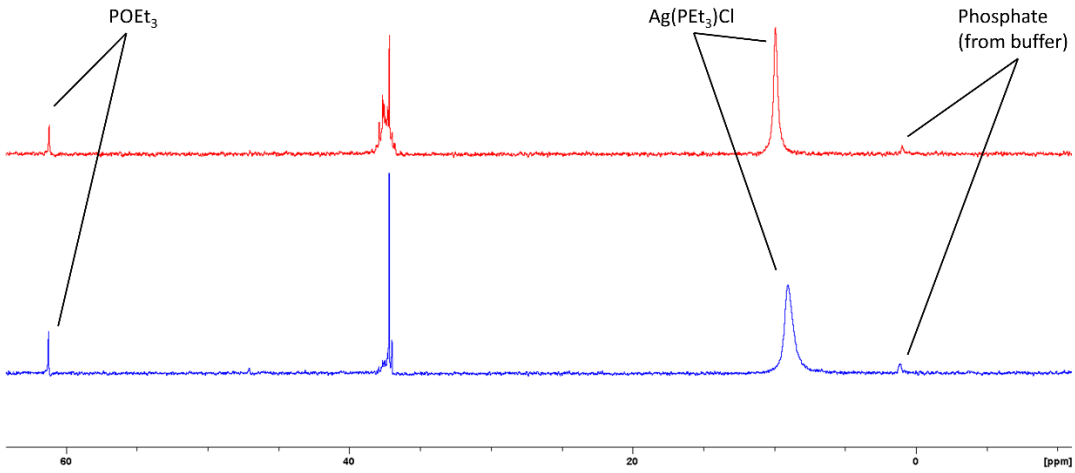

Fig.4: ^{31}PNMR analysis of $[Ag(PEt_3)_2]NO_3$ (161.97 MHz, 298 K). Acquisition performed in a mixture of 250 µL MH Broth, 650 µL CH_3OH and 200 µL CD_3OD. The spectra were acquired at t_0 (blue) and after 72 h (red).

Strain[a]	R profile[b]	[Ag(PEt$_3$)Cl]		[Ag(PEt$_3$)Cl] + PMBN		[Ag(PEt$_3$)Br]		[Ag(PEt$_3$)Br] + PMBN		[Ag(PEt$_3$)I]		[Ag(PEt$_3$)I] + PMBN		[Ag(PEt$_3$)$_2$]NO$_3$		[Ag(PEt$_3$)$_2$]NO$_3$ + PMBN	
		[μg mL^{-1}]	[μM]	[μg mL^{-1}]	[μM]	[μg mL^{-1}]	[μM]	[μg mL^{-1}]	[μM]	[μg mL^{-1}]	[μM]	[μg mL^{-1}]	[μM]	[μg mL^{-1}]	[μM]	[μg mL^{-1}]	[μM]
15	ESC^r NEM^r FQ^r AG^r	2	7.56	1	3.82	2	6.54	1	3.27	4	11.33	2	5.67	8	19.70	8	19.70
16	ESC^r NEM^r FQ^r AG^r COL^r	2	7.56	2	7.56	2	6.54	2	6.54	4	11.33	4	11.33	8	19.70	8	19.70
17	ESC^r NEM^r FQ^r AG^r	1	3.82	0.5	1.91	1	3.27	0.5	1.63	2	5.67	0.5	1.42	8	19.70	1	2.46
18	NEM^r FQ^r AG^r	0.5	1.91	0.5	1.91	0.5	1.63	0.5	1.63	2	5.67	1	2.83	2	4.92	2	4.92
19	–[c]	0.5	1.91	0.25	0.96	0.5	1.63	0.25	0.82	1	2.83	0.5	1.42	1	2.46	1	2.46

Table 5. MIC [μg/mL and μM)] values obtained for silver compounds in Gram-negative strains in the absence or presence of the permeabilizing agent polymyxin B nonapeptide (PMBN). See Table 3 for strain features and notes.

Conclusions

We have analysed the stability profiles in different conditions (organic solvent, PBS, biological media) and the antimicrobial properties on clinical isolates of a small group of neutral gold(I) or silver(I) complexes of the type $[M(PEt_3)X]$ (M=metal, X=halide), as well as of selected complexes bearing a positive or negative charge, that is, $[Au(PEt_3)_2]Cl$, $K[Au(CN)_2]$ and $[Ag(PEt_3)_2]NO_3$. Comparative analysis of the results allowed us to define the following structure–activity relationships:

1. The thiosugar ligand is not essential for the antimicrobial activity of AF and apparently does not favor an increased gold uptake.

2. The identity of the X ligand in the $[Au(PEt_3)X]$ series is not relevant for the activity; similar antimicrobial profiles were seen observed for the three homologous complexes.

3. The gold–diphosphine cationic complex is as active as the $[Au(PEt_3)X]$ derivatives, implying that the positive charge and the presence of two phosphine ligands are not functionally relevant features.

4. Altogether, the above results indicate the $[Au(PEt_3)]^+$ moiety as the "true pharmacophore" in this series of metal complexes; their antimicrobial activity probably arises from gold coordination to appropriate targets after ligand exchange.

5. The anionic $[Au(CN)_2]^-$ complex showed strongly reduced activity: this might be the consequence of the greater stability of the cyanide–gold bond.

6. Replacement of gold(I) with silver(I) causes a net reduction in the measured antimicrobial activity. This might be the consequence of the rather large instability of these complexes clearly detected in the MH broth. Alternatively, the observed reduction in antimicrobial effects might be due to a reduced ability of silver(I) to inhibit bacterial targets.

7. The susceptibility of Gram-negative strains to gold compounds is increased in the presence of a permeabilizing agent (PMBN), indicating that one of the mechanisms of resistance to these compounds in such pathogens is their reduced uptake.

8. Among the various possible protein targets, in analogy with the case of auranofin, thioredoxin reductase might represent a likely target even for the gold and silver analogues [21].

Thus, we have shown here that comparative analysis of the respective antimicrobial profiles is a valid tool for selecting the "best performers" to be further evaluated as

innovative and more efficient antimicrobial metal-based drugs. Hints were obtained toward deciphering the mechanism of action and designing better metal-based antimicrobial agents and drug combinations.

Experimental Section

Chemicals and reagents

Chemicals and reagents were purchased and used without further purification. Auranofin was obtained from Vinci-Biochem (Vinci, Italy). Chloro(triethylphosphine)gold(I) was purchased from Sigma–Aldrich.

NMR analysis

NMR experiments were performed on a Bruker Ultrashield 400 spectrometer. Calibration was made according to the residual peak of the solvent. Raw data were analyzed using Topspin software (Bruker). Spectra are available in the Supporting Information.

UV/Vis analysis

The spectrophotometric analysis of $K[Au(CN)_2]$ was performed on a Varian Cary 50 Bio UV/Vis spectrophotometer.

MIC value determination

MICs were determined using a standard broth microdilution assay on 96-well plates, as recommended by the Clinical and Laboratory Standards Institute [22]. Assays were performed in triplicate using cation-supplemented MH broth (Becton Dickinson, Franklin Lakes, NJ) and a bacterial inoculum of 5V104 CFU per well, in a final volume of 100 mL. AF and $[Au(PEt_3)X]$ and $[Ag(PEt_3)X]$ compounds were initially dissolved in DMSO and then diluted to the test concentrations in MH broth. Cationic diphosphine and anionic dicyano compounds were initially dissolved in sterile doubly distilled water and then diluted as described above. Results were recorded after 18–20h of incubation at 37 °C. For Gram-positive strains, the tested concentrations ranged from 0.062 to 8 mg/mL for all the substances. MICs for Gram-negatives for the tested compounds, alone or in the presence of the permeabilizing agent PMBN, were determined as described above for Gram-positive strains according to the Clinical and Laboratory Standards Institute. PMBN was used at a final concentration of 25 mg/mL [23]. For these strains, AF, $[Au(PEt_3)_2]Cl$ and $K[Au(CN)_2]$ were tested at concentrations from 0.25 to 32 mg/mL, whereas the other substances were tested at concentrations from 0.062

to 8 mg/mL. MICs were determined for all strains and compounds in at least three separate experiments. Main resistance phenotypes of the tested strains are shown in Tables 1–4.

Synthesis

[Au(PEt_3)Br]. According to a modified reported method [24], [Au(PEt_3)Cl] (48.6 mg) was stirred in N,N-dimethylformamide (3 mL) with KBr (5 equiv) at RT. After 18 h the mixture was dried under vacuum and the resulting solid was re-dissolved in a mixture of dichloromethane (10 mL) and demineralized H_2O (10 mL). The mixture was transferred into a separation funnel and more demineralized H_2O (10 mL) was added. After separation, the aqueous phase was again extracted with dichloromethane (10 mL). The recombined organic phase was then washed with saturated NaCl solution (20 mL), dried with Na_2SO_4, filtered and evaporated under reduced pressure. The crude product was re-dissolved in chloroform (3 mL), then diethyl ether (7 mL) and hexane (20 mL) were added. The flask was kept at -20 °C for 96 h to allow crystals to grow. Yield 73.6% (40.1 mg).

^{1}HNMR (CD_3OD, 400.13 MHz, 298 K): δ= 1.943 (dq, J_{HH}= 7.64 Hz, J_{HP}= 10.48 Hz, 6H), 1.215 (dt, J_{HH}= 7.60 Hz, J_{HP}= 19.12 Hz, 9H) ppm;

^{13}CNMR (CD_3OD, 100.61 MHz, 298 K): δ= 19.04 (d, J_{CP}= 36.45 Hz), 9.44 ppm;

^{31}PNMR (CD_3OD, 161.97 MHz, 298 K): δ= 36.38 ppm;

elemental analysis calcd (%) for $C_6H_{15}AuBrP$: C 18.24, H 3.83; found: C 18.36, H 3.55.

Au(PEt_3)I. [Au(PEt_3)Cl] (40 mg) was stirred in ethanol with KI (5 equiv) at RT. After 3 h, the mixture was dried under vacuum and the resulting white solid was kept at -20°C overnight. The product was then extracted five times with dichloromethane (3 mL). The recombined organic phase was washed three times with water (3 mL) and dried with $MgSO_4$. The solvent was evaporated under vacuum to a final volume of 3 mL, and the product was precipitated by addition of pentane (50 mL). After filtration, the white product was dried under vacuum overnight. Yield 70%.

^{1}HNMR (CD_3OD, 400.13 MHz, 298 K): δ= 1.955 (dq, J_{HH}= 7.68 Hz, J_{HP}= 10.44 Hz, 6H), 1.235 (dt, J_{HH}= 7.60 Hz, J_{HP} =19.12 Hz, 9H) ppm;

^{13}CNMR (CD_3OD, 100.61 MHz, 298 K): δ= 19.20 (d, J_{CP}= 34.55 Hz), 9.27 ppm;

^{31}PNMR (CD_3OD, 161.97 MHz, 298 K): δ= 41.17 ppm;

elemental analysis calcd (%) for $C_6H_{15}AuIP$: C 16.30, H 3.21; found: C 16.01, H 3.21, calcd H: 3.42.

$[Au(PEt_3)_2]Cl$. $[Au(PEt_3)Cl]$ (40 mg) was stirred at RT and under inert conditions (Schlenk technique) with a solution of triethylphosphine in tetrahydrofuran (1M, 1 mL, 10 equiv). After 3 h, stirring was stopped and the reaction mixture was kept under a flow of nitrogen overnight to evaporate both tetrahydrofuran and unreacted triethylphosphine. After evaporation, the product was recovered in the form of large colorless crystals. The crude product was dried under reduced pressure to remove all traces of unreacted materials. Yield 77 %.

^{1}HNMR (CD_3OD, 400.13 MHz, 298 K): δ= 2.055 (q, J_{HH}= 7.64 Hz, 12H), 1.264 (br s, 18H) ppm;

^{13}CNMR (CD_3OD, 100.61 MHz, 298 K): δ= 19.20 (br), 9.43 ppm;

^{31}PNMR (CD_3OD, 161.97 MHz, 298 K): δ= 47.83 ppm;

elemental analysis calcd (%) for $C_{12}H_{30}AuClP_2$: C 30.75, H 6.45; found: C 31.28, H 6.25.

$K[Au(CN)_2]$. WARNING: SOME STEPS IN THIS PROCEDURE INVOLVE THE FORMATION OF FULMINATING GOLD (EXPLOSIVE MATERIAL) AND USE OF KCN (HIGHLY TOXIC). According to a modified reported method [25], a solution of $HAuCl_4$ (1 M, 2.5 mL) was stirred in a beaker with aqueous NH_3 (3 M, 10 mL). The resulting suspension was gently warmed (at about 60 °C) for 3 h. The fulminating gold that formed was carefully filtered using a Buchner funnel and washed well with distilled water. To minimize the risk of explosions, in this step the fulminating gold was kept wet. The moist product was transferred into a beaker with the filter and distilled water (20 mL) was added. The suspension was stirred at RT, KCN (350 mg, 2.15 equiv) was added and the mixture turned quickly into a clear pale red solution. The white crystalline product was precipitated by evaporation by gently heating the solution with stirring. The crude product was then washed in a Buchner funnel with ethanol (2 mL) and dried under reduced pressure. Yield: 252.6 mg (35.1 %).

^{13}CNMR (D_2O, 100.61 MHz, 298 K): δ= 154.97 ppm;

UV/Vis: (10^{-4}M in PBS, pH 7.4): λmax=205, 212, 230, 240 nm;

Elemental analysis calcd (%) for $C2AuKN_2$: C 8.34, N 9.72; found: C 8.46, N 9.88.

[Ag(PEt3)Cl]. Under inert conditions, AgCl (200 mg) was added to a solution of PEt_3 in tetrahydrofuran (1M, 1.1 mL, 0.8 equiv). The heterogeneous mixture was stirred at RT

for 4 h, then the liquid phase was evaporated under reduced pressure. The crude product was suspended in dichloromethane (5 mL) and the solid was filtered off. The liquid phase was evaporated to afford the pure product (260 mg, 71.6 %).

^{1}HNMR (CD_3OD, 400.13 MHz, 298 K): δ= 1.764 (m, 6H), 1.193 (dt, J_{HH}= 7.66 Hz, J_{HP}= 17.96 Hz, 9H) ppm;

^{13}CNMR (CD_3OD, 100.61 MHz, 298 K): δ= 18.07 (d, J_{CP}= 18.70 Hz), 9.76 ppm;

^{31}PNMR (CD_3OD; 161.97 MHz, 298 K): δ= 8.83 ppm;

elemental analysis calcd (%) for $C_6H_{15}AgClP$: C 27.56, H 5.78; found: C 27.93, H 5.82.

[Ag(PEt3)Br]. Under inert conditions, AgBr (300 mg) was added to a solution of PEt_3 in tetrahydrofuran (1M, 1.2 mL, 0.8 equiv). The heterogeneous mixture was stirred at RT for 3 h, then the liquid phase was evaporated under reduced pressure. The crude product was suspended in dichloromethane (5 mL) and the solid was filtered off. The liquid phase was evaporated to afford the pure product (380 mg, 77.8 %).

^{1}HNMR (CD_3OD, 400.13 MHz, 298 K): δ= 1.747 (m, 6H), 1.193 (dt, J_{HH}= 7.65 Hz, J_{HP}= 17.73 Hz, 9H) ppm;

^{13}CNMR (CD_3OD, 100.61 MHz, 298 K): δ= 18.19 (br), 9.71 ppm;

^{31}PNMR (CD_3OD; 161.97 MHz, 298 K): δ= 6.68 ppm;

elemental analysis calcd (%) for $C_6H_{15}AgBrP$: C 23.56, H 4.94; found: C 23.73, H 5.33.

[Ag(PEt_3)I]. Under inert conditions, AgI (260 mg) was added to a solution of PEt_3 in tetrahydrofuran (1M, 0.9 mL, 0.8 equiv). The heterogeneous mixture was stirred at RT for 1.5 h, then the liquid phase was evaporated under reduced pressure. The crude product was suspended in dichloromethane (5 mL) and the solid was filtered off. The liquid phase was evaporated to afford the pure product (270 mg, 79.7 %).

^{1}HNMR ($CDCl_3$, 400.13 MHz, 298 K): δ= 1.664 (m, 6H), 1.169 (dt, J_{HH}= 7.99 Hz, J_{HP}= 15.98 Hz, 9H) ppm;

^{13}CNMR (CDCl3, 100.61 MHz, 298 K): δ= 18.53 (d, J_{CP}= 12.74 Hz), 10.39 ppm;

^{31}PNMR (CDCl3; 161.97 MHz, 298 K): δ= -8.39 ppm;

Elemental analysis calcd (%) for C6H15AgIP: C 20.42, H 4.28; found: C 20.51, H 4.36.

$[Ag(PEt_3)_2]NO_3$. Under inert conditions, $AgNO_3$ (162.1 mg) was added to a solution of PEt_3 in tetrahydrofuran (1M, 1.9 mL, 2 equiv). After a few seconds the solid was totally dissolved. The solution was stirred at RT for 2 h, then the solvent and the unreacted phosphine were removed under reduced pressure to give a viscous liquid (335.2 mg, 86.5 %).

^{1}HNMR (CD_3OD, 400.13 MHz, 298 K): δ= 1.787 (m, 12 H), 1.190 (br s, 18H) ppm;

^{13}CNMR (CD_3OD, 100.61 MHz, 298 K): δ= 17.85 (d, J_{CP}=12.55 Hz), 9.72 ppm;

^{31}PNMR (CD_3OD; 161.97 MHz, 298 K): δ= 8.49 ppm;

elemental analysis calcd (%) for $C_{12}H_{30}AgNO_3P_2$: C 35.48, H 7.44, N 3.45; found: C 35.79, H 7.47, N 3.30.

References

[1] T. G. Benedek, J. Hist. Med. Allied Sci. 2004, 59, 50 – 89.

[2] C. F. Shaw, III, Chem. Rev. 1999, 99, 2589 – 2600.

[3] S. Singh, R. Sivakumar, J. Infect. Chemother. 2004, 10, 307 – 315.

[4] J. A. Lemire, J. J. Harrison, R. J. Turner, Nat. Rev. Microbiol. 2013, 11, 371 – 384.

[5] N. Farrell in Metal Complexes as Drugs and Chemotherapeutic Agents from Comprehensive Coordination Chemistry II, Vol. 9 (Eds.: J. A. McCleverty, T. J. Meyer), Elsevier, Amsterdam, 2004, pp. 809 – 840.

[6] C. L. Ventola, P. T. 2015, 40, 277 – 283.

[7] a) M. I. Cassetta, T. Marzo, S. Fallani, A. Novelli, L. Messori, Biometals, 2014, 27, 787 – 791; b) J. P. Owings, N. N. McNair, Y. F. Mui, T. N. Gustafsson, A. Holmgren, M. Contel, J. B. Goldberg, J. R. Mead, FEMS Microbiol. Lett. 2016, 363, fnw148; c) Y. Hokai, B. Jurkowicz, J. Fernàndez-Gallardo, N. Zakirkhodjaev, M. Sanaffl, T. R. Muth, M. Contel, J. Inorg. Biochem. 2014, 138, 81 – 88; d) N. S. Torres, J. J. Abercrombie, A. Srinivasan, J. L. Lopez-Ribot, A. K. Ramasubramanian, K. P. Leung, Antimicrob. Agents Chemother. 2016, 60, 5663 – 5672; e) J. M. Madeira, D. L. Gibson, W. F. Kean, A. Klegeris, Inflammopharmacology 2012, 20, 297 – 306; f) L. Aguinagalde, R. Dìez-Martìnez, J. Yuste, I. Royo, C. Gil, 2. Lasa, M. Martìn-Fontecha, N. I. Marìn-Ramos, C. Ardanuy, J. Linares, P. Garcì, E. Garcì, J. M. Sànchez-Puelles, J. Antimicrob. Chemother. 2015, 70, 2608 – 2617; g) C. Roder, M. J. Thomson, Drugs R&D 2015, 15, 13 – 20.

[8] a) P. Hikisz, Ł. Szczupak, A. Koceva-Chyła, A. Gfflspiel, L. Oehninger, I. Ott, B. Therrien, J. Solecka, K. Kowalski, Molecules 2015, 20, 19699 – 19718; b) B.-J. Chen, N. S. Jamaludin, C.-H. Khoo, T.-H. See, J.-H. Sim, Y.-K. Cheah, S. N. A. Halim, H.-L. Seng, E. R. T. Tiekink, J. Inorg. Biochem. 2016, 163, 68 – 80; c) V. Andermark, K. Gçke, M. Kokoschka, M. A. Abu El Maaty, C. T. Lum, T. Zou, R. W.-Y. Sun, E. Aguilj, L. Oehninger, L. Rodr&guez, H. Bunjes, S. Wçlfl, C.-M. Che, I. Ott, J. Inorg. Biochem. 2016, 160, 140 – 148; d) L. Ortego, J. Gonzalo-Asensio, A. Laguna, M. D. Villacampa, M. C. Gimeno, J. Inorg. Biochem. 2015, 146, 19 – 27; e) A. AbdelKhalek, N. S. Abutaleb, K. A. Elmagarmid, M. N. Seleem, Sci Rep. 2018, 8, 8353.

[9] S. Jackson-Rosario, D. Cowart, A. Myers, R. Tarrien, R. L. Levine, R. Scott, W. T. Self, J. Biol. Inorg. Chem. 2009, 14, 507 – 519.

[10] T. Shankar, M. Haroon, A. F. N. Mostafa, T. J. P. Sobreira, V. E. Hedrick, L. N. Paul, M. N. Seleem, Sci. Rep. 2016, 6, 22571.

[11] S. E. Jackson-Rosario, W. T. Self, J. Bacteriol. 2009, 191, 4035 – 4040.

[12] S. E. Jackson-Rosario, W. T. Self, Metallomics 2010, 2, 112 – 116.

[13] a) B. M. Sutton, E. McGusty, D. T. Walz, M. J. DiMartino, J. Med. Chem. 1972, 15, 1095 – 1098; b) M. El-Etri, W. M. Scovell, Inorg. Chem. 1990, 29, 480 – 484; c) T. Marzo, D. Cirri, C. Gabbiani, T. Gamberi, F. Magherini, A. Pratesi, A. Guerri, T. Biver, F. Binacchi, M. Stefanini, A. Arcangeli, L. Messori, ACS Med. Chem. Lett. 2017, 8, 997 – 1001.

[14] a) M. J. Mays, P. A. Vergnano, J. Chem. Soc. Dalton Trans. 1979, 0, 1112 – 1115; b) G. Brauer, Handbook of Preparative Inorganic Chemistry, Academic Press, New York, 1965, pp. 1065 – 1066.

[15] L. Messori, L. Marchetti, L. Massai, F. Scaletti, A. Guerri, I. Landini, S. Nobili, G. Perrone, E. Mini, P. Leoni, M. Pasquali, C. Gabbiani, Inorg. Chem. 2014, 53, 2396 – 2403.

[16] M. C. Crudden, D. P. Allen, Coord. Chem. Rev. 2004, 248, 2247 – 2273.

[17] H. Tsubery, I. Ofek, S. Cohen, M. Fridkin, J. Med. Chem. 2000, 43, 3085 – 3092, and references therein.

[18] A. Cannatelli, M. M. D'Andrea, T. Giani, V. Di Pilato, F. Arena, S. Ambretti, P. Gaibani, G. M. Rossolini, Antimicrob. Agents Chemother. 2013, 57, 5521 – 5526.

[19] a) M. R. Churchill, B. G. DeBoer, Inorg. Chem. 1975, 14, 2502–2507; b) M. R. Churchill, J. Donahue, F. J. Rotella, Inorg. Chem. 1976, 15, 2752 – 2758.

[20] S. J. Berners-Price, R. K. Johnson, Al. J. Giovenella, L. F. Faucette, C. K. Mirabelli, P. J. Sadler, J. Inorg. Biochem. 1988, 33, 285–295.

[21] M. B. Harbut, C. VilchHze, X. Luo, M. E. Hensler, H. Guo, B. Yang, A. K. Chatterjee, V. Nizet, W. R. Jacobs, Jr., P. G. Schultz, F. Wang, Proc. Natl. Acad. Sci. USA 2015, 112, 4453–4458.

[22] Clinical and Laboratory Standards Institute, Methods for Dilution Antimicrobial Susceptibility Tests for Bacteria that Grow aerobically; Approved Standard—Tenth Edition, 2015, M07-A10, CLSI, Wayne, PA.

[23] D. Schneider, A. Schier, H. Schmidbaur, Dalton Trans. 2004, 1995–2005.

[24] P. Viljanen, M. Vaara, Antimicrob. Agents Chemother. 1984, 25, 701–705.

[25] P. M. Yangyuoru, J. W. Webb, C. F. Shaw, III, J. Inorg. Biochem. 2008, 102, 584 – 593.

5. Gold(I) compounds as promising chemotherapeutic agents

Introduction

Auranofin [2,3,4,6-tetra-o-acetyl-L-thio-β-D-glyco-pyranosato-S-(triethyl- phosphine)-gold(I)] (AF) is a clinically established oral chrysotherapeutic agent that is used for the treatment of some severe forms of rheumatoid arthritis [1]. During the past few years, this drug has attracted renewed attention in the medicinal chemistry scientific community as a prospective anticancer and antimicrobial agent according to innovative drug repurposing strategies [2−4]. In particular, AF has been, or still is, the object of clinical trials in the US as an anticancer agent [5,6]. We thought that selective and limited chemical modifications of AF might lead to a modulation and hopefully an improvement of its pharmacological profile. To this regard, it is worth reminding that Frank Shaw, on the ground of similar arguments, prepared and characterized a few years ago seleno-auranofin, a derivative of auranofin where the thiosugar ligand is replaced by the corresponding selenosugar ligand, and obtained remarkable biological results [7]. Accordingly, we decided to prepare a derivative of AF where the thiosugar ligand is replaced by one iodide ligand and to test this compound in comparison to AF and its commercially available chloride analogue. In principle, replacement of the thiosugar or chloride ligand with iodide should afford a compound of increased lipophilicity, thus enhancing drug bioavailability; at the same time, substitution of such a large ligand as thioglucose tetraacetate with a monatomic ligand, i.e., iodide, should not affect substantially the drug's pharmacological profile as the thiosugar ligand is believed to act mainly as a carrier ligand and, also, as a good leaving group, while the $[Au(PEt_3)]^+$ moiety is assumed to be the "true pharmacophore". In nice agreement with this view, previous studies showed that $Au(PEt_3)Cl$ manifests biological properties similar though not identical to those of AF [8].

Experimental

Synthesis

$Au(PEt_3)I$ was synthesized as described in Chapter 4 starting from commercially available $Au(PEt_3)Cl$. A logP value of 4.6 was found for $Au(PEt_3)I$ making this complex by far the most lipophilic of the series. Indeed, logP values of 1.7 and 1.6 were, respectively measured for $Au(PEt_3)Cl$ and AF (see chapter 2 for details on the method for logP

determination). Single crystals of Au(PEt_3)I, suitable for X-ray diffraction studies, were obtained by adding pentane to a concentrated solution of the compound in dichloromethane. The solution was kept at −20 °C for 1 week. After this time needle-shaped crystals were formed (Figure 1).

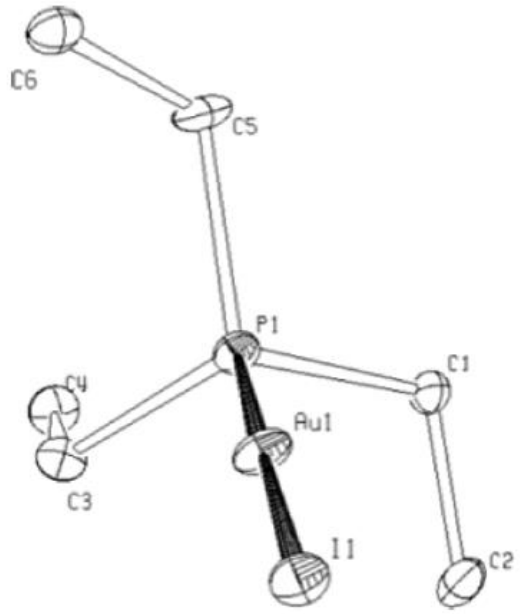

Fig.1: X-ray structure of complex Au(PEt_3)I. The gold(I) ion is linearly coordinated to the I(1) and P(1) atoms, with distance of 2.5898(1) and 2.268(2) Å, respectively. The angle P(1)−Au(1)−I(1) is 178.89(6)°.

The crystal structure was solved to 0.73 Å resolution. The geometry as well as the distances reported in Figure 1 are in good agreement with bond lengths and angles found in similar compounds retrieved from the CSD (v. 5.37 February 2016). It is worth reminding that the Au−I bond length generally increases as the hindrance of the substituents of the P atom decreases (P-tBu_3, P-iPr_3, P-Et_3 of 2.56, 2.58, and 2.59 Å, respectively) [9].

TrxR inhibition assay

Thioredoxin reductase activity was determined by measuring the ability of the enzyme to directly reduce DTNB in the presence of NADPH. Rat liver TrxR (Sigma-Aldrich) was diluted with water to a concentration of 60 nM (2 U/mL). Aliquots of 25 µl of the enzyme solution were preincubated, for 5 min at 37°C, with 25 µl of 0.1 M K-phosphate

buffer pH 7.0, 5 mM EDTA and 0.25 mM NADPH, containing different concentrations of the gold complexes (from 1 µM to 1 nM). Afterwards, the reaction was started with 1 mM DTNB and monitored spectrophotometrically at 412 nm, for about 10 min. The noninterference of the compounds with assay components was confirmed by negative control experiments with enzyme-free solution. The IC50 values are the complex concentration decreasing the enzyme activity to 50%reported as means ± SD of three experiments, each carried out in duplicate.

Melting tests

The melting profiles of different DNA/drug mixtures were obtained by the absorbance data of the system (ShimadzuUV-2450 double-beam spectrophotometer) at different temperatures and 260 nm. The temperature is changed (ca. 3 °C increase each point) by means of the thermostatic bath connected to the spectrophotometer. Its exact value inside the cell department is measured through a digital thermometer. The explored range was between 63 °C and 96 °C. After each temperature change, the system is left to equilibrate for 30 min.

Viscosimetric measurements

Viscosity measurements were done using a Micro-Ubbelohde viscometer whose temperature is controlled by a thermostat (25 ± 0.1 ºC). Time of flow is measured by a digital stopwatch; the data used for each sample are the average of at least five repeated experiments (error within 5%). In all the measurements DNA concentration was kept constant at $2.5x10^{-5}$ M, whereas the drug concentration is varied in the $0 \leq rb \leq 1.0$ range. Each sample/mixture was left to equilibrate for 72h to ensure reaction completion. Particular case was devoted to the procedure of capillary cleaning and drying after each measurement. The sequence water –acetone – water – ethanol – N2 flux is used. The DNA elongation is evaluated as the cubic root of the relative viscosity $\eta/\eta^\circ = (t-t_{solv})/(t_{DNA}-t_{solv})$ where t, t_{solv} and t_{DNA} are the efflux times in the capillary viscometer of the mixture, of the buffer (NaCl 0.1M, NaCacodylate 0.01M, pH 7) and of DNA alone respectively. Note that, under the described reaction condition, the efflux times are in the order of 8 minutes, so that small changes can be measured with high accuracy.

Assessments of Acute toxicity in vivo for $Au(PEt_3)I$

5-week-old, female athymic mice (Envigo) have been treated with $Au(PEt_3)I$ to assess acute toxicity of this potential anticancer Au-based drug. For this test was used the following protocol: intraperitoneal injections 2 time/week (3 weeks treatment) on three different groups (each of three mice). Each group was treated with a different dose of $Au(PEt_3)I$ (10, 15 and 30 mg/Kg). After the three weeks of treatment, mice were monitored for an additional week to find possible changes in their behaviour indicating stress or sufferance due to the drug administration. Sacrifice of mice was made at the end of the protocol through preliminary injection of anesthetic (Avertin). The efficacy of the anesthetic was properly tested and verified. Afterward, dissection of mice and collection of organs (i.e. liver, kidneys and spleen) was carried out.

Results and Discussion

$Au(PEt_3)I$ was investigated for its chemical and biological properties in solution in comparison to AF and $Au(PEt_3)Cl$. The solution behaviour of the three species was mainly assessed by ^{31}PNMR spectroscopy. The three compounds were solubilized in trizma base/CH_3COOH, 6 mM, in the presence of 250 µL of H_2O; 650 µL of CH_3OH; 200 µL of CD_3OD, pH 7, and analysed at increasing time intervals. Notably, all three compounds manifest a high stability for several hours with no evidence of ligand detachment. Indeed, changes in the ^{31}PNMR spectra could only be detected after very long incubation times. For $Au(PEt_3)I$, no changes were seen after 72 h; however, after 1 week of incubation, beside the signal falling at 41 ppm (assigned to the phosphorus in the neutral complex), a new signal of low intensity appeared at 47 ppm. This new signal is attributed to phosphorus in the cationic monocharged complex $[Au(PEt_3)_2]^+$, which is likely formed through rearrangement, according to the equilibrium (Scheme 1) [10, 11].

Scheme 1: Ligand Scrambling Reaction of $Au(PEt_3)I$.

The signal increases in intensity until day 14; no further changes in intensity were detected afterward, even after 35 days, indicating that the reaction has reached its equilibrium (Figure 2 for details).

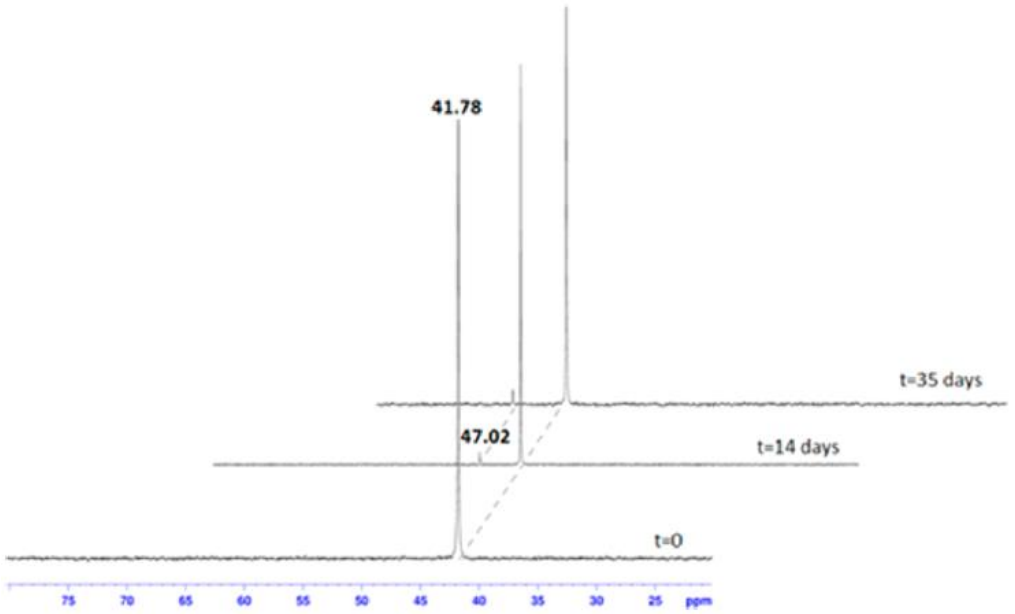

Fig.2: ^{31}PNMR spectra (trizma base/CH_3COOH 6 mM in a mixture of 250 µL of H_2O; 650 µL of CH_3OH; 200 µL of CD_3OD, pH 7) of $Au(PEt_3)I$ recorded at different time intervals.

Formation of $[Au(PEt_3)_2]^+$ was independently confirmed treating $Au(PEt_3)I$ with $AgNO_3$, under the same solution conditions, and then analysing the reaction products by ^{31}PNMR and HR ESI-MS at different times intervals. When recording a ^{31}PNMR spectrum immediately after treatment with $AgNO_3$ we found only a signal falling at 30.43 ppm assignable to $[Au(PEt_3)(H_2O)]^+$ species [12]. After five days, a new ^{31}PNMR spectrum was recorded on the same sample: beside the signal at 30.43 ppm, a new one at 47.85 ppm was detected and assigned to the monopositive cation complex $[Au(PEt_3)_2]^+$. Further confirmation came from ESI-MS analysis. In the spectrum recorded five days after treatment with $AgNO_3$, we found three main signals at 315.1, 333.1, and 433.15 Da assignable, respectively, to the three species $[Au(PEt_3)]^+$, $[Au(PEt_3)(H_2O)]^+$, and $[Au(PEt_3)_2]^+$. Attributions were validated through theoretical simulation of the various species. Finally, to obtain an additional proof that the ^{31}PNMR signal at 47 ppm corresponds to formation of $[Au(PEt_3)_2]^+$ species, we synthesized this complex by treatment of $Au(PEt_3)Cl$ with an excess of triethylphosphine. The ^{31}PNMR analysis of

the resulting product confirmed the obtainment of the desired compound and, accordingly, our assignment (see chapter 4 for further details on the synthesis and NMR spectrum). A quite different situation was found for the ^{31}PNMR spectra of AF and Au(PEt_3)Cl, for which no significant changes were detected even after 35 days of incubation. However, all three compounds show a large stability in solution even when incubated in the presence of NaCl 0.9% as well as in 10 mM PBS buffer, rendering them well suitable for pharmacological testing and application. Next, the antiproliferative properties of the three complexes were measured in vitro against HCT8, HCT116, HT29, and Caco2, four representative cell lines of colorectal cancer (CRC) as well as on HDF (human fibroblast, adult) and HEK293 (human embryonic kidney) cell lines. As displayed in Table 1, all three drugs produce potent cytotoxic effects on the selected CRC cell lines with IC50 values always falling in the 100−700 nM range. Au(PEt_3)I is slightly less cytotoxic than the other two gold complexes.

Complex	**HCT8**	**HCT116**	**HT29**	**Caco2**	**HDF**	**HEK293**
AF	132 ± 16	180 ± 17	359 ± 35	465 ± 53	>5000	>5000
Au(PEt_3)Cl	105 ± 11	154 ± 22	122 ± 15	560 ± 93	>5000	>5000
Au(PEt_3)I	260 ± 28	290 ± 36	318 ± 90	706 ± 232	>5000	>5000

Table 1: IC50 Values (nM) Determined for Au(PEt_3)I, AF, and Au(PEt_3)Cl (24 h Incubation).

In any case, the presence of the thiosugar ligand is not an essential requirement for the cytotoxic action [13], in line with expectations. In addition, upon considering the close similarity in the measured IC50 values, substantial differences in the cellular uptake are unlikely. Remarkably, measuring the cytotoxic effects on two normal cell lines, HDF human fibroblast cells (adult) and HEK293 human embryonic kidney (Table 1), no cytotoxic effect was found for the three study complexes in the range 0−5000 nM. Next, in view of the fact that thioredoxin reductase (TrxR) is a likely important target for AF [14], we have comparatively quantified the inhibitory potency of the three drugs toward this enzyme. Results are summarized in Table 2.

Complex	IC50 (nM)
AF	105 ± 17.3
Au(PEt_3)Cl	51.3 ± 8.5
Au(PEt_3)I	193 ± 22.2

Table 2: Thioredoxin Reductase Activity Assay. IC50 values (nM) were determined treating 2 U/L of TrxR with aliquots of AF, Au(PEt_3)Cl, and Au(PEt_3)I (from 1 μM to 1 nM). Results are reported as average value for three independent experiments ± SD.

It is interesting to note that the obtained IC50 values for TrxR inhibition are in line with those obtained for the cytotoxic effects on CRC cell lines (Table 1). This might imply that the observed cytotoxic effects are somehow related to the ability of these gold complexes to bind and inhibit TrxR. Moreover, results highlight and confirm that Au(PEt_3)Cl is not only the most potent cytotoxic agent but also the most potent TrxR inhibitory agent of the series, though IC50 values for AF and Au(PEt_3)I still fall in the nanomolar range. To better characterize the mechanistic aspects of the interactions occurring between these gold compounds and probable biological targets, we have studied their reactions toward the model protein lysozyme (HEWL) and the GG rich oligonucleotide CTACGGTTTCAC (ODN) through ESI-MS analysis. Notably, upon replacing the thiosugar ligand with a halide ligand, e.g., chloride or iodide, we observed a net change in metallodrug reactivity toward HEWL. Indeed, AF interacts appreciably with HEWL, apparently through formation of noncovalent adducts, where the neutral intact drug is bound to the protein (Figure 3); in contrast, both iodide and chloride derivatives do not react with HEWL even after long incubation times.

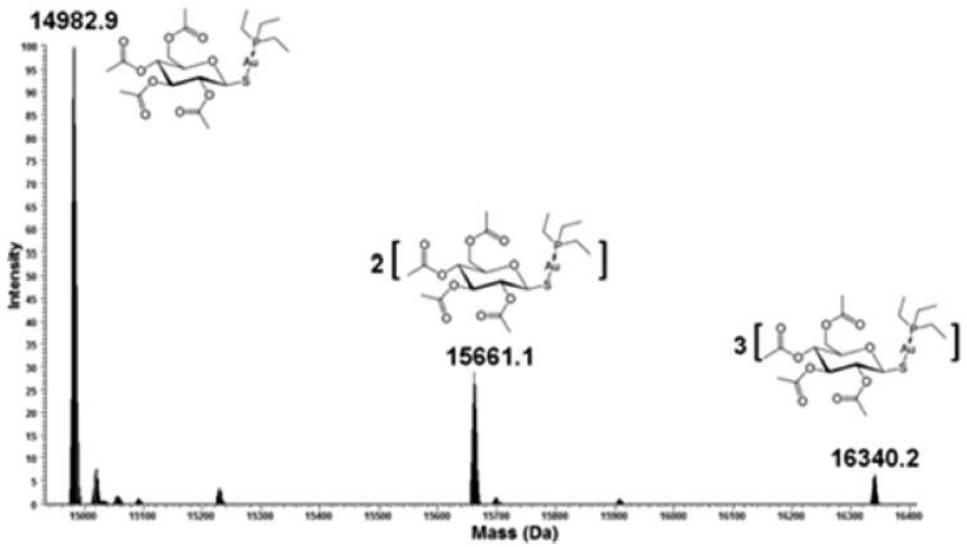

Fig.3: Close-up of deconvoluted ESI-MS spectrum (positive mode) of AF incubated 72 h (37 °C) with HEWL (10^{-4} M) in ammonium acetate buffer, 20 mM, pH 6.8; metal to protein ratio (3:1), 3% DMSO.

This different behaviour might be ascribed to a crucial role of the thiosugar ligand in forming noncovalent protein adducts. Conversely, replacement of the thiosugar ligand with halide ligands greatly enhances reactivity toward oligonucleotide. In fact, both $Au(PEt_3)I$ and $Au(PEt_3)Cl$ coordinate this target through selective release of halide ligands roughly in the same manner (Figure 4); also, similar amounts of the corresponding adducts are formed.

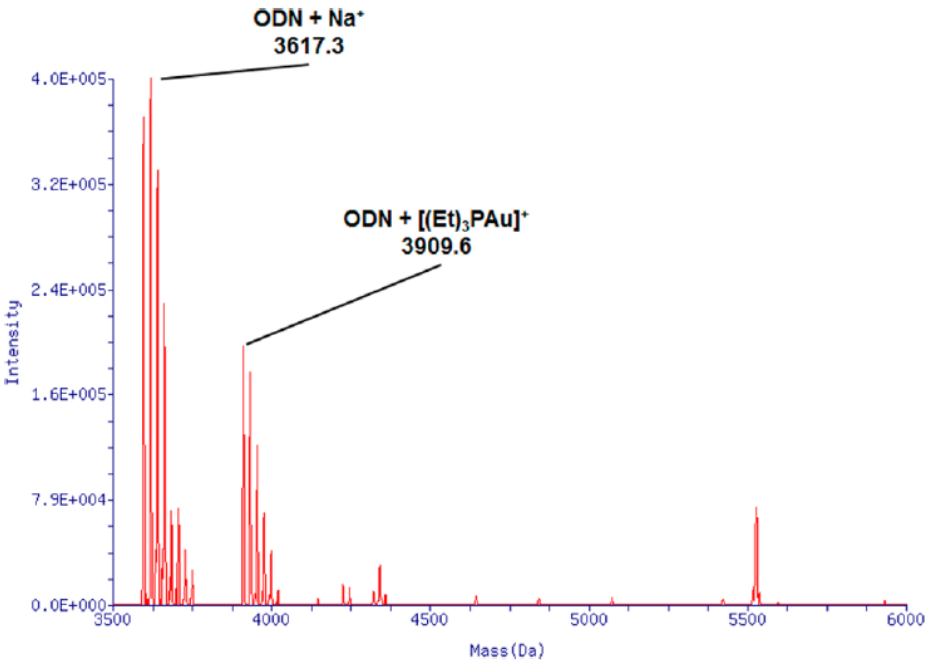

Fig.4: Deconvoluted ESI-MS spectrum (negative mode) of $Au(PEt_3)I$ incubated 72 h (37 °C) with ODN (10^{-4} M) in LC–H_2O metal to protein ratio (3:1), 3% DMSO.

In contrast, when performing the same experiment with AF, no adduct formation with ODN was observed; this finding is relevant even considering that AF does not react with double helix DNA as previously reported by Mirabelli and coworkers [15], and the same kind of reactivity is preserved toward the single strand ODN model. Notably, when AF is incubated with ODN, it only produces a main peak at 923 m/z assignable to the species in Figure 5, as previously reported [16].

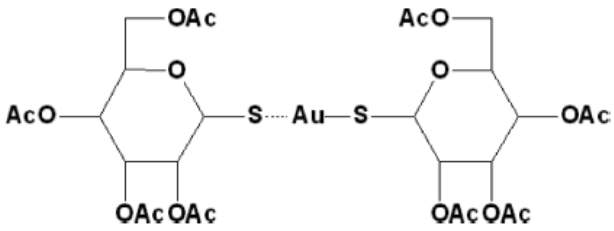

Fig.5: Structure of the main specie produced by AF: structure corresponds to the peak at 923 m/z.

Encouraged by the results obtained with ss ODN, the possible interactions of AF analogues with double-stranded DNA (more precisely, calf thymus DNA) were comparatively investigated by the ethidium bromide (EtBr) assay. DNA is first saturated with the EtBr probe producing a fluorescent intercalation complex (while free dye is non-emissive).

Then, increasing amounts of the drug are added: a fluorescence decrease indicates progressive EtBr displacement and build-up of drug–DNA interactions [17, 18]. We found, indeed, that both $Au(PEt_3)Cl$ and $Au(PEt_3)I$ produce a net fluorescence decrease, while AF does not (Figure 5).

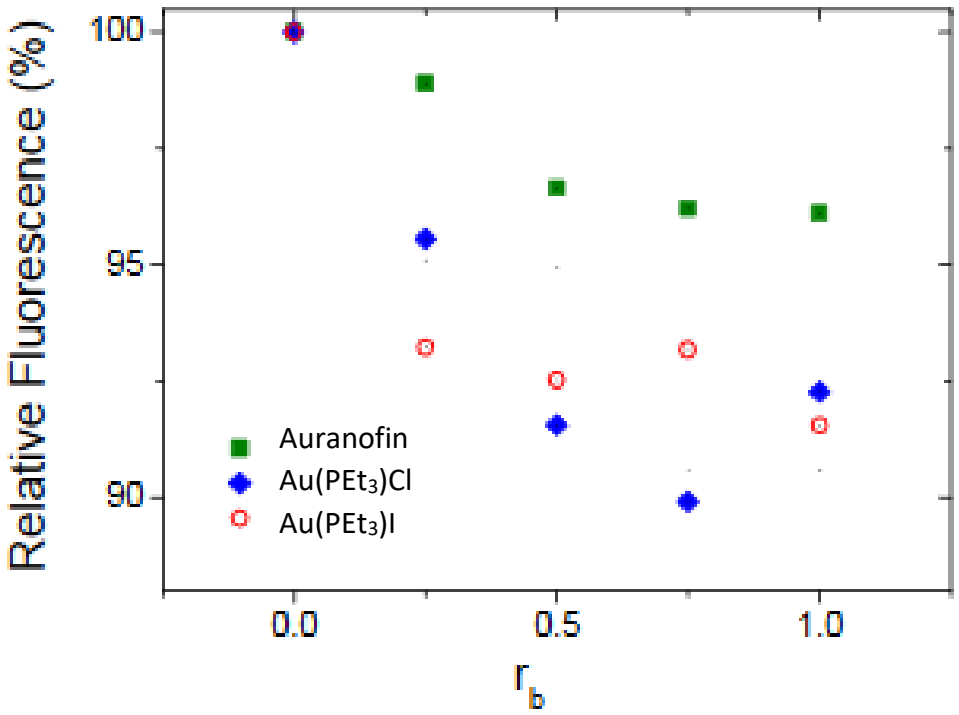

Fig.6: DNA interaction investigated through EtBr displacement.

The emission decrease is limited, in agreement with the non-intercalative nature of the binding, yet significant. Melting temperatures (the temperature of the inflection point of the sigmoid melting profile) of drug–DNA mixtures do not vary appreciably from

those of DNA alone (changes in the melting temperatures are in the range ±2 °C in agreement with monodentate coordination of the drug to DNA strands; Fig.7).

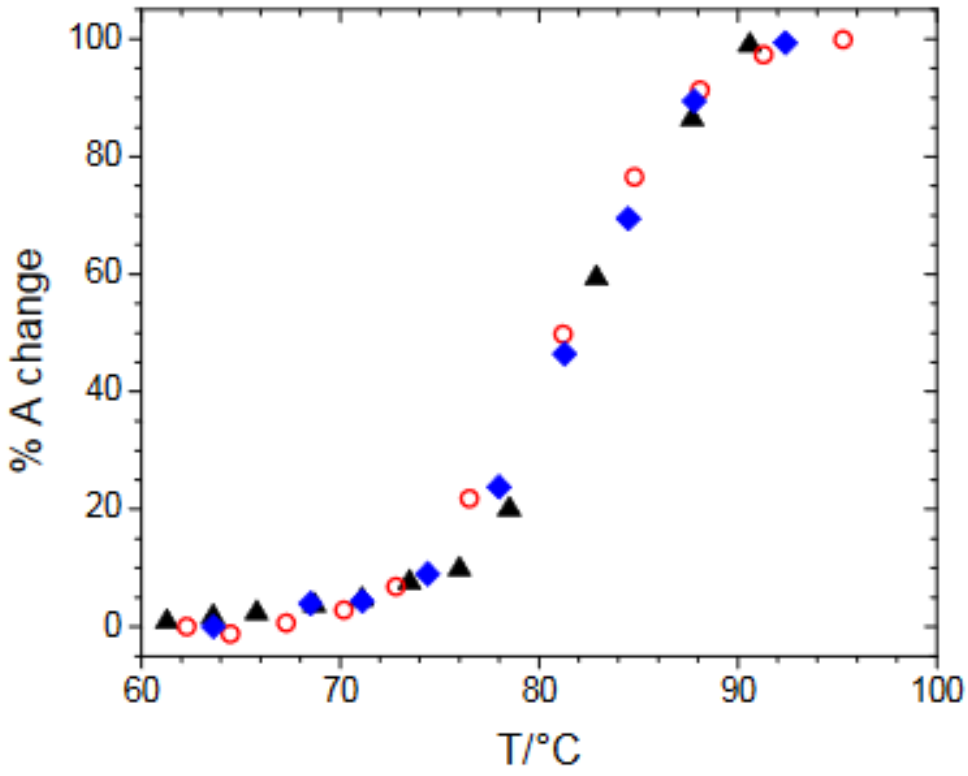

Fig.7: Melting profiles of DNA/AF (triangles), DNA/Au(PEt_3)Cl (diamonds) and DNA/Au(PEt_3)I (circles). [C] DNA = $2.5x10^{-5}$ M, rb = 1.0 in all cases, NaCl 0.1M + NaCacodylate 2.5 mM buffer, pH 7). Melting temperatures were respectively 81.5 °C, 82.1 °C and 81.1 °C.; percentage of absorbance change at 260 nm reported in the plot is calculated as % A change = $100 \times (A - A_0)/(A_\infty - A_0)$ where A is the value read at any temperature, whereas A_0 and A_∞ are the values of the two, respectively initial and final, plateaus as calculated by the sigmoidal fit). The melting temperature of DNA alone was measured and found to be 82.3 °C.

This result is in agreement with the covalent binding of the Au(I) metal ion to one filament as this binding feature is not supposed to significantly alter the energy needed for strands separation. Conversely, viscosity undergoes significant changes for

Au(PEt_3)Cl/DNA and Au(PEt_3)I/DNA systems compared to the control (Figure 8), suggesting that the bound drugs significantly affect the helix flexibility. This strong effect, which is not observed upon AF addition, confirms that the Auranofin analogues manifest a reactivity significantly different from AF and are able to bind ds-DNA.

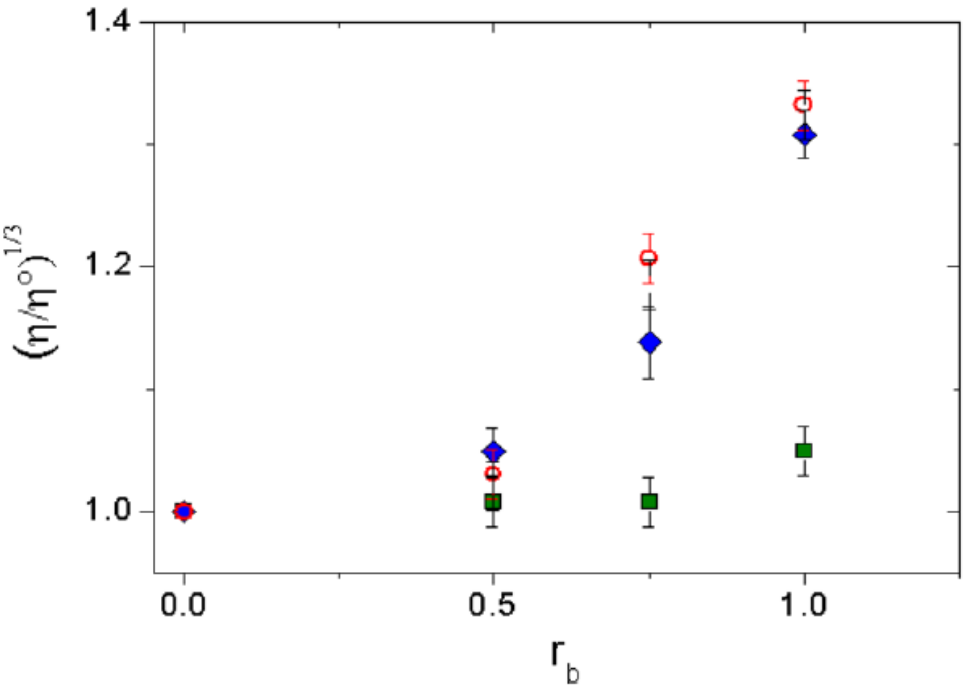

Fig.8: Viscometric plots (25 °C) for Au(PEt_3)I/DNA (open circles), Au(PEt_3)Cl/DNA (diamonds), and AF/DNA (squares) systems. rb = [drug]/[DNA] (base pairs), [DNA] = 2.5 × 10^{-5} M, $\eta/\eta^\circ = (t - t_{solv})/(t_{DNA} - t_{solv})$ where t, t_{solv}, and t_{DNA} are the efflux times in the capillary viscometer of the mixture, of the buffer (NaCl 0.1 M, Na−cacodylate 0.01 M, pH 7) and of DNA alone, respectively.

Finally, in vivo acute toxicity experiments for Au(PEt_3)I were carried out to assess whether this complex is tolerated in murine model. Three doses were tested (i.e., 10, 15, and 30 mg/kg) on three groups of animals (each group consisted in three mice). The weight and the behaviour of mice was monitored every day during all the treatment, and there was no evidence for weight loss; also, no evidence for loss of appetite and mobility reduction were found. Remarkably, neither microscopic or macroscopic alteration was found in liver, kidneys, and spleen. Obtained results highlight that the

treatment has been well tolerated in murine models and that the toxicity profile of this drug is low and similar to that reported for AF [19].

Conclusions

Similarly to AF and $Au(PEt_3)Cl$, $Au(PEt_3)I$ shows a high stability under physiological-like conditions while manifesting a far greater lipophilic character. Interestingly, $Au(PEt_3)I$ retains the large cytotoxic effects of AF and $Au(PEt_3)Cl$ toward four representative CRC cell lines, with the measured IC50 values still falling in the nanomolar range and no cytotoxic effect on human fibroblast cell line and human embryonic kidney cells. This implies that the presence of the thiosugar moiety is not mandatory for the pharmacological action. The TrxR assay reveals that both $Au(PEt_3)Cl$ and $Au(PEt_3)I$ retain the potent inhibitory action of AF (nanomolar range), being consistent with their observed cytotoxic effect, with AF and $Au(PEt_3)Cl$ slightly more active than $Au(PEt_3)I$. However, mechanistic differences were highlighted among the three investigated gold complexes with both $Au(PEt_3)I$ and $Au(PEt_3)Cl$ being unreactive toward HEWL but capable of binding to a standard ss-ODN sequence and to ds-DNA. At variance, AF can bind noncovalently to the model protein but does not form coordinative adducts to ssODN and does not bind calf thymus DNA. In our opinion, the present results are of particular interest for the following reasons:

1. Substitution of the thiosugar with iodide and chloride “tunes” the reactivity of these compounds for model biological targets rendering them more selective toward oligo and polynucleotides. At variance from AF, where the tetraacetate-thiosugar moiety allows formation of noncovalent adducts with lysozyme, this kind of binding is not observed in the cases of $Au(PEt_3)I$ and $Au(PEt_3)Cl$. Yet, it is worth reminding that even AF is not able to form coordinative bonds to HEWL. Binding of gold(I) metal center to histidine and methionine residues of lysozyme was previously described mainly as a naked cation [20]; but this does not occur for AF and its analogues due to the very high stability of the ligands and their steric hindrance. Furthermore, these differences in reactivity toward the model protein HEWL do not correlate with their strong inhibitory power toward TrxR, being this latter aspect most probably related with the very high affinity of gold for the selenium donor and thus for the selenocysteine residue.

2. The enhanced reactivity of the gold(I) center toward the model oligonucleotide and the double helix DNA upon replacement of the thiosugar ligand with halide ligands may be the result of the greater lability of the gold−halide bond compared to the gold−sulfur bond [13]; the guanine residue of nucleic acids that is highly accessible may “assist”

halide detachment. Yet, this augmented reactivity for DNA molecules does not lead to enhanced cytotoxic effects. This might support the view that AF and also its halido analogues exert their strong cytotoxic effects mainly through DNA-independent mechanisms [21].

3. The in vivo acute toxicity test carried out in a murine model, for the treatment with the complex $Au(PEt_3)I$, does not show any side effects, and the treatment has been well tolerated. This evidence is of great significance and warrants further preclinical assessments.

Overall, these findings are of significant interest if one considers that even small differences in biomolecular reactivity may result in large differences in the respective pharmacodynamic and pharmacokinetic profiles. In addition, the far greater lipophilic character of $Au(PEt_3)I$ might lead to an enhanced bioavailability of the latter drug.

References

[1] Shaw, C. F., III Gold-Based Therapeutic Agents. Chem. Rev. 1999, 99, 2589−2600.

[2] Cassetta, M. I.; Marzo, T.; Fallani, S.; Novelli, A.; Messori, L. BioMetals 2014, 27, 787−791.

[3] Fiskus, W.; Saba, N.; Shen, M.; Ghias, M.; Liu, J.; Gupta, S. D.; Chauhan, L.; Rao, R.; Gunewardena, S.; Schorno, K.; Austin, C. P.; Maddocks, K.; Byrd, J.; Melnick, A.; Huang, P.; Wiestner, A.; Bhalla, K. N. Cancer Res. 2014, 74, 2520−2532.

[4] Madeira, J. M.; Gibson, D. L.; Kean, W. F.; Klegeris, A. Inflammopharmacology 2012, 20, 297−306.

[5] Phase I and II Study of Auranofin in Chronic Lymphocytic Leukemia (CLL). https://clinicaltrials.gov/ct2/show/NCT01419691.

[6] Auranofin in Treating Patients with Recurrent Epithelial Ovarian, Primary Peritoneal, or Fallopian Tube Cancer. https://clinicaltrials.gov/ct2/show/NCT01747798.

[7] Hill, D. T.; Isab, A. A.; Griswold, D. E.; DiMartino, M. J.; Matz, E. D.; Figueroa, A. L.; Wawro, J. E.; DeBrosse, C.; Reiff, W. M.; Elder, R. C.; Jones, B.; Webb, J. W.; Shaw, C. F., III Inorg. Chem. 2010, 49, 7663−7675.

[8] Sutton, B. M.; McGusty, E.; Walz, D. T.; DiMartino, M. J. J. Med. Chem. 1972, 15, 1095−1098.

[9] Allen, F. H. Acta Crystallogr., Sect. B: Struct. Sci. 2002, B58, 380−388.

[10] Ahmad, S.; Isab, A. A. Inorg. Chem. Commun. 2001, 4, 362−364.

[11] Ahmad, S.; Isab, A. A. J. Inorg. Biochem. 2002, 88, 44−52.

[12] El-Etri, M. M.; Scovell, W. M. Inorg. Chem. 1990, 29, 480−484.

[13] Mirabell, C. K.; Johnson, R. K.; Hill, D. T.; Faucette, L. F.; Girard, G. R.; Kuo, G. Y.; Sung, C. M.; Crooke, S. T. J. Med. Chem. 1986, 29, 218−223.

[14] Cox, A. G.; Brown, K. K.; Arner, E. S.; Hampton, M. B. Biochem. Pharmacol. 2008, 76, 1097−109.

[15] Mirabelli, C. K.; Sung, C. M.; Zimmerman, J. P.; Hill, D. T.; Mong, S.; Crooke, S. T. Biochem. Pharmacol. 1986, 35, 1427−1433.

[16] Albert, A.; Brauckmann, C.; Blaske, F.; Sperling, M.; Engelhard, C.; Karst, U. J. Anal. At. Spectrom. 2012, 27, 975−981.

[17] Biver, T.; Secco, F.; Tinè, M. R.; Venturini, M.; Bencini, A.; Bianchi, A.; Giorgi, C. J. Inorg. Biochem. 2004, 98, 1531−1538.

[18] Marzo, T.; Pillozzi, S.; Hrabina, O.; Kasparkova, J.; Brabec, V.; Arcangeli, A.; Bartoli, G.; Severi, M.; Lunghi, A.; Totti, F.; Gabbiani, C.; Quiroga, A. G.; Messori, L. Dalton Trans. 2015, 44, 14896−14905.

[19] Auranofin SDS (Safety Data sheet); Cayman Chemical, revision 10/15/2014, according to regulation (EC) No. 1907/2006 as amended by (EC) No. 1272/2008.

[20] Ferraro, G.; Massai, L.; Messori, L.; Cinellu, M. A.; Merlino, A. BioMetals 2015, 28, 745−754.

[21] Rigobello, M. P.; Scutari, G.; Boscolo, R.; Bindoli, A. Br. J. Pharmacol. 2002, 136, 1162−1168.

6. Au(PEt_3)I complex: *in vivo* studies for the treatment of ovarian cancer

Introduction

Encouraged by the results set out in chapter 5, we decided to extend the studies upon *in vivo* models. Moreover, Auranofin (AF) is generally reputed as a reasonably safe drug for human use, even for long chronic treatments [1,2]. On the ground of its antiparasitic and anticancer properties [3-10], AF in the course of the last years has entered many distinct clinical trials, two of them (ovarian and lung cancer) still ongoing and one (leukemia) closed [11−13]. Results of these trials have not been disclosed yet. At the same time, considerable evidence has been gathered that a few specific biomolecular targets such as the enzyme thioredoxin reductase, the proteasome system, the NF-κB pathway and other transcription factors, are crucially involved in mediating the cellular effects of AF as well of other gold (I/III) compounds [14−18]. It has been hypothesized, and then demonstrated, that the biological and pharmacological properties of AF might be kept and hopefully improved/modulated by replacing the thiosugar ligand with other ligands such as various halides. In principle, replacement of the thiosugar ligand with halide ligands may lead to an increased lipophilicity and an enhanced drug bioavailability and biodistribution. However, this modification should not affect substantially the drug's pharmacological profile, as the invariant $[Au(PEt_3)]^+$ moiety is assumed to be the "true pharmacophore" whereas the thiosugar ligand is believed to act mainly as a carrier ligand [18]. Accordingly, the actions of iodido(triethylphosphine)gold(I) complex, Au(PEt_3)I (AFI), and AF, have been comparatively analysed toward ovarian cancer models both in vitro and in vivo. AFI is obtained by replacement of the thiosugar ligand with an iodide ligand according to the reported synthetic procedures [18] (see chapter 4 for detailed synthesis and characterization). The chemical structures of AF and AFI are shown in Figure 1.

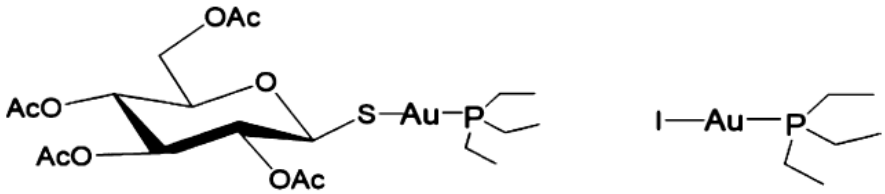

Fig.1: Chemical structures of Auranofin and AFI.

Experimental

Chemical

Auranofin has been purchased from Vinci Biochem srl. AFI was synthesized and characterised as described in Chapter 5.

Assessment of cell death by flow cytometry

Cell death was analysed by TACS Annexin V/PI Kit (Trevigen) according to the manufacturer's instructions. Briefly, control, AF, and AFI A2780-treated treated cells for 72 h with 72 h-exposure IC50, were trypsinized, washed with PBS and resuspended in staining solution for 15 min in the dark. Cells were analysed by FACSCanto flow cytometer (BD Biosciences). Gated cells were plotted on a dot-plot showing Annexin-V staining and propidium iodide (PI) staining. Percentage of apoptotic/necrotic cells was determinate adding Annexin V positive (early apoptotic) cells to Annexin/PI positive ones (late apoptotic) and to PI positive cells (necrotic cells).

Assessment of caspase activity by flow cytometry

For Caspase-3 activity determination control, Auranofinand Et3PAuI A2780-treated cells for 72 h with 72 h-exposure IC50, were trypsinized, washed with PBS and resuspended in FAM-FLICATM Caspases solution (Caspase FLICA kit FAM-DEVD-FMK, ImmunoChemistry Technologies) for 1 h at 37°C, following the manufacturer's instruction. Cells were washed with PBS and analysed by FACSCanto flow cytometer (BD Biosciences).

Cell growth inhibition studies (Sulforhodamine B assay)

The cytotoxic effects of the complexes were evaluated on the growth of A2780. Both compounds were initially diluted in DMSO as stock solutions (20 mM), further dilutions have been performed in PBS (0.5% DMSO present at the higher tested concentration). Exponentially growing cells were seeded in 96-well microplates at a density of $5*10^3$ cell/well. After cell inoculation, the microtiter plates were incubated under standard culture conditions (37°C, 5% CO_2, 95% air and 100% relative humidity) for 24 h prior to the addition of study compounds. After 24 h, the medium was removed and replaced with fresh medium containing drug concentrations ranging from 0.003 to 100 µM for a continuous exposure of 24 and 72 h for both study compounds. For comparison purposes the cytotoxicity effects of cisplatin measured in the same experimental conditions were also determined. According to the procedure the assay was terminated by the addition of cold trichloroacetic acid (TCA). Cells were fixed in situ by

10% TCA and stained by sulforhodamine B (SRB) solution at 0.4% (w/v) in 1% acetic acid. After staining, unbound dye was removed by washing five times with 1% acetic acid and the plates were air dried. Bound stain was subsequently solubilized with 10 mM tris base, and the absorbance was read on an automated plate reader at a wavelength of 540 nm. The IC50 drug concentration resulting in a 50% reduction in the net protein content (as measured by SRB staining) in drug treated cells as compared to untreated control cells was determined after 72 h of drug exposure.

Tolerability studies

Nude mice were randomly grouped according to their body weight with four mice per test substance, which was administered intraperitoneally using two different doses (20 mg/kg and 40 mg/kg). The complexes have been solubilized in DMSO and then diluted in bidistillated water with 5% DMSO present in the final solution. Only one administration was performed, followed by a three weeks observation period; in this time, we monitored daily possible signs of toxicity including weight loss, mobility reduction, dehydration, hunched posture, ruffled fur, and loss of appetite or lethargy. Animals were euthanized if their body weight loss exceeded 15% within the first 24 h after treatment or 20% at any other point in the study.

Biodistribution studies

For the assessment of biodistribution of AF, AFI and, nude mice (female 5 weeks old) were randomly grouped according to their body weight with three mice per test substance, which was administered with intraperitoneal injection using a single dose (10 mg/kg). Mice from each group were anesthetized, bled, and sacrificed, and organs dissected (spleen, liver, kidney, heart) at 24 hours. After blood collection, tissues were weighed and solubilized, and the amount of gold in each tissue was determined through ICP-AES analysis after mineralisation with HNO_3. The determination of gold concentration in the blood or in the organs was performed by a Varian 720-ES Inductively Coupled Plasma Atomic Emission Spectrometer (ICP-AES) equipped with a CETAC U5000 AT+ ultrasonic nebulizer, in order to increase the method sensitivity. Before the analysis, samples were weighed in PE vials and digested in a thermo-reactor at 80 °C for 24 h with 2 mL of HNO_3 (35 % suprapure grade) 0.5 mL of H_2O_2 suprapure grade. After digestion, the samples were diluted to 6 mL with ultrapure water (≤18 MΩ). 5.0 mL of each sample were spiked with 1 ppm of Ge used as an internal standard and analysed. Calibration standards were prepared by gravimetric serial dilution from a commercial standard solution of Au at 1000 mg L^{-1}. The wavelength used for Au determination was 267.594 nm whereas for Ge the line at 209.426 nm was used. The

operating conditions were optimized to obtain maximum signal intensity, and between each sample, a rinse solution of HNO_3 (35 % suprapure grade) was used in order to avoid any “memory effect”.

Results and discussion

Replacement of the thiosugar ligand with iodide results into a greatly increased lipophilic character (a logP value of 4.6 has been measured by ICP-AES in the chapter 5) with respect to both $Au(PEt_3)Cl$ and AF (this latter compound has been previously described and used experimentally for rheumatoid arthritis treatment) [19] for which logP values of 1.7 and 1.6 were measured, respectively [18]. In spite of that, AFI is still appreciably soluble in aqueous solutions, where it manifests a very high stability as documented by a previous systematic NMR analysis, carried out in different environments including biological media [18,20]. As reported in Figure 2, ^{31}PNMR results clearly demonstrate a high stability of AFI, with no changes in the structure of the molecule, even in the presence of a large excess of sodium chloride (up to 100 mM).

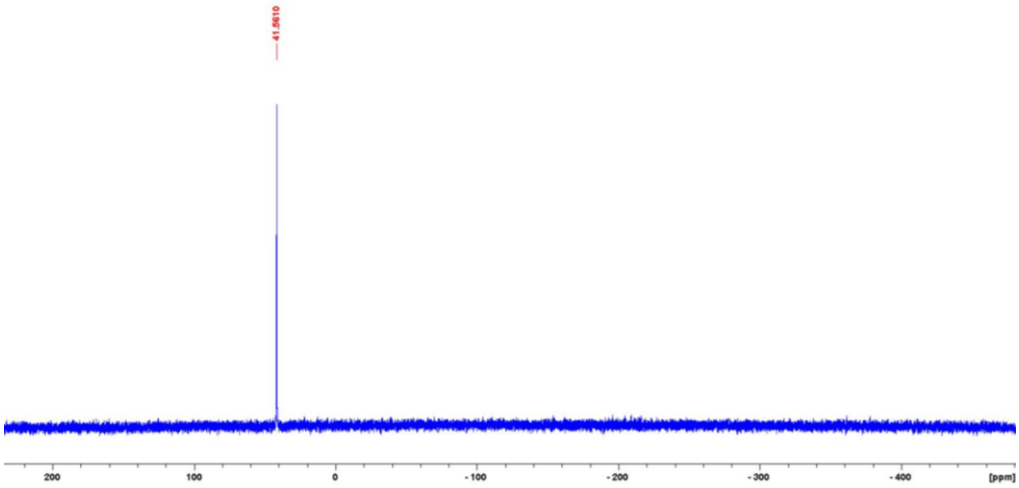

Fig.2: ^{31}PNMR spectrum recorded after incubation (24h) of AFI in 250 μL MeOD + 250 μL NaCl 100mM. The signal detected at 41.56 ppm is in agreement with previous characterizations (see chapter 4).

The documented stability in physiological-like conditions makes the compound an ideal candidate for biological testing. The antiproliferative properties of AFI compared to AF have been investigated in vitro toward A2780 human ovarian cancer cells. As displayed

in Table 1, both compounds produce potent cytotoxic effects with IC_{50} values falling in the high nanomolar range.

	IC_{50} (μM) ± SD		
cell lines	Et_3PAuI	Auranofin	cisplatin
A2780	0.394 ± 0.174	0.754 ± 0.139	1.53 ± 0.66

Table 1: Inhibitory effects of AF, AFI, and Cisplatin on A2780 cells following 72 h drug exposure as determined by the Sulforhodamine B assay.

AFI is slightly more cytotoxic than AF and both result more effective than cisplatin, the well-known anticancer metal compound. These results are consistent with those previously obtained in colon cancer cell lines for the same gold compounds and recently published literature [18] further supporting the concept that the presence of the thiosugar ligand is not an essential requirement for the cytotoxic action and that substantial differences in the cellular uptake, despite the difference in the logP value, between AFI and AF are unlikely to occur. Remarkably, in agreement with a previous observation [18] no appreciable cytotoxic effects were detected for AFI in normal cell lines, i.e., human fibroblasts (HDF cell line) and human embryonic kidney cells (HEK293) over the concentration range 0−5000 nM. Then, we examined whether AFI and AF are able to induce apoptosis in A2780 cells; accordingly, we performed flow cytometry analysis of annexin V/propidium iodide-stained A2780 cells, treated with these two gold compounds, at the respective IC50 values, for 72 h. As shown in Figure 3A, the percentage of apoptotic cells in AF- and AFI-treated samples is significantly increased (control vs AF, $p = 0.0121$; control vs AFI, $p = 0.0107$).

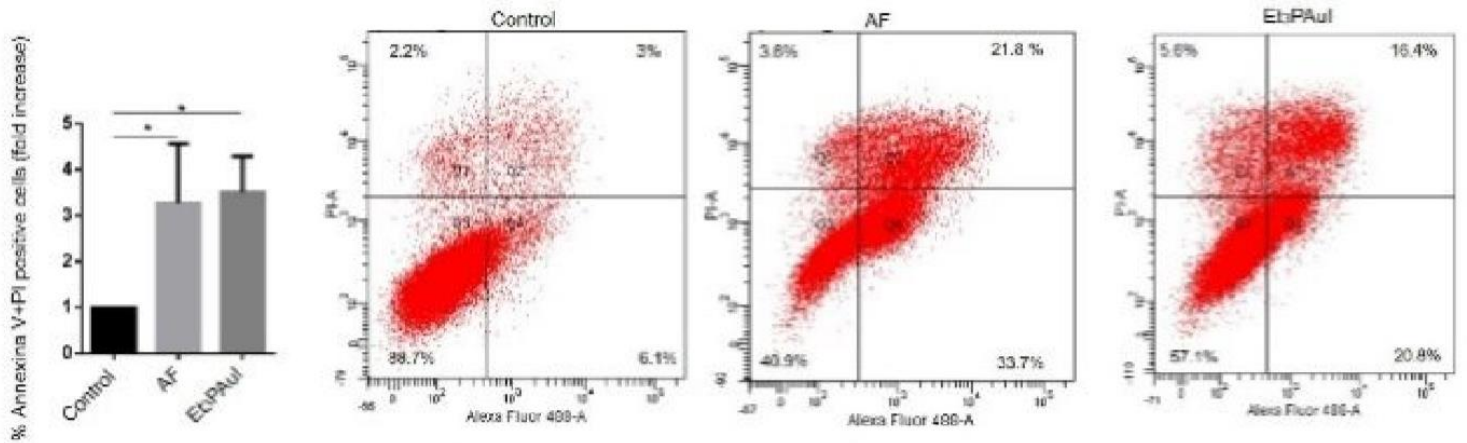

Fig.3A: Gold compounds exert apoptosis induction in A2780 cell line. Flow cytometry analysis of annexin V/propidium iodide-stained A2780 cells treated for 72 h with gold compounds at the respective IC50 values. The histogram reports the mean fold increase of apoptotic/necrotic cells (A+/PI-, A+/PI+ and A/PI+ cells) respect to control conditions. Representative dot plots were shown in the panels on the right.

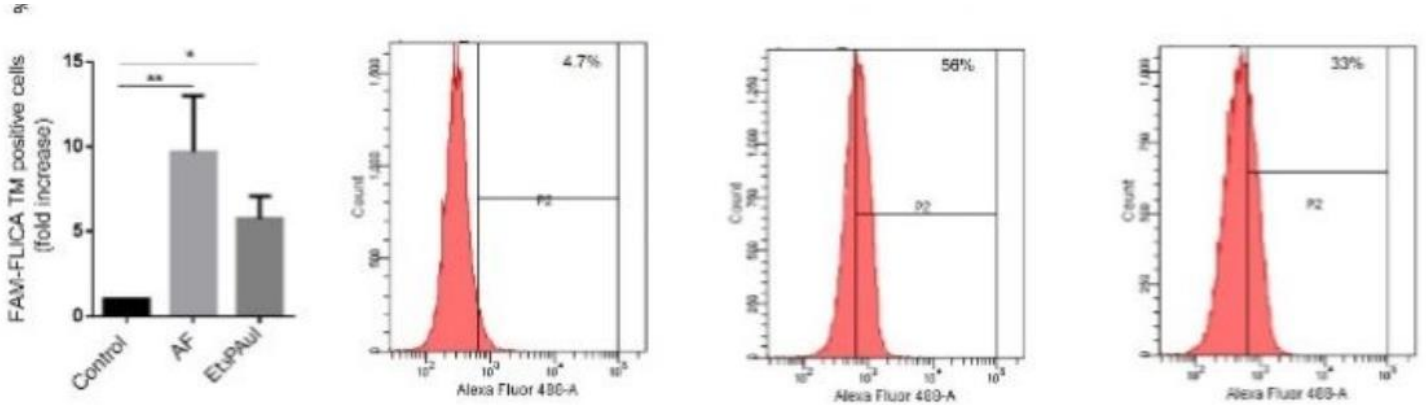

Fig.3B: Caspase-3 Assay of A2780 cells treated with gold compounds at the respective IC50 values for 72 hours. The histogram reports the fold increase of FAM-FLICATM positive cells (P2) respect to control cells. Representative dot plots were shown in the panels on the right.

In order to evaluate and quantitate apoptosis via caspase activity, we checked the activity of caspase 3 by FAM-FLICA Caspase-3 Assay Kit (Fig.3B). Four independent experiments were performed for both assays reported in Fig.3A and Fig.3B. The statistical analysis was carried out using one-way ANOVA test followed by Tuckey's multiple comparisons test using Graphpad Prism v 6.0 (*$p<0.05$, **$p<0.01$). The induction of apoptosis observed for AF and its iodide analogue may be related with the strong thioredoxin reductase inhibition potency. Indeed, the IC_{50} values for the inhibition of the enzyme are generally in nice agreement with cytotoxicity values [18]. The results collected evidenced that both gold compounds induce apoptosis through a caspase 3 activation, with AF being slightly more effective than AFI (control vs AF, $p = 0.0037$; control vs AFI, $p = 0.04$). AFI was subsequently evaluated in vivo in comparison to AF in two different ovarian cancer models, i.e., a xenograft subcutaneous and an orthotopic model. Preliminarily, drug tolerability studies were carried out to assess the in vivo safety of AFI. The single-dose tolerability was evaluated in athymic nude mice over a 3-week observation period. AFI was administered by intraperitoneal (ip) injection using two different doses (20 and 40 mg/kg). Only a single administration was performed, followed by a 3-week observation period; animals were controlled daily, and no signs of sufferings such as weight loss, mobility reduction and appetite reduction were registered. In addition, a pilot singlicate study for gold biodistribution has been carried out and a generalized higher accumulation for AFI, both in organs and in the peripheral blood, was highlighted (Figure 4).

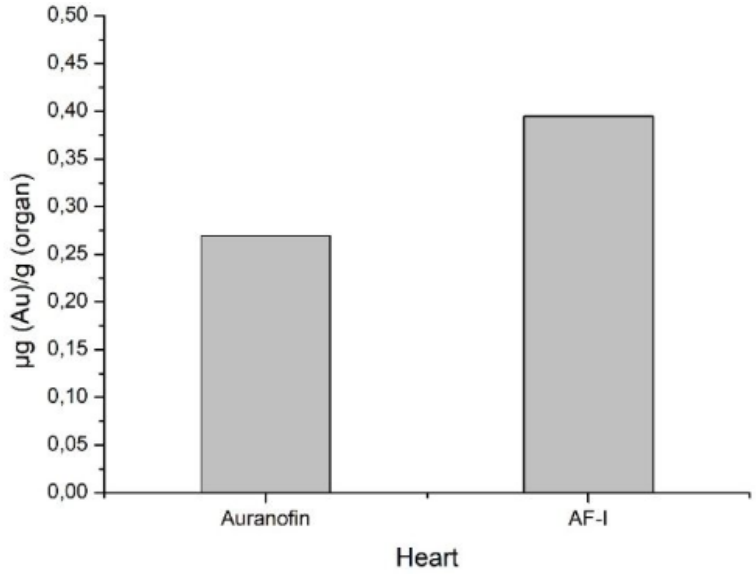

Fig.4A: Biodistribution plots for Auranofin and AFI.

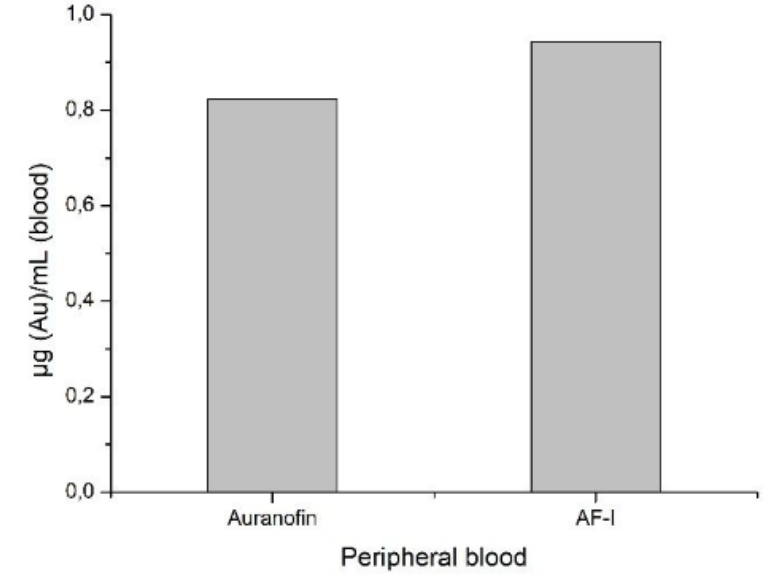

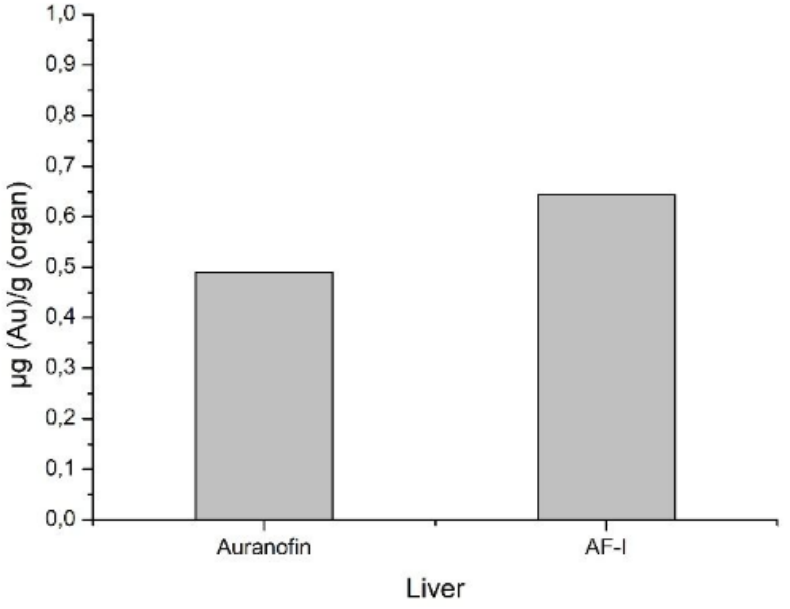

Fig.4B: Biodistribution plots for Auranofin and AFI.

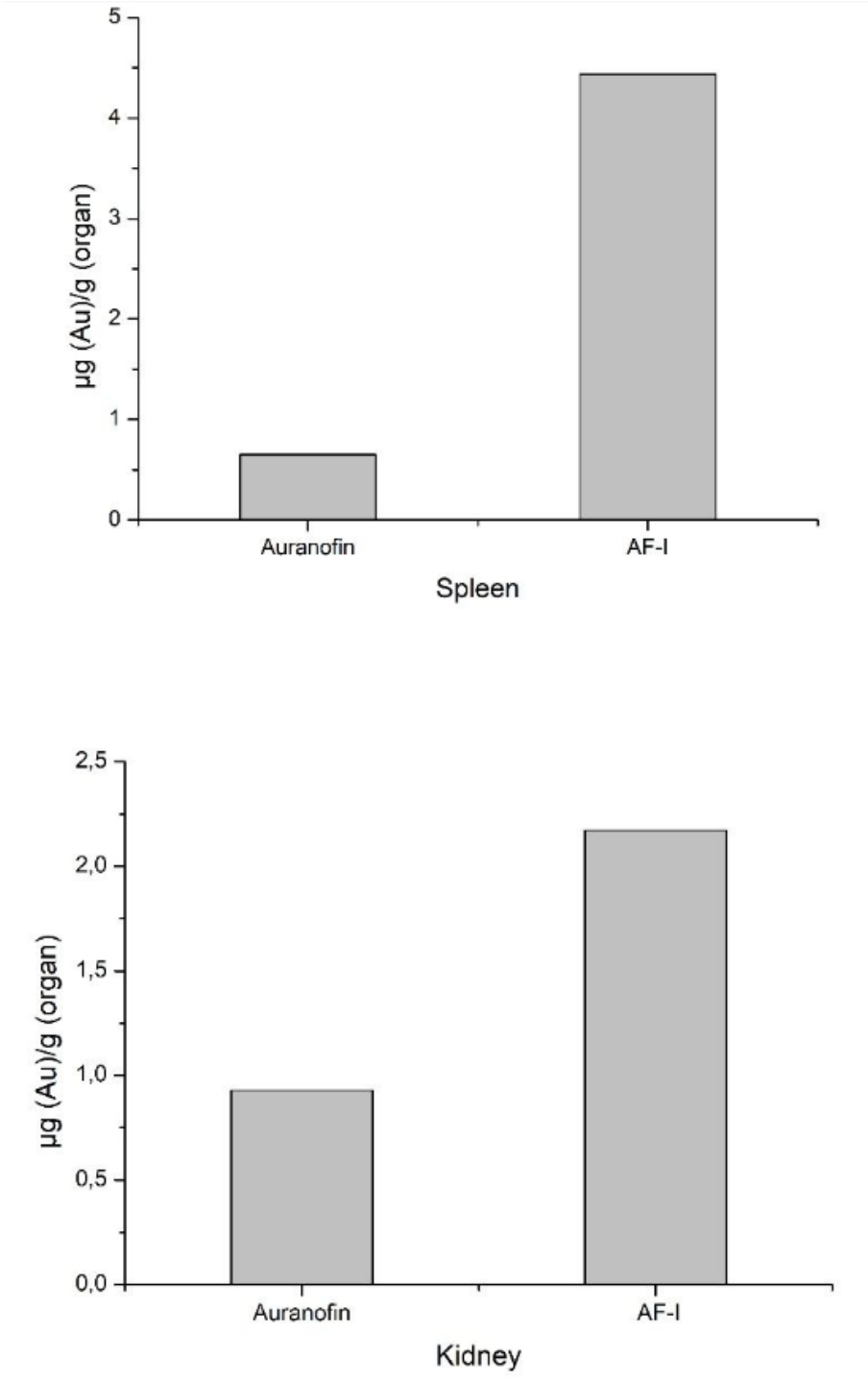

Fig.4C: Biodistribution plots for Auranofin and AFI.

Based on the above observations, we can hypothesize that the detected differences in the in vivo activity of the two compounds could be due to their different lipophilic character leading to an enhanced bioavailability and more favourable pharmacokinetics for AFI. The xenograft model consisted of $1x10^6$ A2780 cells implanted subcutaneously (sc) in both flanks of the animals. The growth of the tumor masses was measured daily with caliper and the treatment started when the volume of the masses reached 60 mm^3. The treatment was performed by intraperitoneal injections (three times a week for 2 weeks of treatment) of AF and AFI, both 15 mg/kg. The growth of the tumor masses was monitored over 21 days and time course is shown in Figure 5A and 5B respectively.

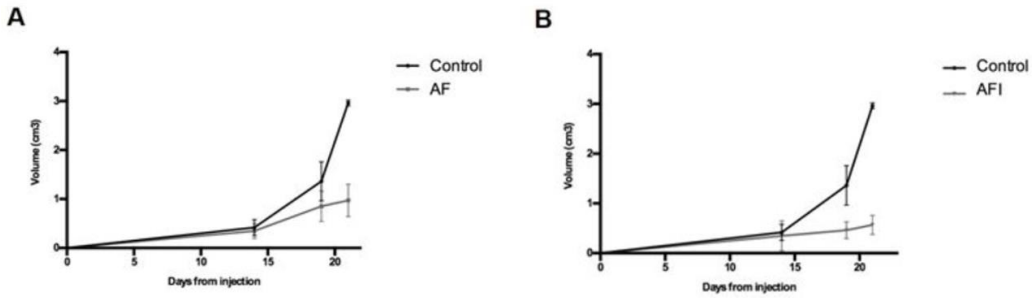

Fig.5: In vivo anticancer activity evaluation of gold compounds in a xenograft subcutaneous (sc) model of ovarian cancer cell line. (A, B) Time course of tumor growth in control, AF, and AFI treated mice (4 animals per group), injected with A2780 cells sc. Treatments started when the volume of the masses reached 60 mm^3 (after 7 days from cells injection); the administration was performed by intraperitoneal injections (three times a week for two weeks of treatment) of AF and AFI compounds (15 mg/kg). Data are reported as the mean ± SD.

At the end of the experiments, mice were sacrificed and the explanted masses measured; the volume (cm^3) was calculated using the ellipsoid equation [21]. Remarkably, treatment with both AFI and AF was accompanied by a strong decrease of the tumor volume determined at the sacrifice (Figure 6, control: 2.96 ± 0.06 vs AFI: 0.56 ± 0.20, $p < 0.01$; control: 2.96 ± 0.06 vs AF: 0,79 ± 0,27, $p < 0.01$).

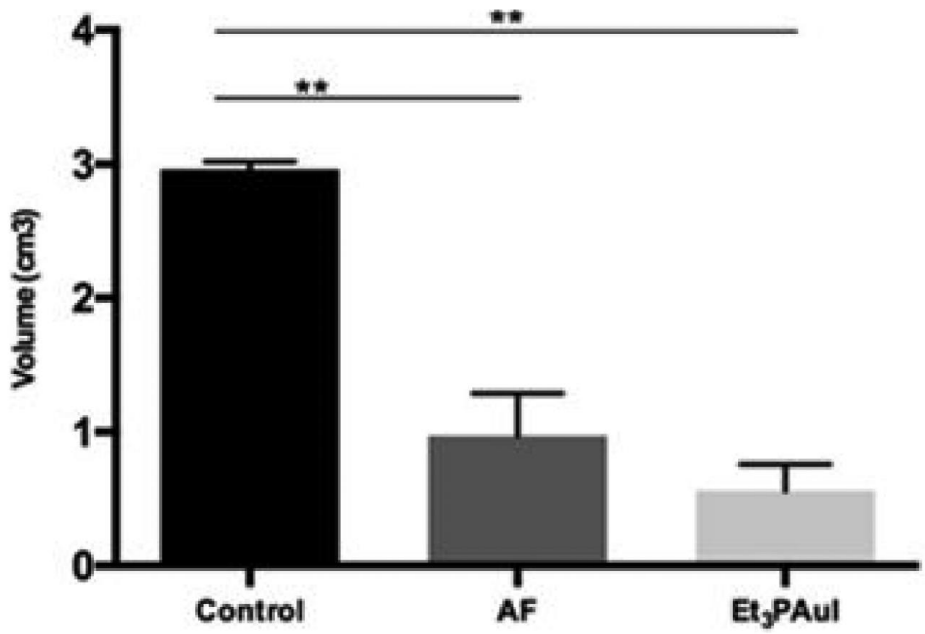

Fig.6: In vivo anticancer activity evaluation of gold compounds in a xenograft subcutaneous (sc) model of ovarian cancer. Mean volume of tumor masses obtained at the sacrifice, after 3 weeks from injection of A2780 cells. Data are reported as the mean ± SD (*$p < 0.05$, **$p < 0.01$).

The above experimental protocol did not alter the behaviour, vitality, or weight of treated mice. Subsequently, the in vivo anticancer activity of AFI versus AF was assessed in an orthotopic model of ovarian cancer, a model that better represents the cancer behaviour and response to therapy. Thirty female athymic nude mice were injected in the ovarian bursa ($5x10^5$ cells each mouse) with A2780 cells transfected with the firefly luciferase gene (A2780-luc). Autopsy confirmed that ovarian cancer occurred in all animals and representative images of the procedure and of tumor masses are reported in Figure 7A. The animals were divided in three groups of treatment (10 mice each): controls, AF treated and AFI treated. The administration schedule was the following: mice received compounds (15 mg/kg) ip three times a week for 2 weeks. The rationale for such a treatment schedule relied on the schedule reported by Mirabelli et al [5] and on the above-reported biodistribution data (Fig.4) showing that administration of 15 mg/kg gives rise to a peak peripheral blood concentration of 823.19 and 944.17 ng/mL, for AF and AFI, respectively, after 24 h. Mice were monitored daily, and the luciferase activity signal was quantified weekly (representative panels are reported in Figure 7B). Both gold compounds effectively reduced the tumor burden

(Figure 7B); notably, AFI is already very effective in antitumor activity after few doses (i.e., 1 week of treatment) leading to an almost complete tumor remission, as evidenced by the drastic reduction of the bioluminescent signal (ROI levels) compared to the control group (control: 20260 ± 4631 vs AFI: 4729 ± 2881; $p < 0,01$) (see graph in Figure 7C). The tumor masses of the sacrificed animals after 3 weeks of treatment were collected and measured with caliper; the volume (cm^3) was calculated using the ellipsoid equation even for this model [21]. Most important, the tumor masses of the animals treated with AFI showed a very strong reduction of the volume compared both to the control group (control vs AFI $p < 0.05$) and to the AF group (AF: 6.86 ± 1.57 vs AFI: 1.00 ± 0.70, $p < 0.01$) (Figure 7D). This latter evidence points out that AFI is a more effective anticancer drug compared with AF in our animal model.

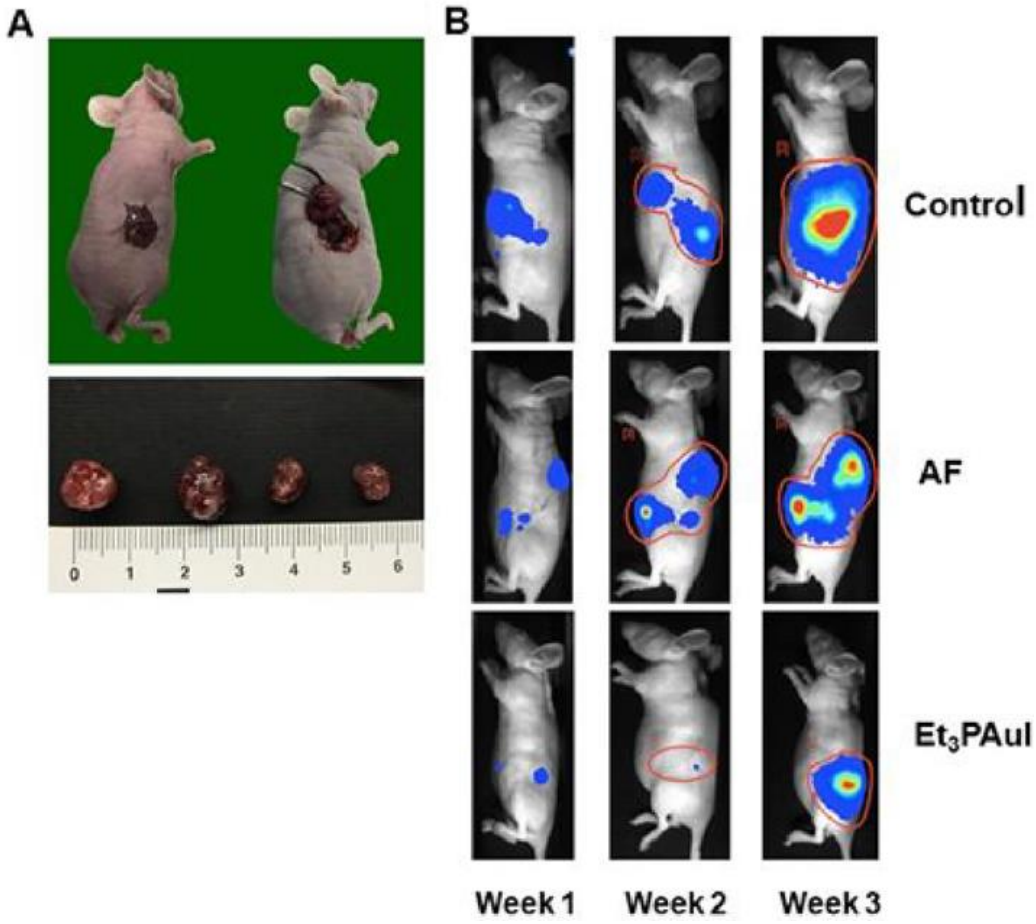

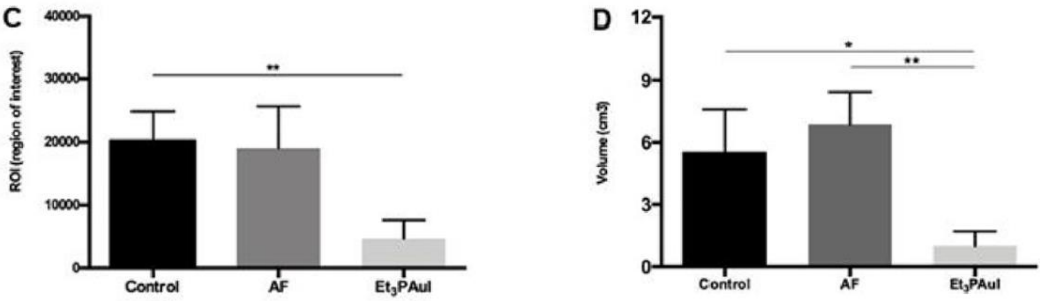

Fig.7: (A) Orthotopic model establishment: injection of $1x10^6$ A2780-luc cells in the ovary bursa of nude mice. Representative macroscopic images of ovarian tumor masses obtained are showed in the bottom panels. (B) Representative pseudocolor BLI images tracking A2780-luc cells emission in mice, 7, 14, and 21 days after A2780-luc injection. Color bar represents light intensity levels reported as counts per minute (cpm). (C) Levels of ROI after 1 week of treatment; data are reported as mean of each group (n = 10 animals/group) ± SD (**p < 0.01). (D) Volume of tumor masses (mean ± SD) at the sacrifice after 3 weeks from injection of A2780-luc cells (control group, n = 8; AF, n = 5; AFI, n = 5). *p < 0.05, **p < 0.01.

Conclusions

In conclusion, we have shown here that a specific structural modification of the repurposed gold(I) drug AF, now under consideration in clinical trials for cancer treatment, i.e., the substitution of the thiosugar ligand with iodide, affords a distinct gold(I) complex AFI, whose anticancer profile in vitro roughly resembles that of AF. This confirms that, even in the present ovarian cancer model, the thiosugar ligand is not mechanistically indispensable and that the $[Au(PEt_3)]^+$ moiety is likely to be the true pharmacophore. Very interestingly, in our in vivo models, AFI, has turned out to be far more effective than AF in contrasting tumor growth. Particularly impressive are the results and the differences between AF and AFI observed in the orthotopic model of ovarian cancer. AFI is found to induce a very large tumor regression after only 1 week of treatment, as pointed out by the decrease of the bioluminescent signal. A conspicuous shrinkage of the tumor is still evident after 3 weeks. The enhanced anticancer activity observed in this orthotopic model might well arise from the far greater lipophilicity of AFI, which might lead to a more favorable pharmacokinetics and biodistribution. Notably, the improved in vivo anticancer activity of AFI over AF does not bring about any increased systemic toxicity, making AFI a promising new drug candidate. In view of its far superior efficacy in animal models, AFI merits a more

extensive preclinical testing as it might be a valuable alternative to AF in cancer clinical trials.

References

[1] Bombardier, C.; Ware, J.; Russell, I. J.; Larson, M.; Chalmers, A.; Read, J. L. Auranofin therapy and quality of life in patients with rheumatoid arthritis. Results of a multicenter trial. Am. J. Med. 1986, 81, 565−578.

[2] Shaw, C. F. Gold-Based Therapeutic Agents. Chem. Rev. 1999, 99, 2589−2600.

[3] Cassetta, M. I.; Marzo, T.; Fallani, S.; Novelli, A.; Messori, L. Drug repositioning: auranofin as a prospective antimicrobial agent for the treatment of severe staphylococcal infections. BioMetals 2014, 27, 787−791.

[4] Capparelli, E. V.; Bricker-Ford, R.; Rogers, M. J.; McKerrow, J. H.; Reed, S. L. Phase I Clinical Trial Results of Auranofin, a Novel Antiparasitic Agent. Antimicrob. Agents Chemother. 2017, 61, e01947.

[5] Mirabelli, C. K.; Johnson, R. K.; Sung, C. M.; Faucette, L.; Muirhead, K.; Crooke, S. T. Evaluation of the in vivo antitumor activity and in vitro cytotoxic properties of auranofin, a coordinated gold compound, in murine tumor models. Cancer Res. 1985, 45, 32−39.

[6] Simon, T. M.; Kunishima, D. H.; Vibert, G. J.; Lorber, A. Cellular antiproliferative action exerted by auranofin. J. Rheumatol. Suppl. 1979, 5, 91−97.

[7] Mirabell, C. K.; Johnson, R. K.; Hill, D. T.; Faucette, L. F.; Girard, G. R.; Kuo, G. Y.; Sung, C. M.; Crooke, S. T. Correlation of the in vitro cytotoxic and in vivo antitumor activities of gold(I) coordination complexes. J. Med. Chem. 1986, 29, 218−223.

[8] Hou, G.-X.; Pan-Pan, L.; Shengyi, Z.; Mengqi, Y.; Jianwei, L.; Jing, Y.; Yumin, H.; Wen-Qi, J.; Shijun, W.; Peng, H. Elimination of stem-like cancer cell side-population by auranofin through modulation of ROS and glycolysis. Cell Death Dis. 2018, 9, 89.

[9] Rios Perez, M. V.; Roife, D.; Dai, B. B.; Kang, Y.; Li, X.; Pratt, M.; Fleming, J. B. Auranofin to prevent progression of pancreatic ductal adenocarcinoma. J. Clin. Oncol. 2016, 34, 236.

[10] Roh, J. L.; Jang, H.; Kim, E. H.; Shin, D. Targeting of the Glutathione, Thioredoxin, and Nrf2 Antioxidant Systems in Head and Neck Cancer, Antioxid. Antioxid. Redox Signaling 2017, 27, 106−114.

[11] Auranofin in Treating Patients With Recurrent Epithelial Ovarian, Primary Peritoneal, or Fallopian Tube Cancer. https://clinicaltrials.gov/ct2/show/NCT01747798.

[12] Sirolimus and Auranofin in Treating Patients With Advanced or Recurrent Non-Small Cell Lung Cancer or Small Cell Lung Cancer. https://clinicaltrials.gov/ct2/show/NCT01737502.

[13] Phase I and II Study of Auranofin in Chronic Lymphocytic Leukemia (CLL). https://clinicaltrials.gov/ct2/show/NCT01419691.

[14] Scalcon, V.; Bindoli, A.; Rigobello, M. P. Significance of the mitochondrial thioredoxin reductase in cancer cells: An update on role, targets and inhibitors. Free Radical Biol. Med. 2018, 127, 62−79.

[15] Magherini, F.; Fiaschi, T.; Valocchia, E.; Becatti, M.; Pratesi, A.; Marzo, T.; Massai, L.; Gabbiani, C.; Landini, I.; Nobili, S.; Mini, E.; Messori, L.; Modesti, A.; Gamberi, T. Antiproliferative effects of two gold(I)-N-heterocyclic carbene complexes in A2780 human ovarian cancer cells: a comparative proteomic study. Oncotarget 2018, 9, 28042−28068.

[16] Pratesi, A.; Gabbiani, C.; Michelucci, E.; Ginanneschi, M.; Papini, A. M.; Rubbiani, R.; Ott, I.; Messori, L. Insights on the mechanism of thioredoxin reductase inhibition by Gold Nheterocyclic carbene compounds using the synthetic linear Selenocysteine containing C-terminal peptide hTrxR(488−499): An ESI-MS investigation. J. Inorg. Biochem. 2014, 136, 161−169.

[17] Micale, N.; Schirmeister, T.; Ettari, R.; Cinellu, M. A.; Maiore, L.; Serratrice, M.; Gabbiani, C.; Massai, L.; Messori, L. Selected cytotoxic gold compounds cause significant inhibition of 20S proteasome catalytic activities. J. Inorg. Biochem. 2014, 11, 79−82.

[18] Marzo, T.; Cirri, D.; Gabbiani, C.; Gamberi, T.; Magherini, F.; Pratesi, A.; Guerri, A.; Biver, T.; Binacchi, F.; Stefanini, M.; Arcangeli, A.; Messori, L. Auranofin, Et3PAuCl, and Et3PAuI Are Highly Cytotoxic on Colorectal Cancer Cells: A Chemical and Biological Study. ACS Med. Chem. Lett. 2017, 8, 997−1001.

[19] Sutton, B. M.; Mc Gusty, E.; Walz, D. T.; Di Martino, M. J. Oral gold. Antiarthritic properties of alkylphosphinegold coordination complexes. J. Med. Chem. 1972, 15, 1095−1098.

[20] Marzo, T.; Cirri, D.; Pollini, S.; Prato, M.; Fallani, S.; Cassetta, M. I.; Novelli, A.; Rossolini, G. M.; Messori, L. Auranofin and its Analogues Show Potent Antimicrobial Activity Covering Multiresistant Pathogens: Structure-Activity Relationships. ChemMedChem 2018, 13, 2448−2454.

[21] Crociani, O.; Zanieri, F.; Pillozzi, S.; Lastraioli, E.; Stefanini, M.; Fiore, A.; Fortunato, A.; D'Amico, M.; Masselli, M.; De Lorenzo, E.; Gasparoli, L.; Chiu, M.; Bussolati, O.; Becchetti, A.; Arcangeli, A. hERG1 channels modulate integrin signaling to trigger angiogenesis and tumor progression in colorectal cancer. Sci. Rep. 2013, 3, 3308.

7. Silver(I) carbenes as a new class of chemotherapeutic agents

Introduction

Since cisplatin was first approved by the US Food and Drug Administration (FDA) for cancer treatment in 1978, the development of new and more effective metal-based anticancer drugs has been a primary challenge for scientists [1]. Despite great efforts made in the past few decades, only two other platinum-based drugs (i.e., carboplatin and oxaliplatin) and one arsenic-based drug (i.e., As_2O_3, trisenox) [2] have received approval worldwide as anticancer agents. In addition, even considering the important improvements in the administration protocols, some of the major problems associated to the use of Pt drugs still remain unsolved [3]. A family of metal-based compounds with promising features is that of carbene complexes. Metal–N-heterocyclic carbene (NHC) complexes have been extensively investigated in recent years for various applications, including medical and pharmacological ones. Particularly attractive for biomedical purposes is the high stability of these complexes, which is often greater than for the corresponding metal complexes with phosphane ligands [4]. This is one of the reasons why the synthesis and characterization of the carbene complexes of several transition metals has gained so much attention. Many gold, copper, platinum, palladium, iridium, ruthenium, and silver carbenes have now been tested as experimental drugs with promising results [5]. Beyond the above motivations, the interest in anticancer applications of carbene complexes is also driven by the observation that gold or silver carbene compounds seem to have non genomic targets for their pharmacological activity. In this frame, many research groups worldwide have reported the capacity of gold-based carbenes to bind thioredoxin reductase (TrxR), an important enzyme involved in cellular redox homeostasis; apparently metal binding occurs at the level of the redox-active C-terminal motif bearing a selenocysteine residue [6]. In 2013, Rigobello and co-workers published a paper on the synthesis, characterization, and anticancer properties of two novel silver- or gold-based carbene complexes bearing a 1-(anthracen-9-ylmethyl)-3-methylimidazol-2-ylidene ligand with fluorescence properties. These compounds showed pronounced in vitro anticancer properties and were also found to be strong inhibitors of TrxR. Remarkably, the silver complex was more efficient than its gold counterpart in contrasting cancer cell proliferation as well as in inhibiting TrxR activity [7]. We were interested to evaluate whether small structural modifications of the 1-(anthracen-9-ylmethyl)-3-

methylimidazol-2-ylidene silver chloride complex ([Ag(MIA)]Cl), such as replacement of the imidazole methyl substituent with an ethyl group, might appreciably affect the chemical and biological profiles of the resulting compound. We soon realized that upon ligand modification, when the product is slowly crystallized from the reaction mixture, the structure of the silver center turned out to be different. Indeed, at variance with the parent complex bearing the methyl substituent at the imidazole 3-position, a structure of the type $[Ag(NHC)_2]X$ was the only one afforded both in the solid state and in solution. Thus, we report herein the synthesis and chemical and biological features of this fluorescent complex characterized by the ability to inhibit TrxR apparently through direct binding to the active site redox motif. Remarkably, this latter process has been conveniently investigated by high-resolution ESI-MS using the C-terminal dodecapeptide of thioredoxin reductase hTrxR (488–499) bearing the active site redox motif, with a method already established in our laboratory [6a, b].

Results and Discussion

Synthesis and characterization of $[Ag(EIA)_2]Cl$

We first prepared the studied complex according to the synthetic procedure reported in the Experimental Section below. The complex was designed by modifying the ligand reported by Rigobello and co-workers in their work (see Figure 1). After synthesis of the modified ligand, we intended to prepare its 1:1 silver complex, i.e., Ag(EIA)Cl. In contrast to expectations, through slow crystallization of the product, as described in the Experimental Section, we obtained selectively and in good yield a product which turned out to correspond to the bifunctional silver complex $[Ag(EIA)_2]Cl$.

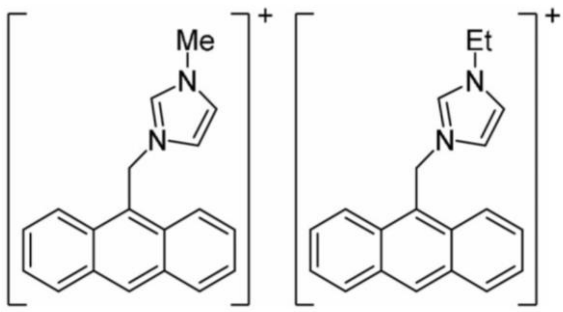

Fig.1: Structures of the ligand previously reported (left) [7] and of the modified ligand 5 used in this work (right, see Scheme 1).

Crystal structure

The crystal structures of the free ligand i.e. 1-(anthracen-9-ylmethyl)-3-ethyl-1H-imidazol-3-ium chloride (5) and of $[Ag(EIA)_2]Cl$ show that the ligand in both molecules retains the same conformation with respect to the mean planes containing the anthracene ring and the ethylimidazole moiety (88.55 in (5) compared with 82.25 in $[Ag(EIA)_2]Cl$). In contrast, the torsion angle of the ethyl pendant varies from -44.15° in (5) to 77.17° in $[Ag(EIA)_2]Cl$. The solid-state crystal structure of $[Ag(EIA)_2]Cl$ confirms the bifunctional structure already described in solution (Figure 2). Further crystallographic data are reported in Experimental Section (Table 4).

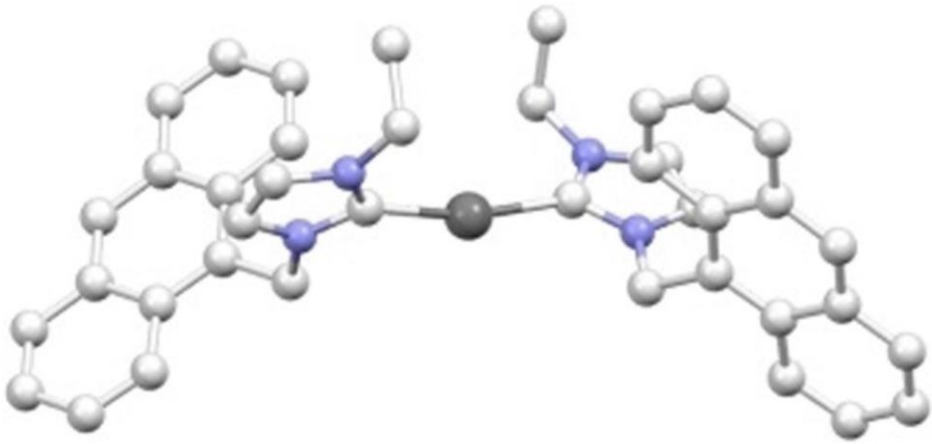

Fig.2: X-ray structure of complex $[Ag(EIA)_2]Cl$: C-Ag bond length: 2.093(4) Å; C-Ag-C' angle: 167.7° (C' is reported by the symmetry operation -x+1,+y,-z-1/2).

These results point out that, at variance with [Ag(MIA)]Cl, the small modification made at the imidazole 3-position strongly affects the nature of the resulting species, leading to a final product characterized by two carbene ligands bound to the metal center both in the solid state and in solution.

UV/Vis absorption and emission spectra

To test the complex stability with respect to dissociation in solution, we recorded UV/Vis absorption spectra of $[Ag(EIA)_2]Cl$ in buffered aqueous solutions at physiological pH. $[Ag(EIA)_2]Cl$ displays the typical structured absorption band of the anthracene chromophore, with a maximum at 370 nm (see Figure 3 below). This band does not

show any change within 24 hours, testifying the complex stability in aqueous medium (Figure 3).

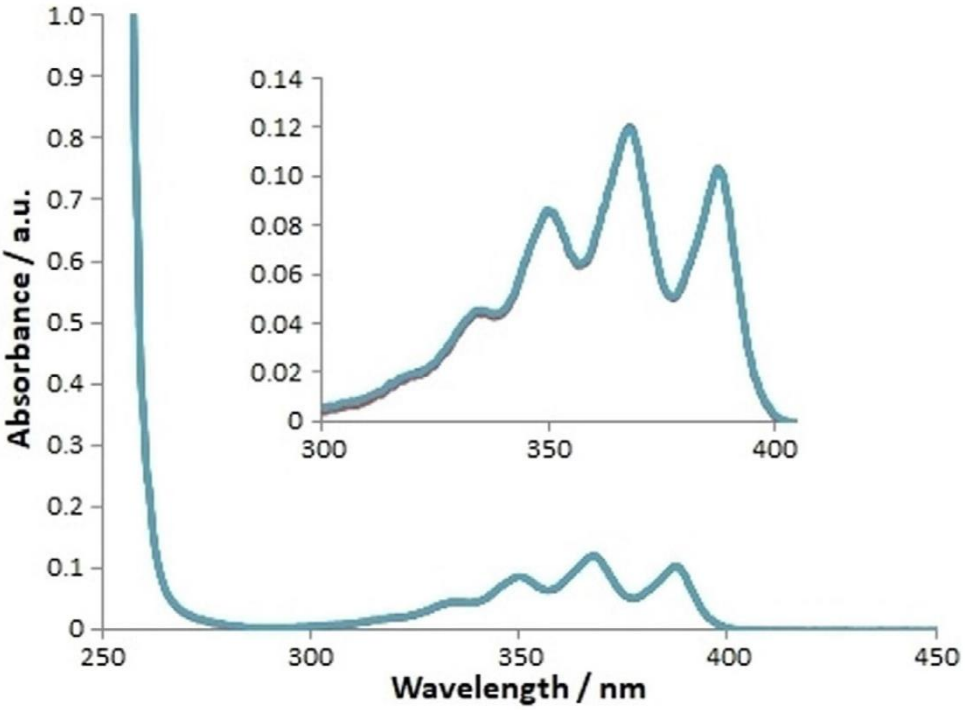

Fig.3: Time course spectra of $[Ag(EIA)_2]Cl$ (10^{-5}M, phosphate buffer 50 mM pH 7.4, 1% DMSO) for 24 h

In Figure 4 the emission spectra of $[Ag(EIA)_2]Cl$ and of free ligand are reported at different excitation wavelengths. At 350 nm of excitation wavelength the spectrum of $[Ag(EIA)_2]Cl$ shows three main emission bands falling at 395, 420, and 440 nm. Interestingly, the presence of the silver atom does not significantly affect the spectrophotometric properties of the ligand; these are substantially unaltered and almost superimposable to those of the free ligand.

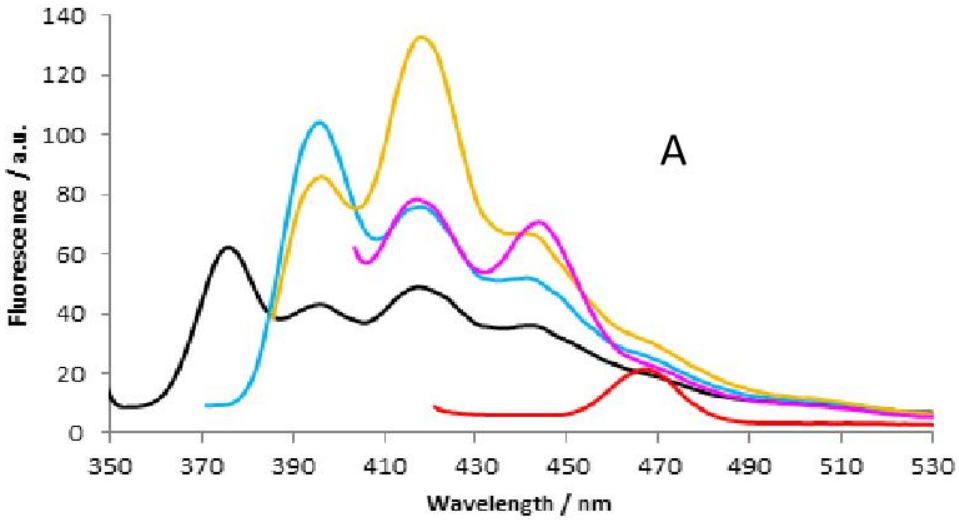

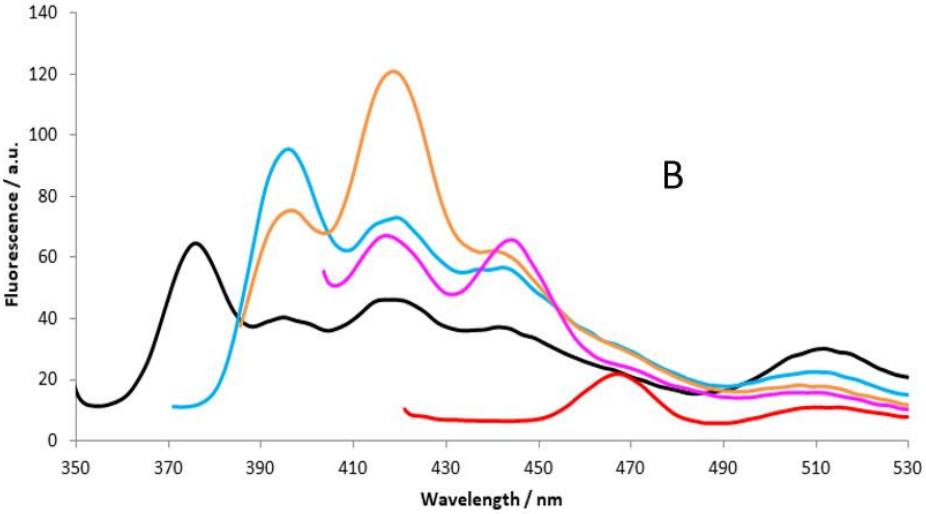

Fig.4: Emission spectra of ligand (A) and $[Ag(EIA)_2]Cl$ (B) (10^{-8} M in 50 mM phosphate buffer pH 7.4 in presence of 0.001 % DMSO): black line λexc=335 nm, blu line λexc=350 nm, orange line λexc=368 nm, pink line λexc=388 nm and red line λexc=405 nm.

Cytotoxic effects and cellular uptake

Next, the in vitro cytotoxic effects of $[Ag(EIA)_2]Cl$ toward human SH-SY5Y neuroblastoma cells were measured in comparison with cisplatin (the clinically established drug in the treatment of neuroblastoma) and [Ag(MIA)]Cl. The results highlighted that $[Ag(EIA)_2]Cl$ possesses cytotoxic properties greater than both compounds. In particular, an IC_{50} value of 1.059 +/- 0.042 μM was determined, which is about 10- and 2-fold lower than cisplatin and [Ag(MIA)]Cl, respectively (Table 1).

Complex	IC_{50} [μM][a]
$[Ag(EIA)_2]Cl$	1.059 ± 0.042
cisplatin	9.987 ± 0.506
[Ag(MIA)]Cl	2.093 ± 0.704

[a] Results are the average ± SD of three independent experiments.

Table 1: IC_{50} values in SH-SY5Y cells determined for $[Ag(EIA)_2]Cl$, cisplatin, and [Ag(MIA)]Cl.

Uptake experiments were subsequently performed to assess whether the different logP values of these compounds (which may be tentatively associated with different capacities to permeate the cell membrane) significantly affect cellular accumulation. Indeed, the three compounds show rather different logP values: -2.4 for cisplatin [8] and 0.90 and 0.50 for $[Ag(EIA)_2]Cl$ and [Ag(MIA)]Cl, respectively. Results of the uptake experiments are reported in Table 2.

Complex	[μg metal]/[μg protein][a]
[Ag(EIA)2]Cl	$(1.4 \pm 0.2) \times 10^{-3}$ (a)
cisplatin	$(1.6 \pm 0.3) \times 10^{-4}$ (b)
[Ag(MIA)]Cl	$(2.1 \pm 0.7) \times 10^{-4}$ (b)

[a] Values with the same letter are not statistically different at the 5% significance level according to the Tukey test.

Table 2: Metals level measured after 30 min exposure of SH-SY5Y cells to $[Ag(EIA)_2]Cl$, cisplatin, and [Ag(MIA)]Cl at 10 mm.

It is observed that $[Ag(EIA)_2]Cl$ shows a far higher ability to enter cells, with its uptake being about 10-fold greater than cisplatin and about 6-fold greater than [Ag(MIA)]Cl. The increased cell internalization of $[Ag(EIA)_2]Cl$ is probably correlated with its higher lipophilicity. In turn, the greater cell internalization might explain its higher cytotoxicity.

TrxR inhibition by $[Ag(EIA)_2]Cl$

Because the cellular redox system and, more specifically, TrxR are the likely targets for the cytotoxic effects of gold and silver carbene complexes [6, 7, 9], we decided to determine the inhibitory potency of $[Ag(EIA)_2]Cl$ toward this enzyme (Table 3).

Complex	IC_{50} [μM][a]
$[Ag(EIA)_2]Cl$	0.493 ± 0.04

[a] Value was determined by treating TrxR ($1\ U\ L^{-1}$) with $[Ag(EIA)_2]Cl$ (from 0.1 nM to 1 mM); the result is the average ± SD of three independent experiments.

Table 3: Thioredoxin reductase activity assay.

The experiments were done according to the procedure detailed in the Experimental Section [10]. The obtained IC_{50} value, falling in the sub-micromolar range, indicates that $[Ag(EIA)_2]Cl$ strongly inhibits TrxR, with its inhibitory potency in good agreement with its cytotoxic effects toward the SH-SY5Y cancer cell line.

MS studies of the interaction between $[Ag(EIA)_2]Cl$ and the C-terminal dodecapeptide of hTrxR.

To determine the molecular basis of TrxR inhibition, $[Ag(EIA)_2]Cl$ was incubated with the C-terminal dodecapeptide of hTrxR typically used as a model for the interaction of metal compounds with this enzyme (Figure 5) [6]. Indeed, this latter dodecapeptide, with the sequence Ac-SGGDILQSGCUG-NH_2, corresponds to the tryptic C-terminal fragment (488–499) of hTrxR.

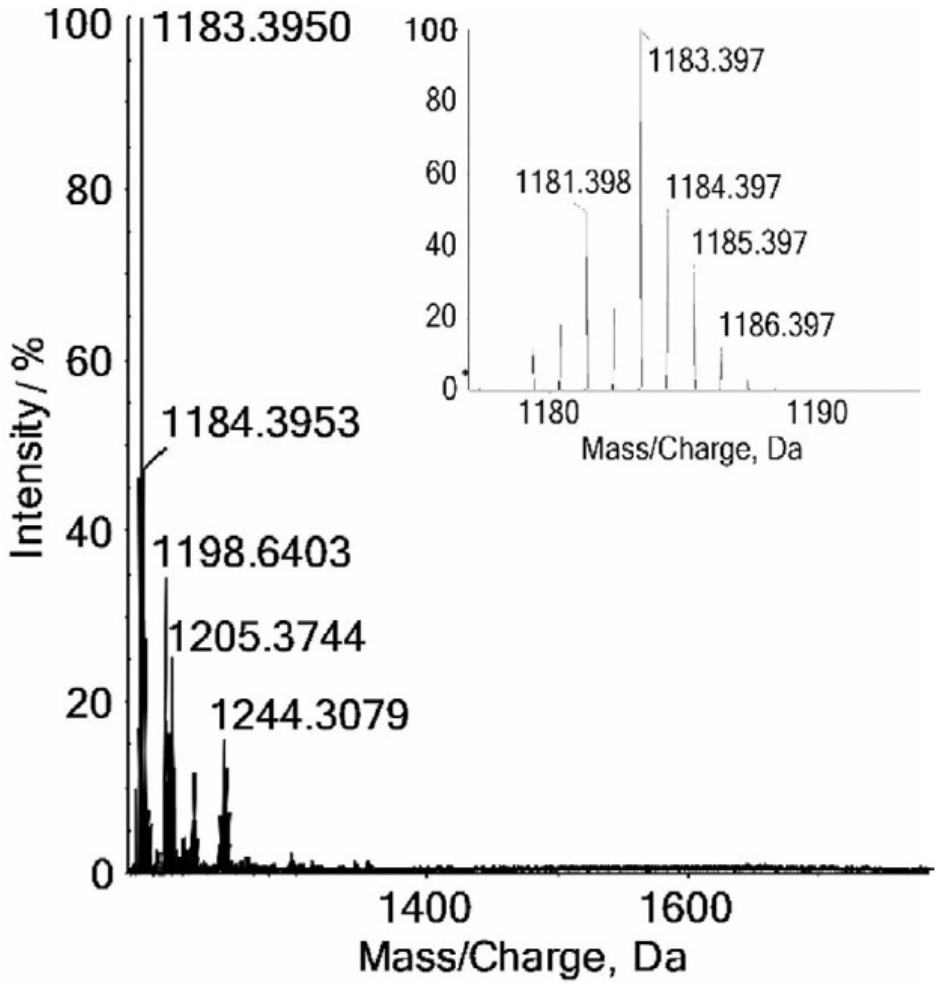

Fig.5: ESI-MS spectrum of the C-terminal dodecapeptide hTrxR (Ac-SGGDILQSGCUG-NH_2) dissolved in MilliQ water (10^{-4}M). The inset shows the characteristic selenium isotopic pattern.

In the peptide sequence, the N-terminal residue is acetylated and the C-terminus is amidated to avoid undesired interactions with the metal compound. The mass spectrum of this peptide is displayed in Figure 5, showing an intense peak at m/z 1183.39 Da. The inset shows greater detail of the characteristic isotopic pattern due to the presence of a selenocysteine residue. The ESI-MS spectrum recorded for $[Ag(EIA)_2]Cl$ in the presence of the dodecapeptide bearing the redox-active motif of TrxR, revealed that the metal compound reacts rapidly with this peptide. Indeed, after

2 h of incubation at 37 °C, the mass spectrum (Figure 6) clearly shows the presence of two main signals: one at m/z 1469.54 Da (corresponding to the monoadduct), and one at m/z 1755.69 Da (belonging to the bisadduct) in which one or two carbene ligands, deprived of the metal center, are bound to the peptide.

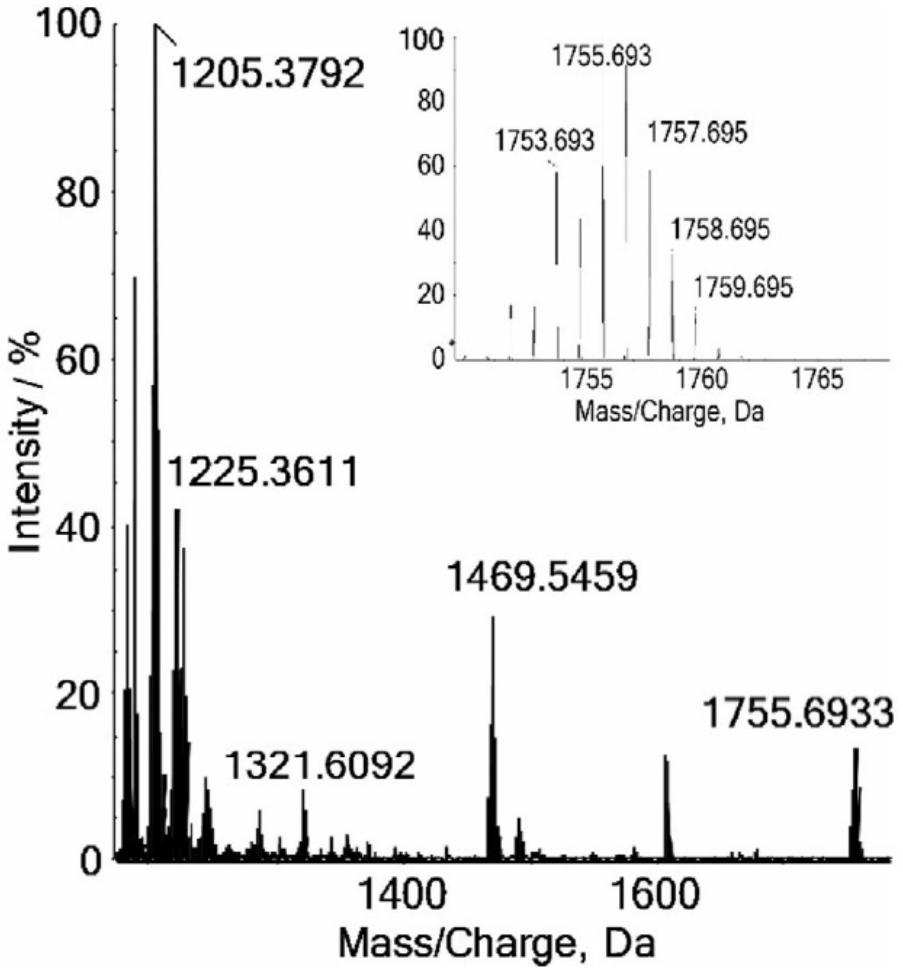

Fig.6: ESI-MS spectrum of the C-terminal dodecapeptide hTrxR (Ac-SGGDILQSGCUG-NH_2) dissolved in MilliQ water (10^{-4}M) in the presence of 5.0 equiv dithiothreitol (DTT) and 1.0 equiv $[Ag(EIA)_2]Cl$ incubated for 2 h at 37 °C. The inset shows the isotopic pattern for the bis-adduct.

Assignments were consistent with theoretical simulations of the isotopic pattern, which are in very good agreement with the experimental data depicted in the insets of Figure 6. The peak at m/z 1205.37 Da is assigned to the unreacted peptide associated with sodium. To confirm this unconventional reactivity, we carried out the same ESI-MS experiments using the complex bis(1-(anthracen-9-ylmethyl)-3-propylimidazol-2-ylidene) silver bromide ([$Ag(PIA)_2$]Br), that is, the same complex with a propyl substituent at imidazole position 3. This complex was synthesized by following the same synthetic route as in the case of [$Ag(EIA)_2$]Cl and characterized accordingly. Its crystal structure was also determined (Experimental Section, Table 4). A reactivity superimposable to that of [$Ag(EIA)_2$]Cl emerged, indicating that the uncommon mechanism of binding described in the case of [$Ag(EIA)_2$]Cl is conserved upon replacement of the ethyl substituent at imidazole position 3 with a propyl group. Additionally, the same incubation was carried out with [Ag(MIA)]Cl: the monofunctional silver complex reported by Rigobello and colleagues [7]. At variance with the two bifunctional silver complexes, i.e., [$Ag(EIA)_2$]Cl and [$Ag(PIA)_2$]Br, no adducts were found. Next, to gain further insight into the mechanistic aspects involved in the pharmacological action of [$Ag(EIA)_2$]Cl, we reacted the silver complex with three model proteins: cytochrome C, ribonuclease A, and lysozyme. We analyzed the incubated solutions through a well-established protocol relying on high-resolution mass spectrometry (HRMS) [11]. Indeed, binding and interaction with non-genomic targets such as proteins is recognized to play a key role for the activity of silver and gold carbene complexes [7, 10]. In contrast to expectations, no evidence of adduct formation was detected, even for incubation times up to 72 h.

Fluorescence microscopy

Finally, to evaluate the intracellular distribution of [$Ag(EIA)_2$]Cl, SH-SY5Y cells were treated with this silver complex for various time periods and then observed by fluorescence microscopy. No fluorescence signal was detectable in the control cells (Figure 7 A). Conversely, a weak blue fluorescence signal appears in the peripheral cytoplasm after about 30 min treatment with [$Ag(EIA)_2$]Cl, reaching its maximum intensity at 60 min. By observation of the fluorescence pattern, the fluorescent complex seems to accumulate within rounded bodies compatible with endocytic vesicles, as suggested by their distribution in the sub-plasmalemmal cytoplasm (Figure 7B).

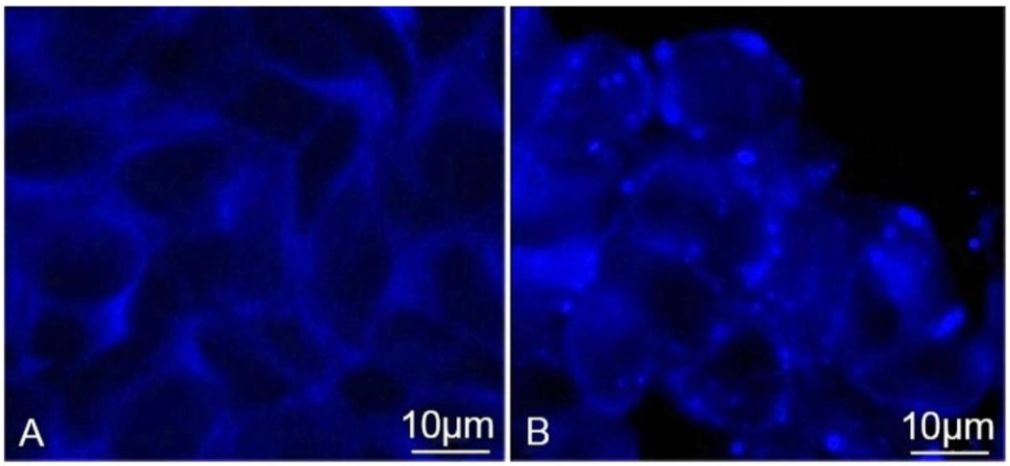

Fig.7: Representative image of SH-SY5Y cells: A) controls, and B) cells treated with 10 μM $[Ag(EIA)_2]Cl$ for 1 h.

Conclusions

There is currently broad interest in the development of metal carbene complexes combining cytotoxic and fluorescence properties. Herein we have reported on the synthesis and chemical characterization of a novel monocationic silver(I) NHC complex, namely bis(1-(anthracen-9-ylmethyl)-3-ethylimidazol-2-ylidene) silver chloride, bearing an anthracenyl fluorescent probe. The complex was fully characterized by NMR, ESI-MS, elemental analysis, and X-ray crystallography. The chemical and biological characterization of this compound has revealed a few peculiar and interesting features. Quite surprisingly, replacement of the methyl group of Ag(MIA)Cl with an ethyl substituent at position 3 of the imidazole ring leads to the formation of a cationic silver complex bearing two carbene ligands. The selective obtainment of the bis-carbene complex is attributable to a number of factors including steric hindrance of the imidazole substituent, already reported by Garrison and Youngs [12]. $[Ag(EIA)_2]Cl$ is highly stable in common organic solvents or in buffered physiological solutions and is unreactive toward small model proteins. These properties make it highly suitable for biological and cellular studies. Remarkably, $[Ag(EIA)_2]Cl$ manifested cytotoxic potency 10-fold higher than cisplatin and 2-fold higher than Ag(MIA)Cl when assayed in a reference neuroblastoma cell line (the respective IC_{50} values are 1.059, 9.987, and 2.093 μM). The in vitro pharmacological activity of $[Ag(EIA)_2]Cl$ correlates well with its capacity to enter cancer cells; this, in turn, probably depends on its greater lipophilicity

than that of Ag(MIA)Cl or cisplatin. $[Ag(EIA)_2]Cl$ potently inhibits TrxR with an IC_{50} value of 0.493 μM; interestingly, this value is in good agreement with the determined cytotoxicity value, supporting the view of TrxR as one of the likely cellular targets. The reaction of $[Ag(EIA)_2]Cl$ toward the C-terminal dodecapeptide of thioredoxin reductase hTrxR (488–499) was investigated by HRMS experiments. Notably, $[Ag(EIA)_2]Cl$ is able to bind tightly the C-terminal fragment, most probably at the level of the S-Se redox motif, through an unconventional mechanism, involving a sort of transmetalation, with concomitant loss of the silver center. This finding is particularly important, and, to the best of our knowledge, such a mode of binding is reported here for the first time. Finally, it is notable that the presence of the anthracene fluorophore allows facile tracking of the complex by fluorescence microscopy analysis; we found that $[Ag(EIA)_2]Cl$ accumulates within rounded-shaped bodies that are compatible with endocytic vesicles.

Experimental Section

Chemistry

Synthesis were carried out through modifications of those reported in the literature [7, 12]. The overall synthetic route is displayed in Scheme 1.

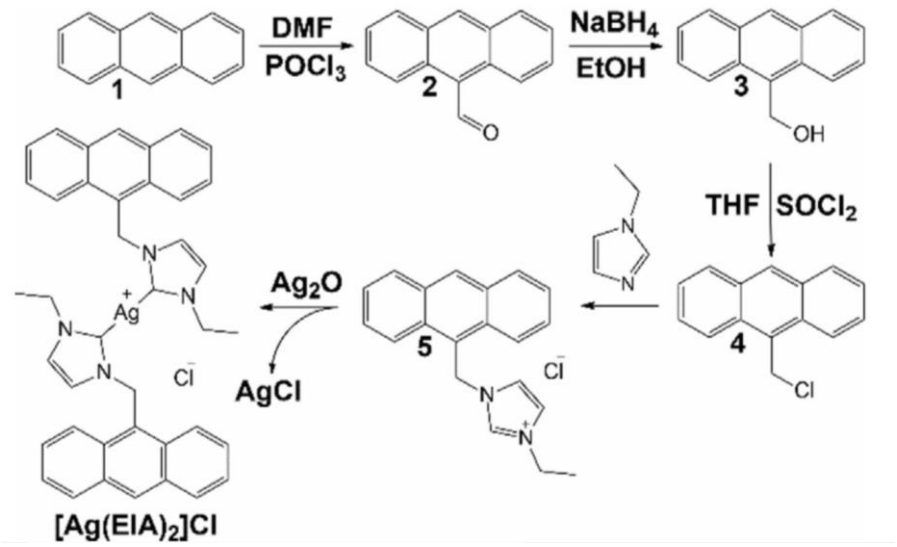

Scheme 1: Synthetic route for bis(1-(anthracen-9-ylmethyl)-3-ethylimidazol-2- ylidene) silver chloride.

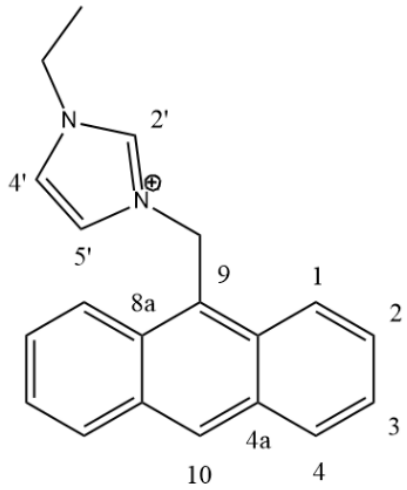

Fig.8: System numeration.

Synthesis of 3-(anthracen-9-ylmethyl)-1-ethyl-1H-imidazol-3-ium chloride (5): To compound (4) (210 mg, 0.9 mmol) was added ethylimidazole(2 ml, 25 mmol). The obtained mixture was stirred for 24 h at room temperature. Next, acetonitrile was added to the mixture to induce precipitation of compound as chloride salt. The resulting solid was filtrated and washed with ether. Yield: 75%.

^{1}HNMR (400.13 MHz, DMSO-d_6) δ: 9.04 (s, 1H, Im H2'), 8.83 (s, 1H, Ant H10), 8.46 (d, 2H, Ant H1, *J* = 8.8 Hz), 8.21 (d, 2H, Ant H4, *J* = 8.3 Hz), 7.77 (s, 1H, Im, H4') 7.67 (pseudo t, 2H, Ant H2), 7.65 (s, 1H, Im, H5'), 7.60 (pseudo t, 2H, Ant H3), 6.47 (s, 2H, AntCH_2Im), 4.09 (q, 2H, ImCH_2CH*3*, *J* = 7.2 Hz), 1.30 (t, 3H, ImCH_2CH_3, *J* = 7.2 Hz);

^{13}CNMR (100.61 MHz, DMSO-d6) δ: 135.46 (Im C2'), 131.02 (Ant C4a), 130.58 (Ant C8a), 130.01 (Ant C10), 129.30 (Ant C4), 127.69 (Ant C2), 125.50 (Ant C3), 123.56 (Ant C9), 123.44 (Ant C1), 122.40 (Im C5'), 122,10 (Im C4'), 44.78 (AntCH_2Im), 44.14 (ImCH_2CH_3), 15.11 (ImCH_2CH_3).

Synthesis of bis(1-(anthracen-9-ylmethyl)-3-ethylimidazol-2-ylidene) silver chloride ([Ag(EIA)$_2$]Cl): Compound 5 (101 mg, 0.31 mmol) was stirred with silver(I) oxide (40 mg, 0.17 mmol) in methanol (7 mL) for 24 h. Then, dichloromethane (20 mL) was added to the mixture and the suspension was filtered over Celite to remove both unreacted Ag_2O and AgCl formed during reaction. After concentration in vacuo, crystallization was

carried out at -20 °C by adding hexane. During the next four days the dark-grey precipitate that slowly appeared was filtered off daily. Finally, the plate-shaped crystals of complex were filtered and washed with hexane. Yield: 61%;

^{1}H NMR (400.13 MHz, MeOD): δ=8.59 (s, 2H, Ant H10), 8.18 (d, 4H, Ant H1, J=8.1 Hz), 8.07 (d, 4H, Ant H4, J= 8.2 Hz), 7.53–7.45 (m, 8H, Ant H2,3), 7.31 (s, 2H, Im H4'), 7.23 (s, 2H, Im H5'), 5.91 (s, 4H, AntCH_2Im), 3.58 (b, 4H, ImCH_2CH_3), 1.13 ppm (b, 6H, ImCH_2CH_3);

^{13}C NMR (100.61 MHz, MeOD): d= 183.57 (Im C2'), 133.05 (Ant C4a), 132.17 (Ant C8a), 130.83 (Ant C10), 130.57 (Ant C4), 128.51 (Ant C2), 126.48 (Ant C3), 124.59 (Ant C9), 123.67 (Ant C1), 123.22 (Im C5'), 121.53 (Im C4'), 48.25 (AntCH_2Im), 47.82 (ImCH_2CH_3), 17.07 ppm (ImCH_2CH_3);

ESI-MS: m/z 681.20;

Elemental analysis of C, N, and H for $C_{40}H_{36}AgClN_4 \cdot 3(CH_2Cl_2)$ [calculated C: 53.20 %, H: 4.36 %, N: 5.77 %, experimental: C: 53.22 %, H: 4.04 %, N: 5.02%].

Synthesis of 3-(anthracen-9-ylmethyl)-1H-imidazole (6): Imidazole (84.9 mg, 1.25 mmol) was stirred overnight in 10 mL of DMF with 172.3 mg (1.25mmol) of K_2CO_3 and 309.3 mg (1.36 mmol) of 4 at 60°C. Subsequently, 50 mL of water were added and the mixture was extracted with CH_2Cl_2, washed with water and dried with Na_2SO_4.Yield: 43%.

^{1}HNMR (400.13 MHz, $CDCl_3$) δ:8.57 (s, 1H, Ant), 8.20 (d, 2H, Ant, *J* = 8.57 Hz), 8.08 (d, 2H, Ant, *J* = 7.83 Hz), 7.57(m, 2H, Ant), 7.51(m, 2H, Ant), 7.48 (s, 1H, Im), 6.99 (s, 1H, Im), 6.86 (s, 1H, Im), 6.09 (s, 2H, AntCH_2Im)

Synthesis of 3-(anthracen-9-ylmethyl)-1-propyl-1H-imidazol-3-ium bromide (7): Compound (6) (49.47 mg, 0.19 mmol) was dissolved in 2 mL of CH_3Cl. Subsequently 5 mL of 1-Bromopropane were added to the solution. The obtained mixture was stirred at 60°C. After 6h diethyl ether was added to the mixture to induce precipitation of compound as bromide salt. Yield: 86%.

^{1}HNMR (400.13 MHz, DMSO-d_6) δ:8.95 (s, 1H, Im), 8.85 (s, 1H, Ant), 8.45 (d, 2H, Ant, *J* = 8.76 Hz), 8.23 (d, 2H, Ant , *J* = 8.32Hz), 7.75 (s, 1H, Im), 7.68 (m, 2H, Ant), 7.66 (s, 1H, Im), 7.62 (m, 2H, Ant), 6.48 (s, 2H, AntCH_2Im), 4.03 (t, 2H, Im$CH_2CH_2CH_3$, *J* = 7.07 Hz), 1.69 (m, 2H, Im$CH_2CH_2CH_3$), 0.73 (t, 3H, Im$CH_2CH_2CH_3$, *J* = 7.37 Hz).

^{13}CNMR (100.61 MHz, MeOD) δ: 137.51, 132.96, 132.50, 131.99, 131.28, 129.62, 127.45, 125.33, 125.19, 124.49, 124.37, 52.14, 46.80, 24.71, 12.08.

Synthesis of bis(1-(anthracen-9-ylmethyl)-3-propylimidazol-2-ylidene) silver bromide ([Ag(PIA)$_2$]Br): 51.7 mg of (7) (0.13 mmol) were stirred with silver(I) oxide (17.9 mg, 0.075 mmol) in methanol (2.5 mL) for 24 h. Then, 10 mL of dichloromethane were added to the mixture and the suspension was filtered for removing the solid phase. After concentration in vacuum, crystallization was allowed at -20° C by adding hexane. During the next four days the dark-grey precipitate that slowly appeared was daily filter-off. Finally, the crystals of complex were filtered and washed with hexane. Yield: 61%.

^{1}HNMR (400.13 MHz, MeOD) δ: 8.61(s, 1H, Ant), 8.19 (d, 2H, Ant, *J* = 8.41 Hz), 8.08 (d, 2H, Ant, *J* = 7.45 Hz), 7.54 (m, 6H, An t+ Im overlapped), 5.92 (s, 2H, AntCH$_2$Im), 3.43(b, 2H, ImCH$_2$CH$_2$CH$_3$), 1.46(b, 2H, ImCH$_2$CH$_2$CH$_3$), 0.57(b, 3H, ImCH$_2$CH$_2$CH$_3$)

^{13}CNMR (100.61 MHz, MeOD) δ: 190.51, 133.09, 132.21, 130.89, 130.67, 130.58, 129.22, 128.50, 126.64, 126.50, 124.60, 123.84, 123.61, 123.23, 54.98, 47.88, 25.67, 11.16

Spectrophotometric analysis: Solution behavior of [Ag(EIA)$_2$]Cl was assessed by spectrophotometric studies performed with a Varian Cary 50 Bio UV/Vis spectrophotometer. For absorption experiments solutions of complex (10^{-5}M) were prepared in dimethyl sulfoxide (DMSO), N,N-dimethylformamide (DMF) or 50 mm phosphate buffer (pH 7.4) in the presence of 1% of organic solvent. Emission spectra of complex (10^{-8}M), in 50 mm phosphate buffer (pH 7.4) with the presence of 0.001% of DMF, were recorded with a PerkinElmer LS55 Luminescence Spectrometer. All the experiments were carried out at 25 °C.

LogP determination: The octanol/water partition coefficient was assessed through a modified shake-flask method previously used in our laboratories [8].

NMR spectroscopy: NMR spectra were acquired on a Bruker Avance III 400 console equipped with a Bruker Ultrashield 400 Plus superconducting magnet (resonating frequencies: 400.13 and 100.61 MHz for ^{1}H and ^{13}C NMR, respectively) and a 5 mm PABBO BB-1H/D Z-GRD Z108618/0049 probe. All spectra were recorded at room temperature (25 +/- 2 °C) in solvents with a deuteration degree of 99.8% and calibrated

on solvent residual signals [13]. $CDCl_3$ was purchased from Sigma–Aldrich, while DMSO-d_6 was purchased from Deutero.de (https://www.deutero.de/).

ESI-MS: Interaction between the silver complex and the synthetic dodecapeptide Ac-SGGDILQSGCUG-NH_2, corresponding to the C terminal tryptic fragment of hTrxR, was assessed by high-resolution ESI-MS [6a, b]. The dodecapeptide was dissolved in LC–MS-grade water (final concentration 10^{-4}M solution), and dithiothreitol (DTT, 5.0 equiv) was added to reduce the S-Se bond. Then, the silver complexes (1.0 equiv) were also added at a 1:3 metal complex/peptide molar ratio, and the mixture was incubated for 2 h at 37 °C. Interaction between $[Ag(EIA)_2]Cl$ and model proteins was carried out as described in our previous works [11]: solutions of cytochrome C, ribonuclease A, and lysozyme (10^{-4}M) were incubated for 72 h at 37 °C with $[Ag(EIA)_2]Cl$ (3:1 complex to protein ratio) in 20 mM ammonium acetate buffer (pH 6.8) in the presence of 3% of organic solvent (DMSO or DMF). Aliquots were sampled after 24, 48, and 72 h. ESI-MS spectra were acquired through direct infusion at 10 mL/min flow rate in a TripleTOF-5600+ mass spectrometer (Sciex, Framingham, MA, USA), equipped with a DuoSpray interface operating with an ESI probe. The ESI source parameters were optimized as follows: positive polarity, ionspray voltage floating 5500 V, temperature 400 °C, ion source gas 1 (GS1) 40, ion source gas 2 (GS2) 30, curtain gas (CUR) 25, declustering potential (DP) 100 V, collision energy (CE) 10 V. For acquisition, Analyst TF software 1.7.1 (Sciex) was used, and deconvoluted masses were obtained by using the Bio Tool Kit micro-application v.2.2 embedded in PeakView_ software v.2.2 (Sciex).

X-ray crystallography: Single crystals suitable for X-ray diffraction experiments for EIA were obtained by adding to the reaction mixture acetonitrile and diethyl ether. This solution was stored at -20 °C for four days. After this time, yellow needle-shaped crystals were obtained. For $[Ag(EIA)_2]Cl$, colorless plate-shaped crystals were straightforwardly obtained as products of the synthesis as described above in the paragraph reporting synthesis of the compound. Similarly, for $[(Ag(PIA)_2]Br$, suitable crystals were obtained as product of the synthesis. Data collection was performed on an Oxford Diffraction Xcalibur3 diffractometer at 100 K and with MoKα radiation (λ = 0.71073 Å). Data collection and reduction were performed through the suite CrysAlis [14]. The absorption correction was applied with the program SCALE3 ABSPACK, also integrated in the CrysAlis suite. The structures were solved by direct methods implemented in SIR97 [15] and refined by full-matrix least-squares on F^2 using the SHELXL software package [16]. All non-hydrogen atoms were refined anisotropically by full-matrix least-squares methods on F^2. All H atoms (except those of H_2O in 5) were

placed in calculated positions with isotropic thermal parameters depending on that of the atom to which they are bound and included in structure factor calculations in the final stage of full-matrix least-squares refinement. In the crystal structure of compound $[Ag(EIA)_2]Cl$, the silver and chlorine atom lie in special position and the occupancy factor is 0.5 for both atoms. Supplementary crystallographic are reported in Table 4. These data can be obtained free of charge from The Cambridge Crystallographic Data Centre.

	5	$[Ag(EIA)_2]Cl$	$[Ag(PIA)_2]Br$
Empirical formula	$C_{20}H_{21}ClN_2O$	$C_{20}H_{18}N_2Cl_{0.5}Ag_{0.5}$	$C_{21}H_{20}N_2Br_{0.5}Ag_{0.5}$
Formula weight	340.84	358.02	394.28
Temperature (K)	100(2)	100(2)	100(2)
Wavelength (Å)	0.71073	0.71073	0.71073
Crystal system, space group	Monoclinicic, P 21/c	Orthorhombic, P bcn	Orthorhombic, P bcn
Unit cell dimensions (Å, °)	a = 9.7330(4) b = 19.5123(7) β = 96.251(3) c = 9.0818(3)	a = 13.6037(4) b = 11.4983(5) c = 22.062(1)	a = 13.6510(4) b = 11.5815(4) c = 22.0821(6)
Volume ($Å^3$)	1714.5(1)	3450.9(2)	3491.2(2)
Z, D_c (mg/cm^3)	4, 1.320	8, 1.378	8, 1,500
μ (mm^{-1})	0.232	0.695	1.758
F(000)	720	1472	1608
Crystal size (mm)			0.1x0.03x0.02
θ range (°)	4.18 to 28.06	4.27 to 29.18	4.245 to 29.46
Reflections collected / unique	3659 / 2828	4121 / 2915	4078/2684
Data / restraints / parameters	2828 / 0 / 226	2915 / 0 / 210	2684 / 0 / 271
Goodness-of-fit on F^2	1.030	1.035	1.057
Final R indices [I>2σ(I)]	R1 = 0.0425, wR2 = 0.0921	R1 = 0.0568, wR2 = 0.1552	R1 = 0.0455, wR2 =0.1027
R indices (all data)	R1 = 0.0632, wR2 = 0.1042	R1 = 0.0832, wR2 = 0.1774	R1 = 0.0770, wR2 = 0.1207

Table.4: Crystallographic Data of compounds 5, $[Ag(EIA)_2]Cl$ and $[Ag(PIA)_2]Br$.

Cell culture: Human SH-SY5Y neuroblastoma cells were cultured in Dulbecco's modified Eagle's medium/Ham's Nutrient Mixture F12 (1:1) (Sigma–Aldrich), supplemented with 10% heat-inactivated fetal bovine serum (FBS, Invitrogen, Carlsbad, CA, USA), 2 mm glutamine, 250 U/mL penicillin G and 250 mg/mL streptomycin (Sigma–Aldrich), in a humidified atmosphere with 5% CO2 at 37 °C.

Cytotoxicity assay: Cell viability was measured using the CellTiter-Blue Reagent (Promega, Milan, Italy). SH-SY5Y cells ($1x10^4$ per well) were seeded in 96-well plates and treated with $[Ag(EIA)_2]Cl$ (0.5–2.5 μM), cisplatin (10–50 μM), and [Ag(MIA)]Cl (2–10 μM) for 24 h. At end treatments, CellTiter-Blue Reagent was added to each well and

incubated for 2 h at 37 °C. Fluorescence was measured in a multiplate reader (Infinite M200PRO, Tecan, Switzerland) at 560/590 nm. The IC50 values for each compound were determined from the specific dose–response curves by nonlinear analysis, using GraphPad Prism 2.0 statistical software (GraphPad Software, San Diego, CA, USA) and expressed as means +/- standard deviation of at least four independent experiments. Drug uptake: SH-SY5Y cells were seeded in six-well plates ($5x10^5$ cells per well) and allowed to adhere. The culture medium was replaced with medium without phenol red and FBS, and the cells were incubated with $[Ag(EIA)_2]Cl$, cisplatin, or [Ag(MIA)]Cl (10 μM) for 30 min. At end of treatments, the cells were harvested in distilled H_2O to induce osmotic shock. The determination of metals concentration in the cell lysates was performed as previously reported [8] in triplicate by a Varian 720-ES inductively coupled plasma atomic emission spectrometer (ICP-AES) equipped with a CETAC U5000 AT+ ultrasonic nebulizer, in order to increase the method sensitivity. Before analysis, fixed volumes of samples were moved in vials and digested in a thermo-reactor at 80 °C for 3 h with 1 mL of aqua regia (HCl supra-pure grade and HNO_3 supra-pure grade in 3:1 ratio) and 5 mL of ultrapure water (R > 18 MΩ). Next, samples were spiked with 1 ppm of Ge used as an internal standard and analyzed. Calibration standards were prepared by gravimetric serial dilution from a commercial standard solution of Pt at 1000 mg/L. The wavelength used for Pt and Ag determination were 214.424 and 338.289 nm, respectively, whereas for Ge the line at 209.426 nm was used. The operating conditions were optimized to obtain maximum signal intensity, and between each sample, a rinse solution of HCl supra-pure grade and HNO_3 supra-pure grade at a 3:1 ratio was used to avoid any "memory effect". The values of Ag or Pt were normalized to cellular proteins, determined by the micro-bicinchoninic acid (BCA) method, and expressed as mg metal per mg protein. Intracellular localization of $[Ag(EIA)_2]Cl$ monitored by fluorescence microscopy: SH-SY5Y cells ($5x10^5$) were seeded on a glass coverslip and treated with 10 mm $[Ag(EIA)_2]Cl$ for 20, 30, 60, and 90 min. Control cells, not treated with this silver complex, were used. At end of treatment, the cells were fixed with 2% paraformaldehyde for 10 min at room temperature and then observed under an epifluorescence Zeiss Axioskop microscope (Mannheim, Germany) using 358 nm excitation wavelength, with a 100X objective. The fluorescence images were captured using a Leica DFC310 FX 1.4-megapixel digital camera, equipped with the Leica software application suite LAS V3.8 (Leica Microsystems, Mannheim, Germany).

TrxR activity assay: The inhibitory effects of complex toward TrxR activity (from rat liver) were determined by quantification of the ability of compound to directly reduce

5,5’-dithiobis(2-nitrobenzoic acid) (DTNB) in the presence of NADPH as reported previously [10].

References

[1] a) T. C. Johnstone, K. Suntharalingam, S. J. Lippard, Chem. Rev. 2016, 116, 3436; b) K. B. Garbutcheon-Singh, M. P. Grant, B. W. Harper, A. M. Krause-Heuer, M. Manohar, N. Orkey, J. R. Aldrich-Wright, Curr. Top. Med. Chem. 2011, 11, 521; c) I. Romero-Canel_n, P. J. Sadler, Inorg. Chem. 2013, 52, 12276.

[2] a) L. Kelland, Nat. Rev. Cancer 2007, 7, 573; b) A. Emadi, S. D. Gore, Blood. Rev. 2010, 24, 191.

[3] a) T. C. Johnstone, G. Y. Park, S. J. Lippard, Anticancer Res. 2014, 34, 471; b) L. Liu, Q. Ye, M. Lu, Y. C. Lo, Y. H. Hsu, M. C. Wei, Y. H. Chen, S. C. Lo, S. J. Wang, D. J. Bain, C. Ho, Sci. Rep. 2015, 5, 10881; c) S. Pillozzi, M. D’Amico, G. Bartoli, L. Gasparoli, G. Petroni, O. Crociani, T. Marzo, A. Guerriero, L. Messori, M. Severi, R. Udisti, H. Wulff, K. G. Chandy, A. Becchetti, A. Arcangeli, Br. J. Cancer 2018, 118, 200.

[4] L. Oehninger, R. Rubbiani, I. Ott, Dalton Trans. 2013, 42, 3269.

[5] a) K. M. Hindi, M. J. Panzner, C. A. Tessier, C. L. Cannon, W. J. Youngs, Chem. Rev. 2009, 109, 3859; b) Y. Gothe, T. Marzo, L. Messori, N. M. Nolte, Chem. Eur. J. 2016, 22, 12487; c) G. Tamasi, A. Carpini, D. Valensin, L. Messori, A. Pratesi, F. Scaletti, M. Jakupec, B. Keppler, R. Cini, Polyhedron 2014, 81, 227– 237.

[6] a) A. Pratesi, C. Gabbiani, M. Ginanneschi, L. Messori, Chem. Commun. 2010, 46, 7001; b) A. Pratesi, C. Gabbiani, E. Michelucci, M. Ginanneschi, A. M. Papini, R. Rubbiani, I. Ott, L. Messori, J. Inorg. Biochem. 2014, 136, 161; c) V. Gandin, A. P. Fernandes, Molecules 2015, 20, 12732.

[7] A. Citta, E. Schuh, F. Mohr, A. Folda, M. L. Massimino, A. Bindoli, A. Casini, M. P. Rigobello, Metallomics 2013, 5, 1006.

[8] T. Marzo, S. Pillozzi, O. Hrabina, J. Kasparkova, V. Brabec, A. Arcangeli, G. Bartoli, M. Severi, A. Lunghi, F. Totti, C. Gabbiani, A. G. Quiroga, L. Messori, Dalton Trans. 2015, 44, 14896.

[9] a) E. Schuh, C. Pfl_ger, A. Citta, A. Folda, M. P. Rigobello, A. Bindoli, A. Casini, F. Mohr, J. Med. Chem. 2012, 55, 5518; b) A. Meyer, L. Oehninger, Y. Geldmacher, H. Alborzinia, S. Wçlfl, W. S. Sheldrick, I. Ott, ChemMedChem 2014, 9, 1794.

[10] T. Marzo, D. Cirri, C. Gabbiani, T. Gamberi, F. Magherini, A. Pratesi, A. Guerri, T. Biver, F. Binacchi, M. Stefanini, A. Arcangeli, L. Messori, ACS Med. Chem. Lett. 2017, 8, 997.

[11] a) A. Merlino, T. Marzo, L. Messori, Chem. Eur. J. 2017, 23, 6942; b) C. Martìn-Santos, E. Michelucci, T. Marzo, L. Messori, P. Szumlas, P. J. Bednarski, R. Mas-Ballest, C. Navarro-Ranninger, S. Cabrera, J. Aleman, J.Inorg. Biochem. 2015, 153, 339; c) L. Massai, A. Pratesi, J. Bogojeski, M. Banchini, S. Pillozzi, L. Messori, Zˇ. D. Bugarcˇic´, J. Inorg. Biochem. 2016, 165, 1; d) E. Michelucci, G. Pieraccini, G. Moneti, C. Gabbiani, A. Pratesi, L. Messori, Talanta 2017, 167, 30; e) L. Messori, T. Marzo, C. Gabbiani,A. A. Valdes, A. G. Quiroga, A. Merlino, Inorg. Chem. 2013, 52, 13827; f) L. Messori, A Merlino, Chem. Commun. 2017, 53, 11622.

[12] J. C. Garrison, W. J. Youngs, Chem. Rev. 2005, 105, 3978.

[13] H. E. Gottlieb, V. Kotlyar, A. Nudelman, J. Org. Chem. 1997, 62, 7512.

[14] CrysAlisPro 1.171.38.41r, Rigaku OD: https://www.rigaku.com/en/products/smc/crysalis, 2015.

[15] A. Altomare, M. C. Burla, M. Camalli, G. L. Cascarano, C. Giacovazzo, A. Guagliardi, A. G. G. Moliterni, G. Polidori, R. Spagna, J. Appl. Crystallogr. 1999, 32, 115.

[16] G. M. Sheldrick, Acta Crystallogr. Sect. A 2008, 64, 112.

8. Final considerations

As Barnett Rosenberg stated in last years of his life, the results obtained by chemists in developing new anticancer compounds have been substantially inadequate (Fig.1). For this reason, all the scientists involved in the field of medicinal bioinorganic research should address their efforts in finding safer and more effective metal-based drugs, to be used as anticancer or antimicrobial agents, being the cancer and bacterial infections two between the most lethal global health problems. As I showed in previous chapters, this family of molecules still has a lot to offer in the field of clinical applications. The wide literature concerning their structural modifications teaches us that the family of transition metal complexes could be an almost limitless repository of valuable drug candidates. We only need of enough hands and motivation for not stopping our research work. Anyway, it is also a moral duty.

Fig.1: “For years I've been saying this is the first platinum-based drug we discovered (Cisplatin). It can't possibly be the best one. It's disappointing that the scientific community has not been able to find better ones” [1]. Barnett Rosenberg (1926-2009), the discoverer of anticancer activity of Cisplatin.

References

[1]: https://msutoday.msu.edu/news/2009/former-msu-professor-developer-of-anti-cancer-drug-dies-at-age-82/